Supplement of The Cryosphere, 16, 941–965, 2022
https://doi.org/10.5194/tc-16-941-2022-supplement

The Cryosphere
Open Access

Supplement of

PISM-LakeCC: Implementing an adaptive proglacial lake boundary in an ice sheet model

Sebastian Hinck et al.

Correspondence to: Sebastian Hinck (sebastian.hinck@awi.de)

S1 Sensitivity experiments

In this section a short overview of all sensitivity runs is given. These are also listed in Table S1. Temporal snapshots of all experiments are shown in Sect. S2 The main experiments discussed in the main manuscript (*LAKE*, *CTRL* and *DEF*) are not discussed here.

Table S1: List of all sensitivity experiments

Experiment name	Description
IncCalv	increased calving; lacustrine thickness calving threshold set to 500m
RedCalv	reduced calving; lacustrine thickness calving threshold set to 20m
MR	adapted sub-shelf melting; melt parameter adapted to account for differences between marine and lacustrine environment
nSG	no slippery grounding line model
TWO	use of set_tillwat_ocean parameterization instead of slippery grounding line model
GIA	adapted Earth model parameters for the Lingle-Clark bed deformation model
FR5	max_fill_rate set to 5m year^{-1}
FR10	max_fill_rate set to 10m year^{-1}
FR50	max_fill_rate set to 50m year^{-1}

S1.1 IncCalv

As it has already been mentioned in the main text, vast ice shelves appeared in the *LAKE* experiment. However, we are uncertain in how far this aspect is realistic. We therefore conducted one experiment with increased thickness calving threshold for lakes. In this experiment almost all floating ice is immediatley calved off. This value was set ten time higher than in the *LAKE* experiment: $\Delta h_L = 500$m.

Increasing the calving rate speeds up the glacial retreat (see figures in Sec. S2). The break-up of the ice dome over Hudson Bay and the ice bridge connecting the LIS and CIS happen about 2000yr earlier that in the *LAKE* experiment.

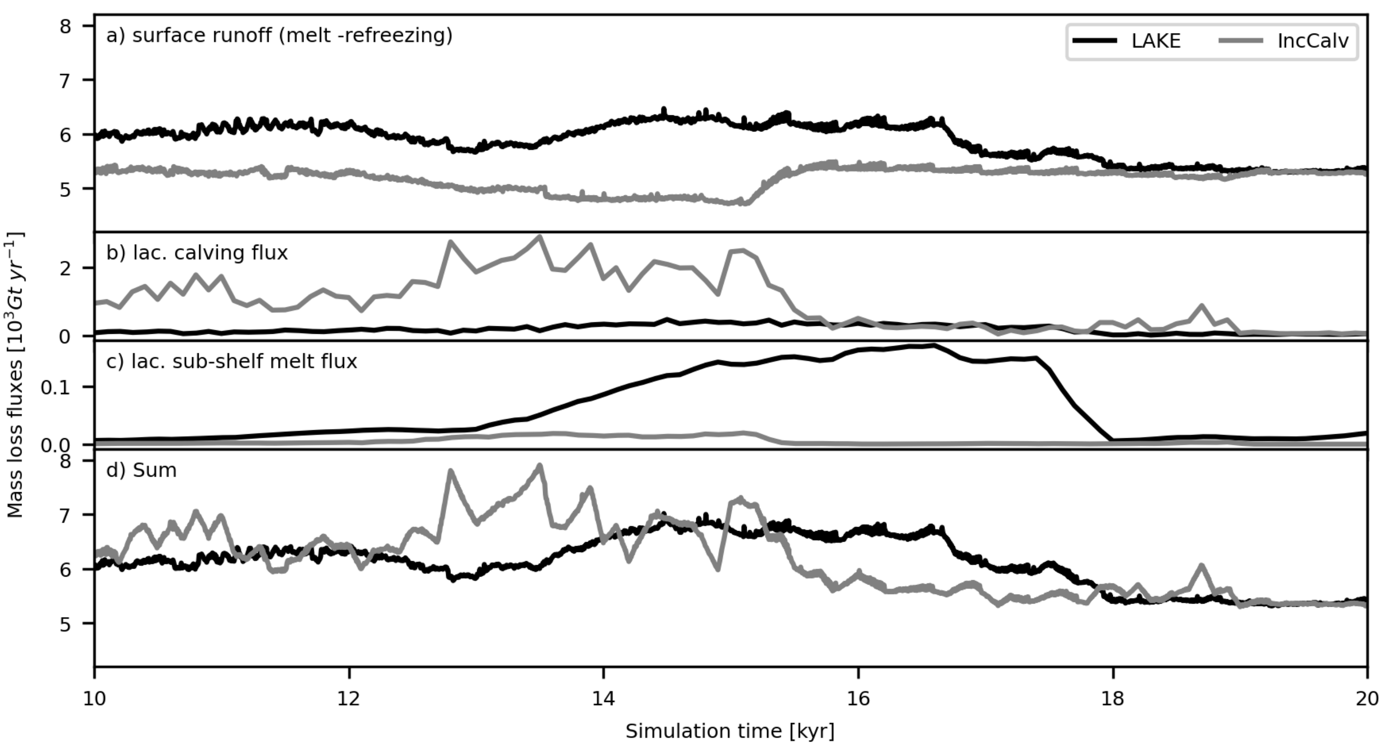

Figure S1: Mass losses for the LIS for the *IncCalv* experiment. Panel (a) shows the surface runoff for the entire LIS. Panels (b) and (c) show the calving and sub-shelf melt fluxes of the LIS at all lacustrine boundaries, respectively. Note, these fluxes are averaged over 100yr. (d) The lines show the accumulated mass losses from the panels above.

Figure S1 shows the mass losses due to lacustrine calving and sub-shelf melting and relates them to the surface runoff. Since no major ice shelves are present, which are due to their low surface elevation subject to high melting, the runoff is strongly reduced, compared to the *LAKE* experiment. The lack of ice shelves is also the reason why the sub-shelf melting is negligible. As long as major proglacial lakes are present, mass losses due to lacustrine calving is substantially higher than in the *LAKE* experiment. Surface runoff contributes most to the ice sheets mass balance.

S1.2 RedCalv

For the *redcalv* experiment the thickness calving threshold for lakes is reduced to 20m. Except for slightly larger ice shelves, the results are hardly different from the *LAKE* experiment (see figures in Sec. S2).

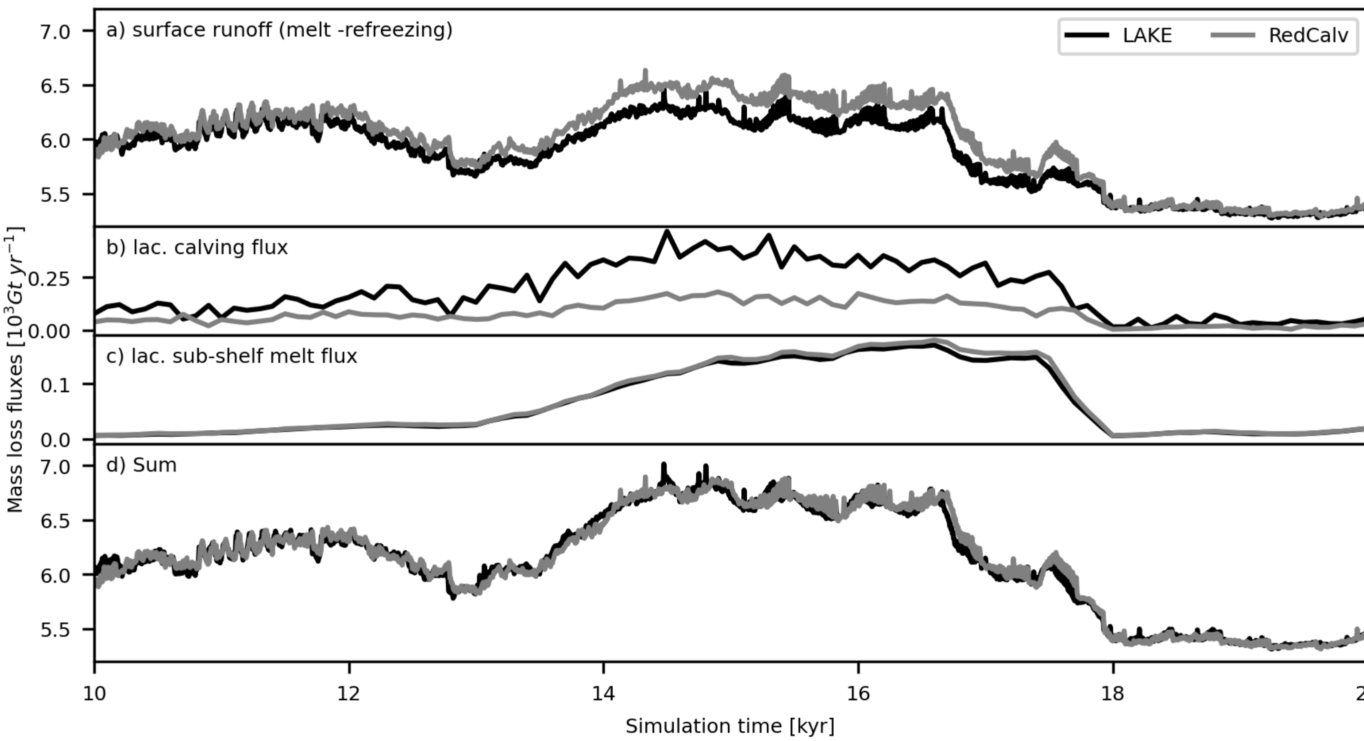

Figure S2: Mass losses for the LIS for the *RedCalv* experiment. Panel (a) shows the surface runoff for the entire LIS. Panels (b) and (c) show the calving and sub-shelf melt fluxes of the LIS at all lacustrine boundaries, respectively. Note, these fluxes are averaged over 100yr. (d) The lines show the accumulated mass losses from the panels above.

Figure S2 shows the mass losses due to lacustrine calving and sub-shelf melting and relates them to the surface runoff. The calving flux is reduced, compared to the *LAKE* experiment, while the sub-shelf melting is almost unchanged. Surface ablation is by far the dominant contribution to mass loss, and is slightly higher than in the *LAKE* experiment. When summing up the contributions from panels (a)-(c) (see panel (d)), it becomes clear, that the gain in runoff balances the reduction in sub-shelf melting.

S1.3 MR

The sub-shelf melting is calculated based on the melt pump scheme by (Beckmann and Goosse, 2003). Although the parameters of the model were adapted for a marine setting around Antarctica, it was used in the previous experiments in the lacustrine setting without adaptation. In the *MR* experiment we estimate the magnitude of the difference between marine and lacustrine melting and adapt a melt parameter of the model accordingly. The details are discussed in the following.

The melt flux is calculated as follows (Martin et al., 2011):

$$M = L^{-1}\ C\ \rho_{SW}\ c_p\ \gamma_{T,O}\ \ (T_O - T_f(S,d)) \tag{S1}$$

Here, L is the latent heat of fusion, C is a tuning parameter, ρ_{SW} is the density of seawater, c_p is the heat capacity of the mixed layer, $\gamma_{T,O}$ is the thermal exchange velocity, T_O is the temperature of the ambient ocean and $T_f(S,d)$ the freezing temperature of water of salinity S at depth d. We rewrite this formula for lakes:

$$\begin{aligned} M &= L^{-1}\ C\ \rho_{FW}\ c_p\ \gamma_{T,L}\ \ (T_L - T_f(S_L,d)) \\ &= L^{-1}\ C\ C_\rho\ \rho_{SW}\ c_p\ C_\gamma\ \gamma_{T,O}\ \ C_T(T_O,T_L,S_L,d)\ (T_O - T_f(S,d)) \end{aligned} \tag{S2}$$

Here, T_L is the temperature of the lake, $\gamma_{T,L}$ is the thermal exchange velocity for a lake, and the C terms are factors to modify from lake to ocean parameterization:

$$C_\rho = \rho_{FW}/\rho_{SW} \approx 1 \tag{S3}$$

accounts for the difference in density. We neglect the density difference here and assume it is 1.

$$C_\gamma = \gamma_{T,L}/\gamma_{T,O} \approx \frac{1}{200} \tag{S4}$$

This value is not easy to estimate, it describes how efficient heat is transported away in the boundary layer. The thermal exchange velocity γ_T is a function of the Nusselt number Nu of the mixed layer (Holland and Jenkins, 1999), which is proportional to the velocity of the mixed layer. We assume that this velocity depends on the density contrast between the meltwater and the ambient water. In a marine environment the buoyancy of meltwater is about 200 times larger than in a lacustrine environment (Funk and Röthlisberger, 1989). We use this as our best guess: $C_\gamma = 200^{-1}$.

$$C_T = \frac{T_L - T_f(S_L, d)}{T_O - T_f(S, d)} \approx 5 \tag{S5}$$

This term can not be expressed as a constant, as it depends on lake and ocean temperatures, depth and salinity. The marine values are set in the model: $S = 35$PSU and $T_O = -1.7°C$, and also $S_L = 0$ for freshwater is fixed. The dependence on the other values is illustrated in Fig. S3. Even though the values vary a lot, we chose $C_T = 5$, which represents this value for $T_L = 2°C$ and $d = 300m$.

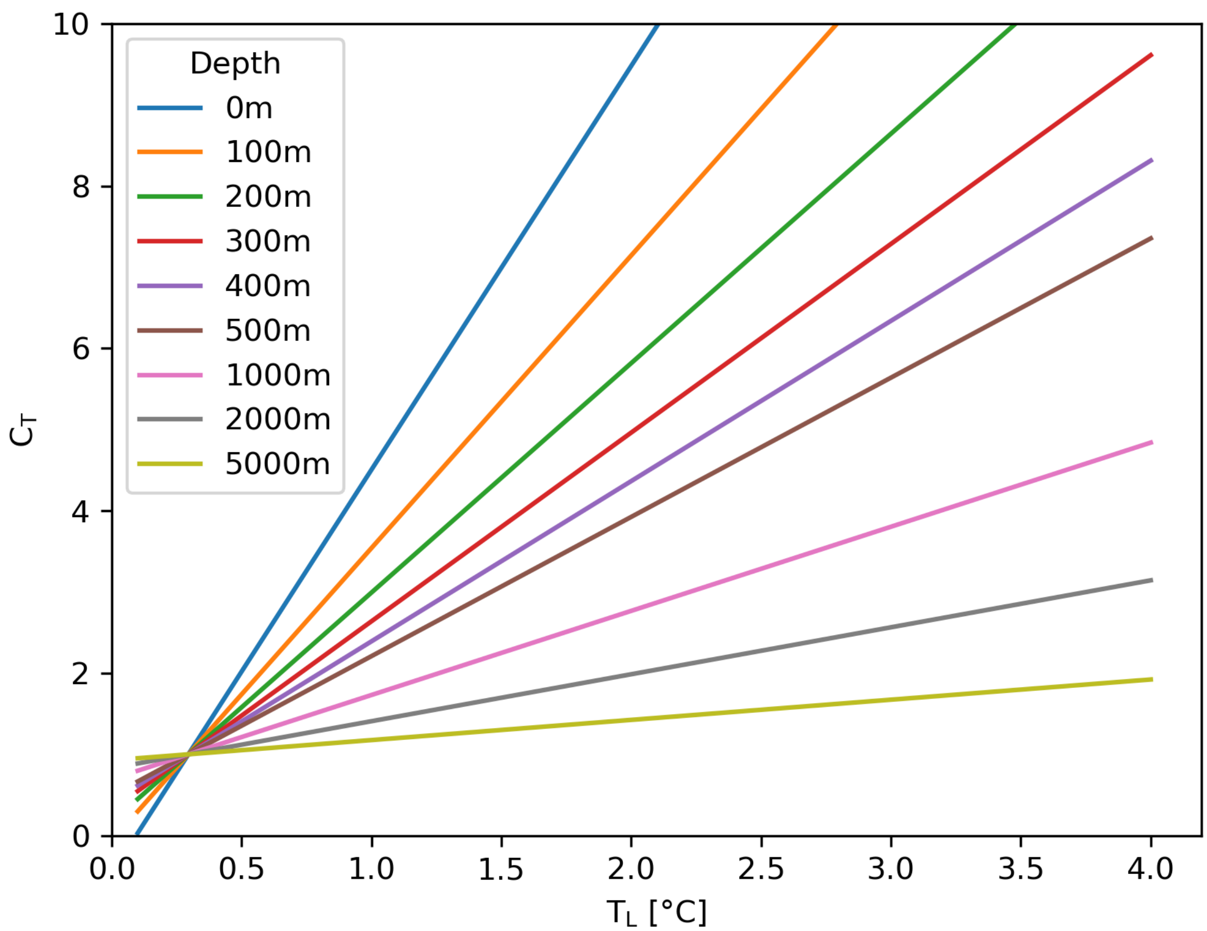

Figure S3: Dependence of C_T on the lake temperature T_L for different depths d.

Since we used $C = 0.01$ for the other experiments, we keep it at that value. With these estimates we can determine our tuning factor C^* for lacustrine settings:

$$C^* = C\ C_\rho\ C_\gamma\ C_T = 2.5 \cdot 10^{-4} \tag{S6}$$

Accordingly, the lacustrine sub-shelf melting is 40 times less effective than its marine counterpart.

We have to note that, when using this tuning factor sub-shelf melting is strongly reduced also at the marine boundaries. To prevent marine ice shelves from growing excessively large, we restrict the ice sheet in the *MR* experiment from expanding outside a prescribed margin. A respective mask was calculated in a way that the ice sheet growth was only restricted in marine areas, not terrestrial or lacustrine regions. This is the reason why the marine parts of the ice sheet differ from the other experiments (compare with Fig. S3).

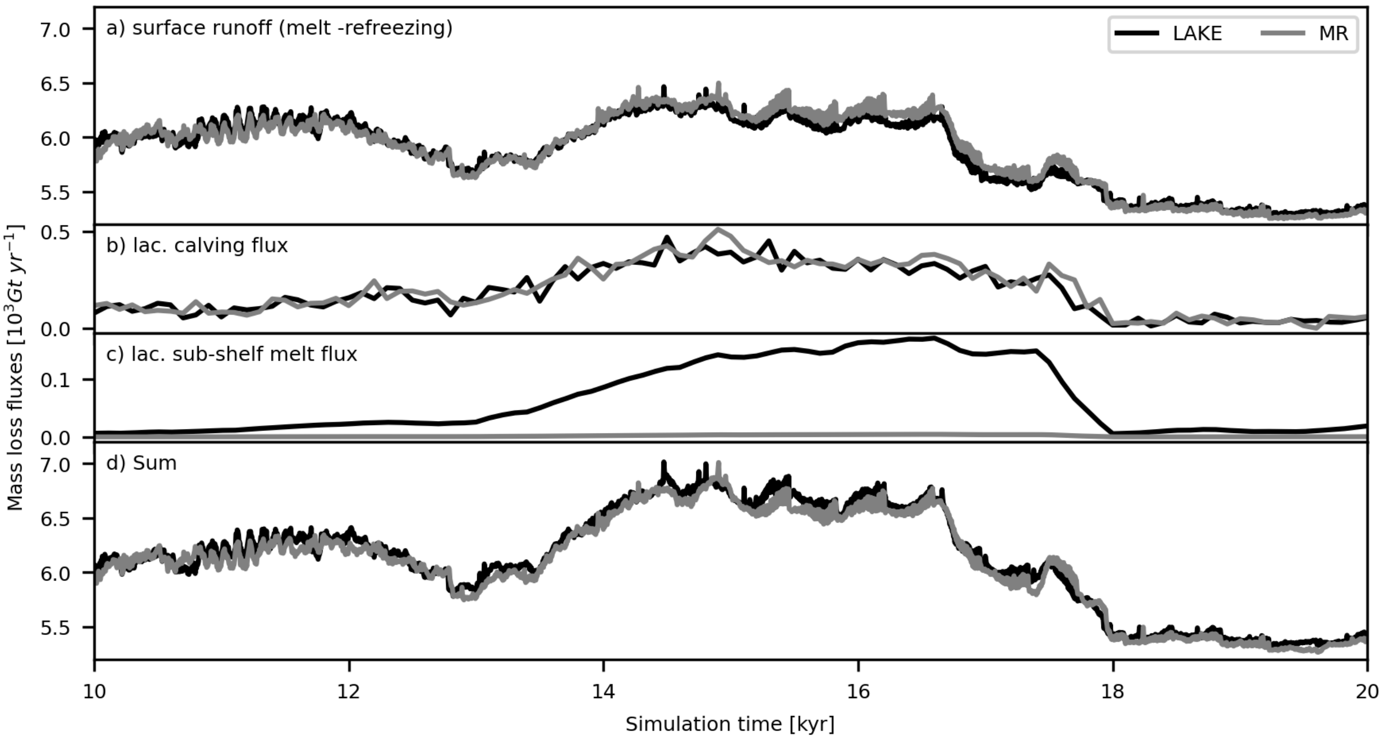

Figure S4: Mass losses for the LIS for the *MR* experiment. Panel (a) shows the surface runoff for the entire LIS. Panels (b) and (c) show the calving and sub-shelf melt fluxes of the LIS at all lacustrine boundaries, respectively. Note, these fluxes are averaged over 100yr. (d) The lines show the accumulated mass losses from the panels above.

Figure S4 shows the mass losses due to lacustrine calving and sub-shelf melting and relates them to the surface runoff. The mass loss due to lacustrine sub-shelf melting is strongly reduced, compared to the *LAKE* experiment, while the lacustrine calving flux is almost unchanged. Surface ablation dominates the ice sheet's mass loss, while lacustrine sub-shelf melting is almost insignificant.

S1.4 nSG

For this run the slippery grounding line treatment of PISM, which was used for the other experiments, is disabled. Compared to the *LAKE* experiment, the transport of ice towards the marine and lacustrine boundaries is drastically reduced. As a consequence, the observed lowering of the ice surface upstream the lacustrine and marine boundaries is also smaller. The self-amplified feedback cycle, consisting of increased melting due to warmer air temperatures and warming temperatures due to surface lowering, that results in the rapid breakup of the ice sheet, as observed in the *LAKE* experiment, does not appear in this run (see figures in Sec. S3).

Although the mass loss is reduced compared to the *LAKE* experiment, the presence of lakes does increase the ice loss at the lacustrine boundaries compared to the *CTRL* experiment (see Fig. S5). At the marine ice margins, this lower mass flux leads to thicker ice shelves and an advanced grounding line.

Due to the thicker ice sheet, the rapid lacustrine advance underneath the grounded ice front, as observed over Hudson Bay for the *LAKE* experiment, does not happen here. Consequently, the self-amplified feedback mechanism, the PLISI, does not happen and the complete breakup of the LIS ice dome over Hudson Bay and the ice bridge to the CIS does not happen until the end of the run. In the final phase of the experiments the southern ice margin is a few hundred kilometers north of the no-lake experiments.

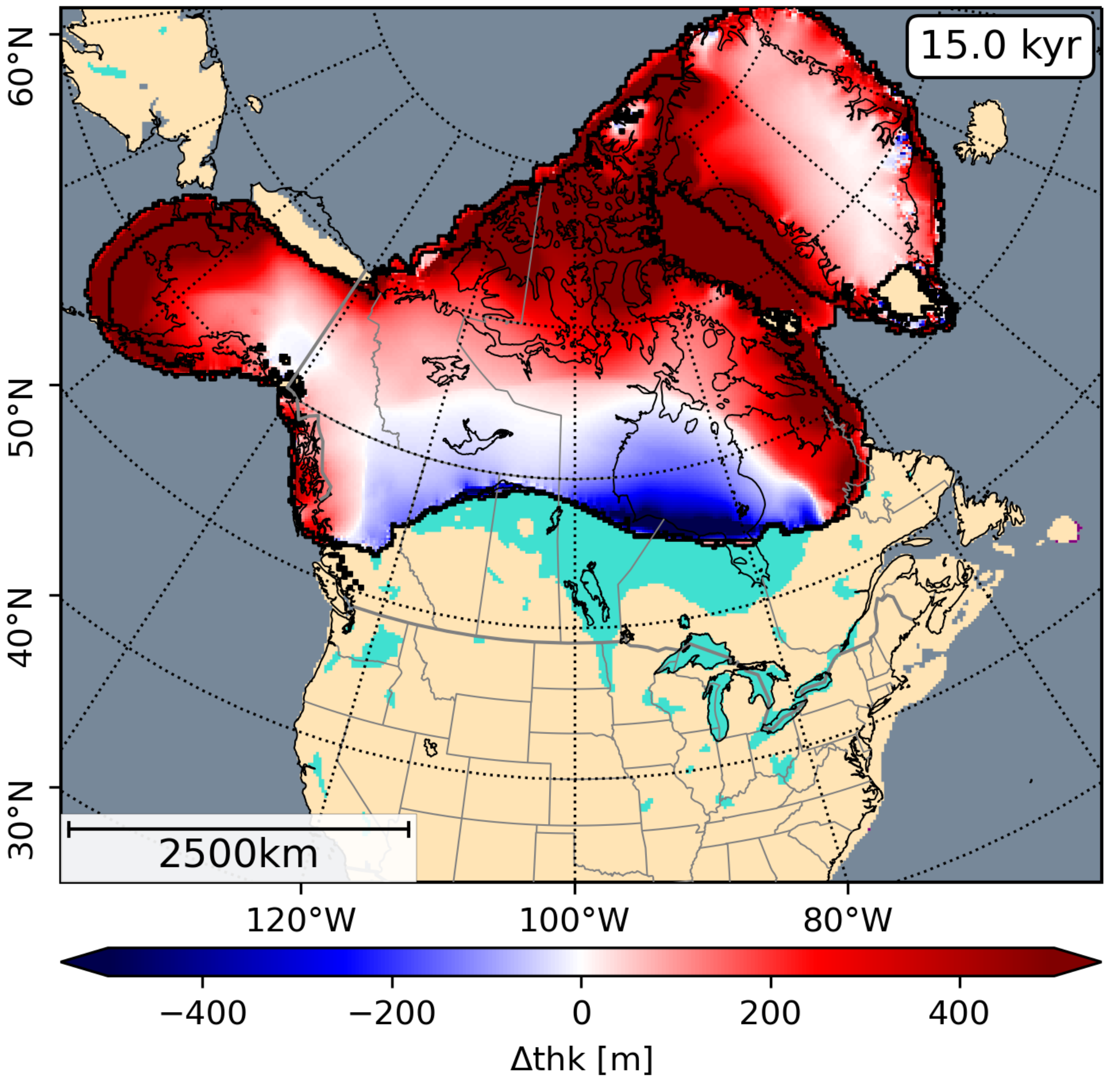

Figure S5: Ice thickness anomaly plot comparing the *nSG* and the *CTRL* experiment. Along the lacustrine margins and upstream of those the impact of the lake boundary, even in absence of the enhanced sliding parameterization, is obvious. At the marine boundaries, however, the mass loss is also strongly reduced, which can be seen in the strong positive anomaly.

S1.5 TWO

Another treatment of the grounding line is proposed in Albrecht et al. (2020). This method is called `tillwater_ocean`, hence the name of the experiment, and is not yet included into an official PISM release [1]. This parameterization assumes the till at grounded ice cells, that have previously been ocean, to be saturated with water. This assumption is similar to the slippery grounding-line approach. As has also been reported by Albrecht et al. (2020), we find the results to be similar to the *LAKE* experiment, where the `slippery_gl` parameterization was used (compare with figures in Sec. S2).

S1.6 GIA

In this experiment different parameters for the Lingle-Clark bed deformation model of PISM were used. Our changes targeted the underlying Earth model, which was chosen accordingly to the parameterization used for NAICE (Gowan et al., 2016). The viscosity of the upper mantle is set to $4 \cdot 10^{20}$Pa s and the lithosphere is assumed to be 120km thick. With these values the flexural rigidity of the lithosphere is calculated accordingly to Bueler et al. (2007): $1.2627 \cdot 10^{25}$Nm.

The results of this run are very similar to the *LAKE* experiment (see figures in Sec. S2). Differences in timing in the glacial retreat are due to the different calculated Earth response. The conclusions drawn from this experiment, however, are the same as for the *LAKE* experiment.

[1] See the corresponding pull request on *Github*: `https://github.com/pism/pism/pull/425`. Accessed: 2021/08/15

S1.7 FR5, FR10 and FR50

Compared to the *LAKE* experiment for these three experiments (*FR5*, *FR10* and *FR50*) only fill rates at which the water level is gradually adjusted is changed (5, 10 and 50m yr^{-1}). Although the rates were drastically increased up to 50 times more rapid, the model stayed numerically stable. However, it can not be determined, whether this is because a reduced time step of 0.25yr was chosen, or simply because no critical situation was triggered.

The more quickly adjusting water level comes closer to the original assumption that the lake basins are always filled. By looking at the overview maps in Sec. S2, no substantial difference in the ice sheet evolution can be determined, compared to the *LAKE* experiment.

References

Albrecht, T., Winkelmann, R., and Levermann, A.: Glacial-Cycle Simulations of the Antarctic Ice Sheet with the Parallel Ice Sheet Model (PISM) – Part 1: Boundary Conditions and Climatic Forcing, The Cryosphere, 14, 599–632, https://doi.org/10.5194/tc-14-599-2020, 2020.

Beckmann, A. and Goosse, H.: A Parameterization of Ice Shelf–Ocean Interaction for Climate Models, Ocean Modelling, 5, 157–170, https://doi.org/10.1016/S1463-5003(02)00019-7, 2003.

Bueler, E., Lingle, C. S., and Brown, J.: Fast Computation of a Viscoelastic Deformable Earth Model for Ice-Sheet Simulations, Annals of Glaciology, 46, 97–105, https://doi.org/10.3189/172756407782871567, 2007.

Funk, M. and Röthlisberger, H.: Forecasting the Effects of a Planned Reservoir Which Will Partially Flood the Tongue of Unteraargletscher in Switzerland, Annals of Glaciology, 13, 76–81, https://doi.org/10.3189/S0260305500007679, 1989.

Gowan, E. J., Tregoning, P., Purcell, A., Montillet, J.-P., and McClusky, S.: A Model of the Western Laurentide Ice Sheet, Using Observations of Glacial Isostatic Adjustment, Quaternary Science Reviews, 139, 1–16, https://doi.org/10.1016/j.quascirev.2016.03.003, 2016.

Holland, D. M. and Jenkins, A.: Modeling Thermodynamic Ice–Ocean Interactions at the Base of an Ice Shelf, Journal of Physical Oceanography, 29, 1787–1800, https://doi.org/10.1175/1520-0485(1999)029⟨1787:MTIOIA⟩2.0.CO;2, 1999.

Martin, M. A., Winkelmann, R., Haseloff, M., Albrecht, T., Bueler, E., Khroulev, C., and Levermann, A.: The Potsdam Parallel Ice Sheet Model (PISM-PIK) – Part 2: Dynamic Equilibrium Simulation of the Antarctic Ice Sheet, The Cryosphere, 5, 727–740, https://doi.org/10.5194/tc-5-727-2011, 2011.

S2 Overview maps

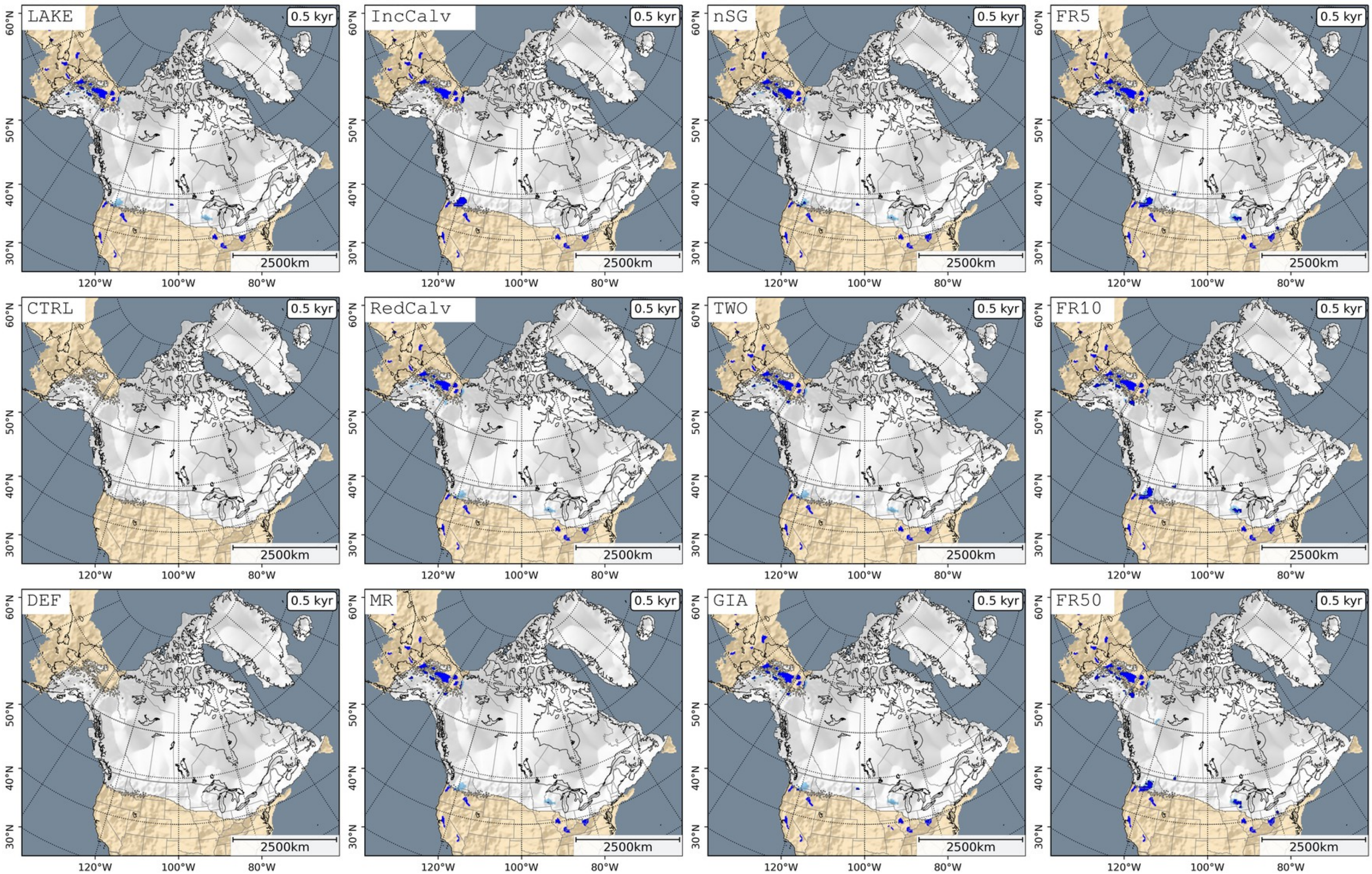

Figure S6: Overview map at 500yr for the different experiments

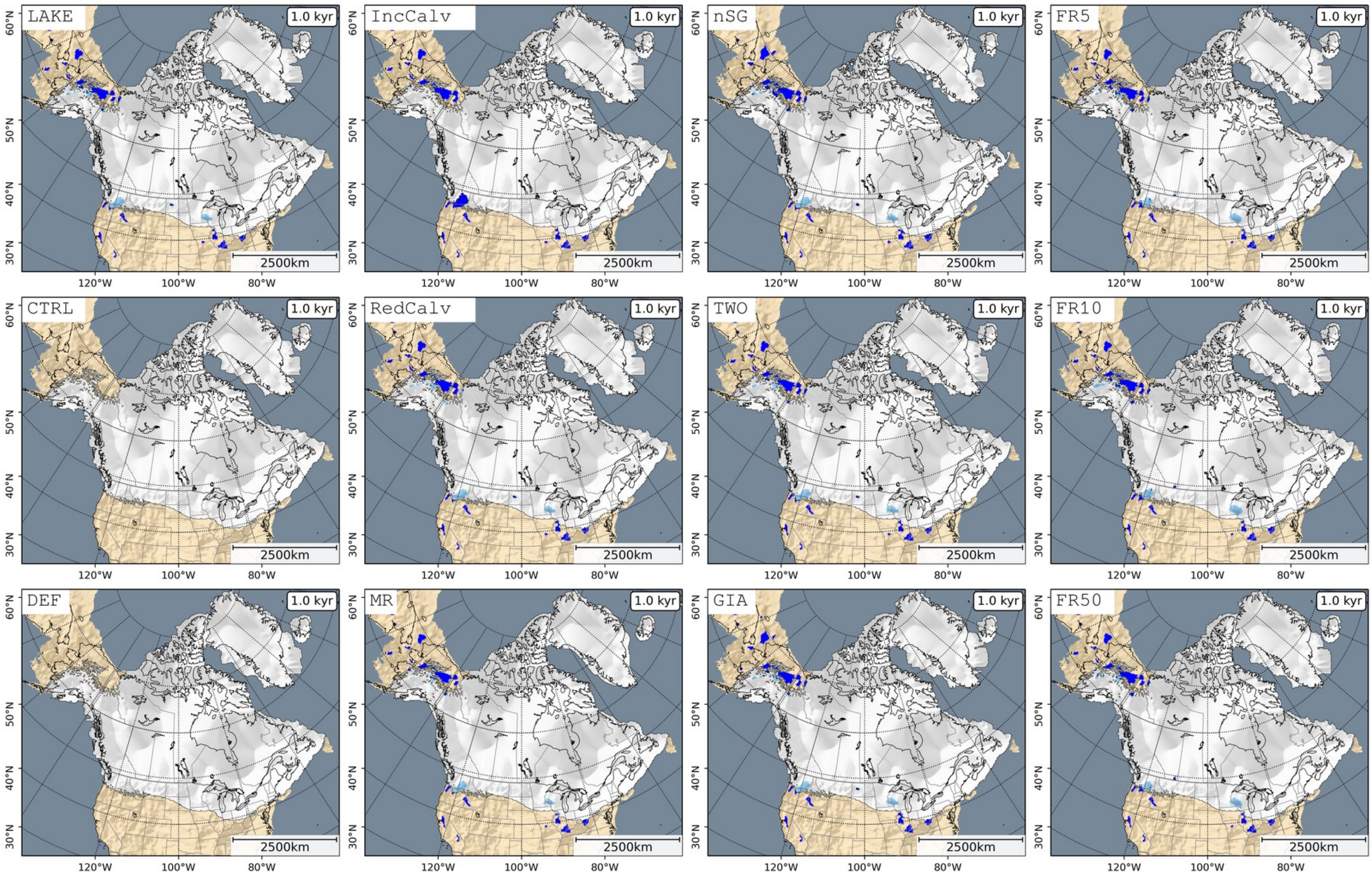

Figure S7: Overview map at 1000yr for the different experiments

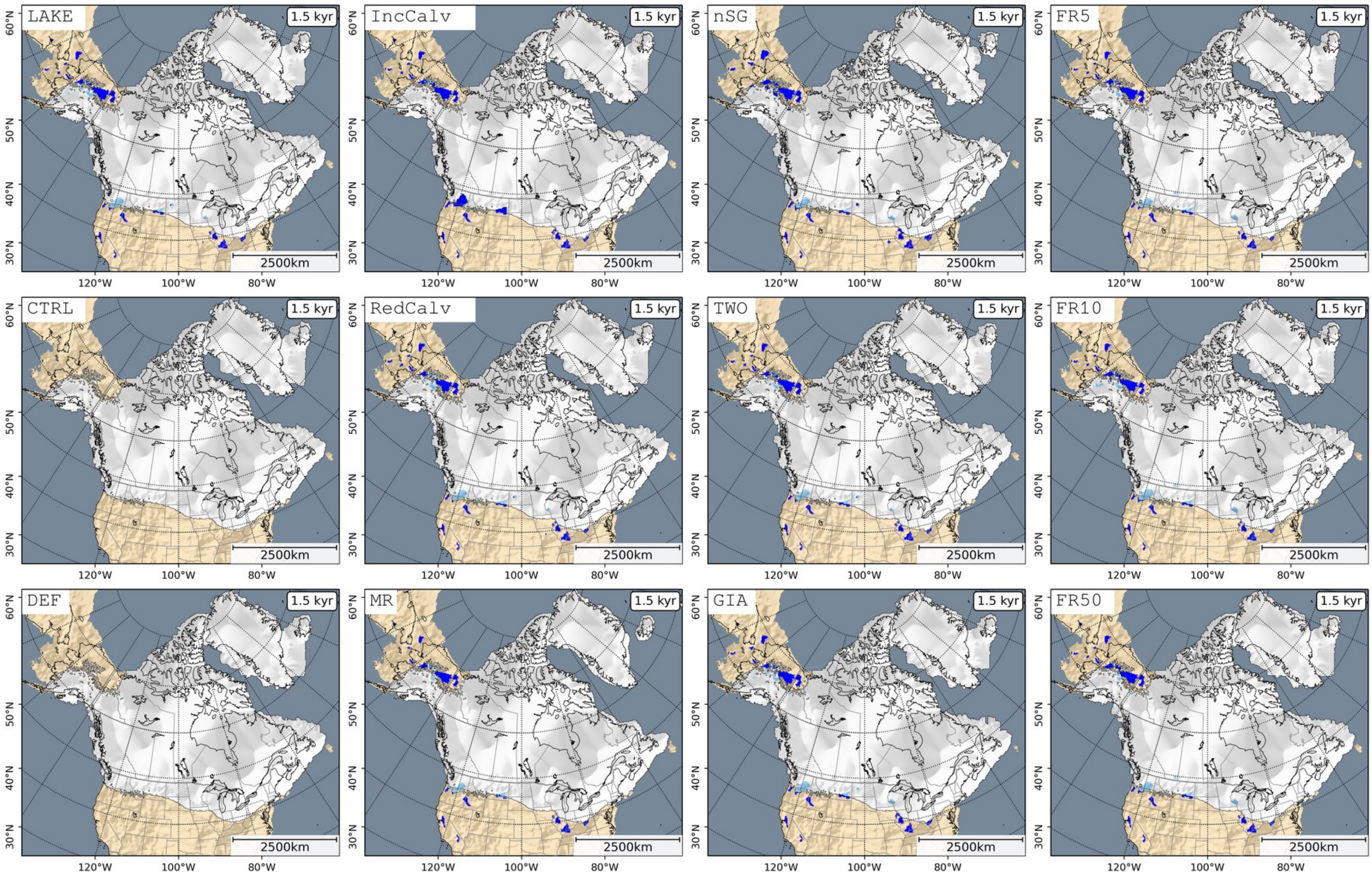

Figure S8: Overview map at 1500yr for the different experiments

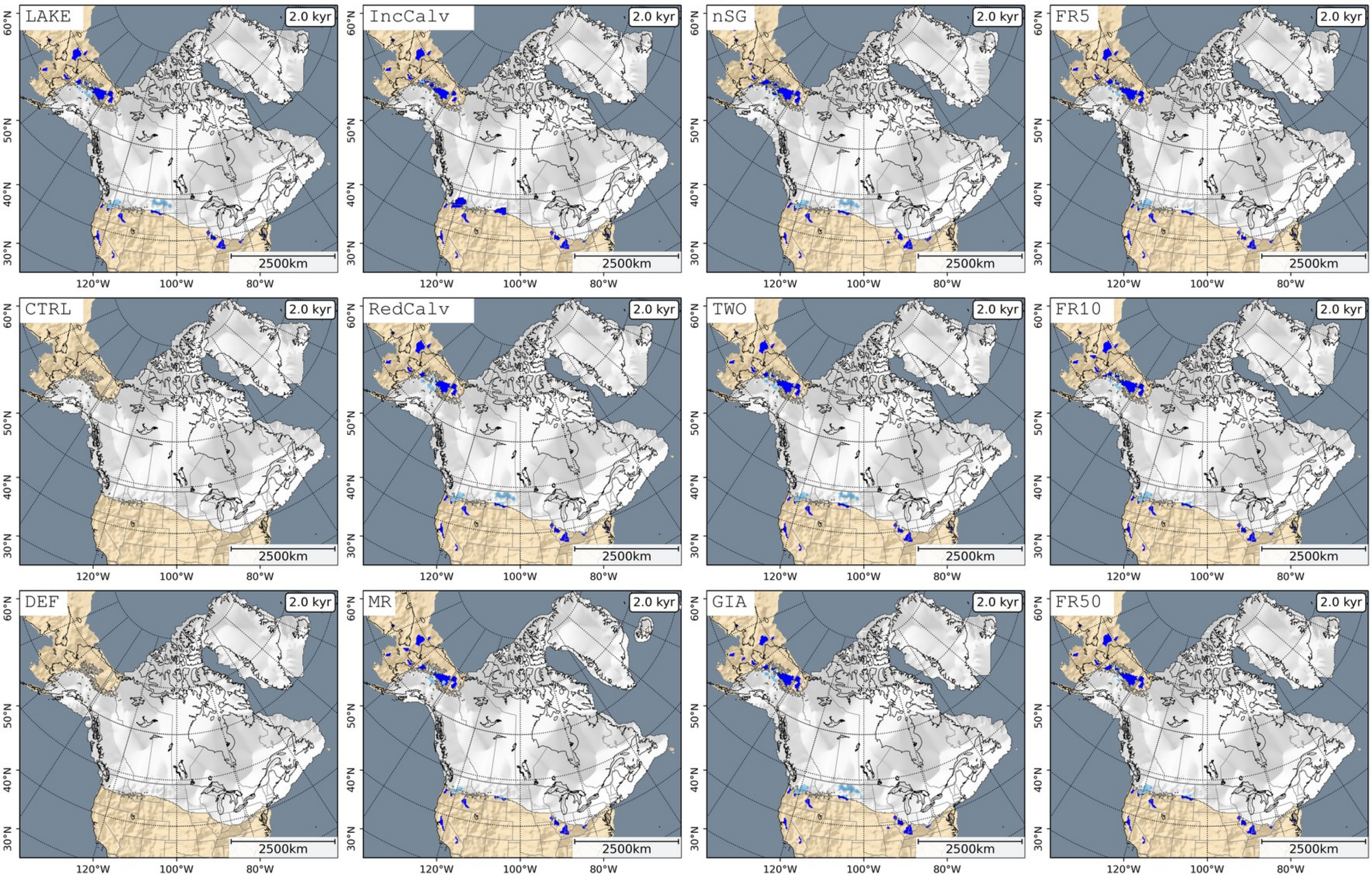

Figure S9: Overview map at 2000yr for the different experiments

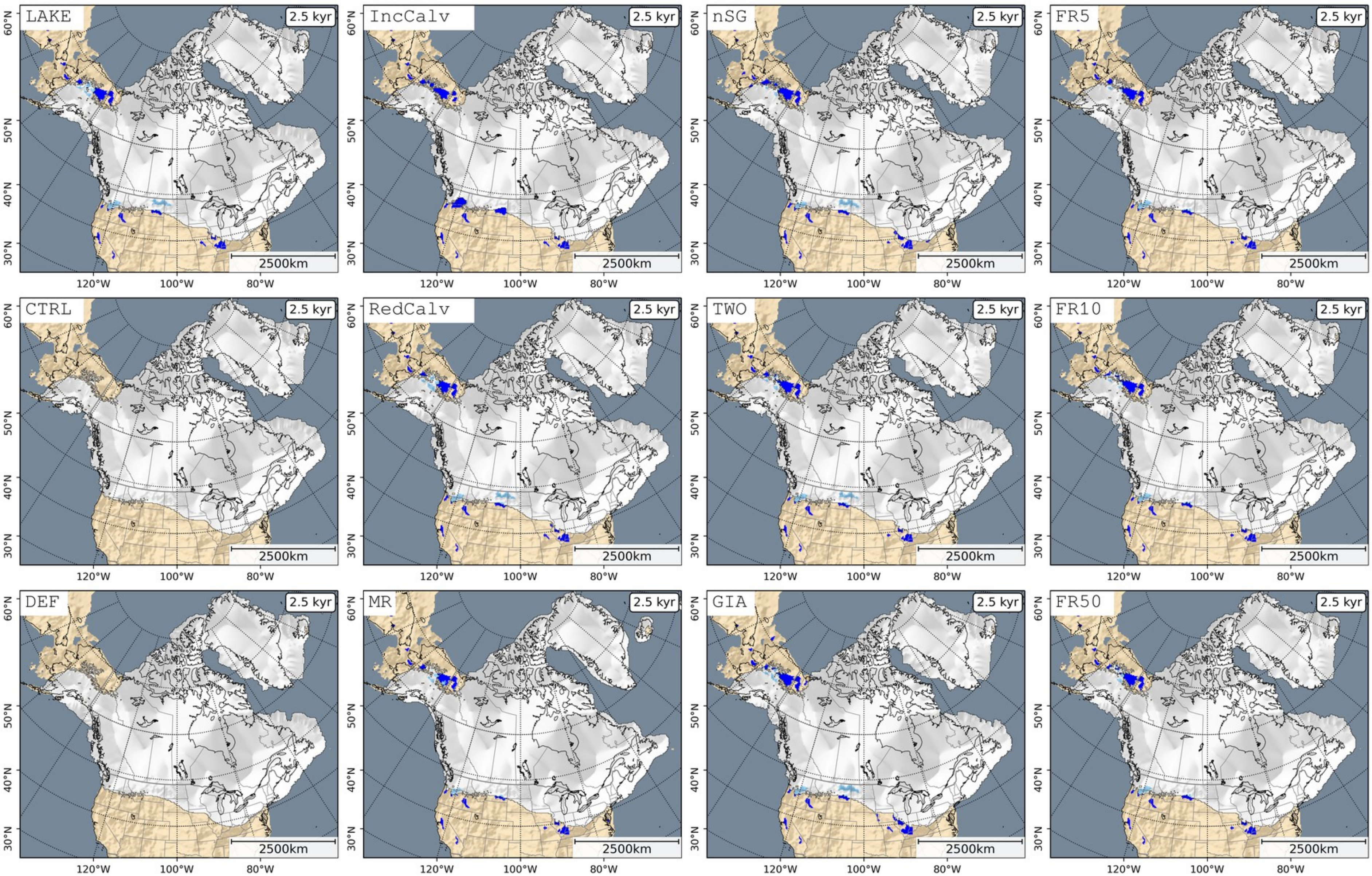

Figure S10: Overview map at 2500yr for the different experiments

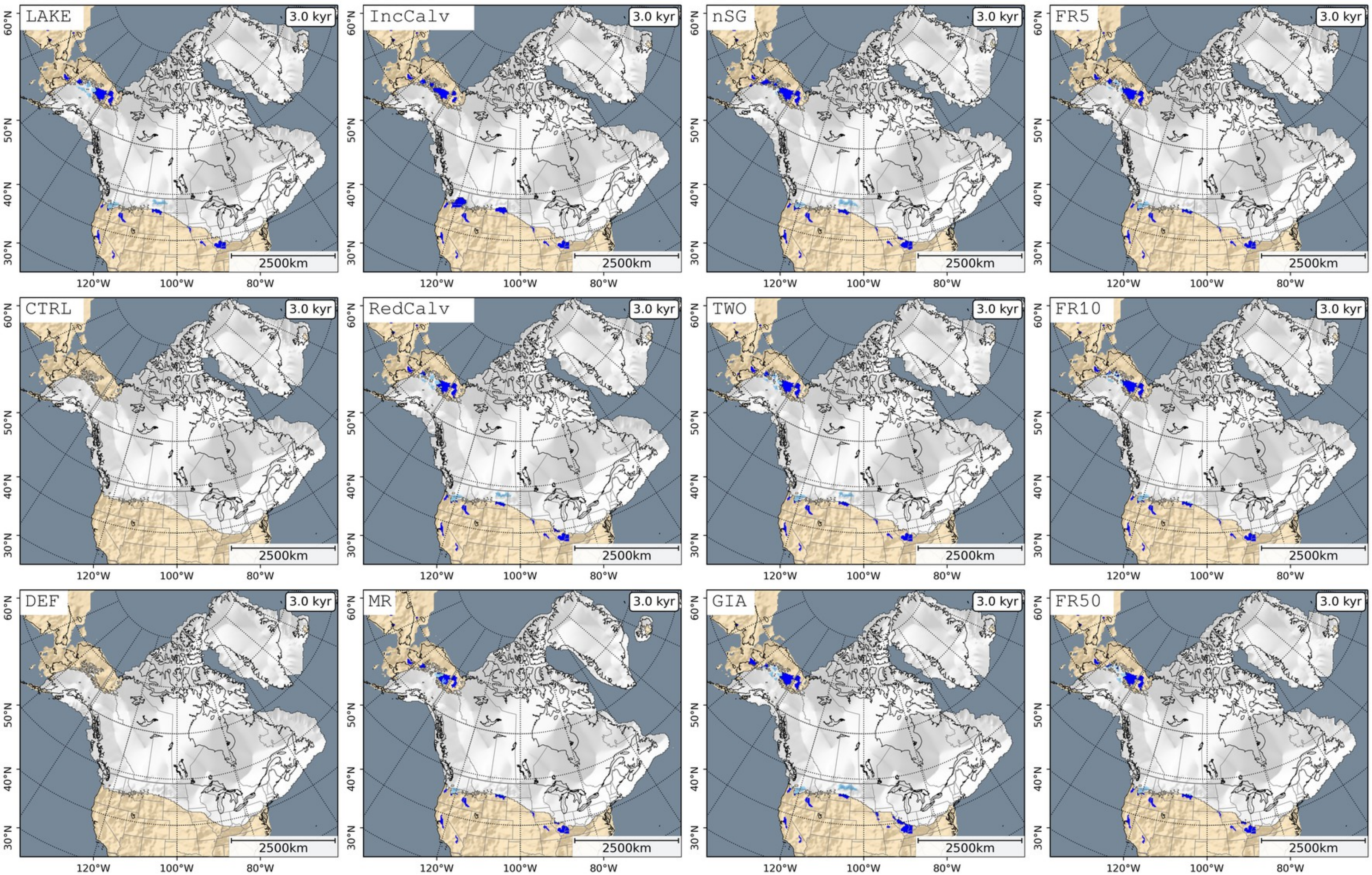

Figure S11: Overview map at 3000yr for the different experiments

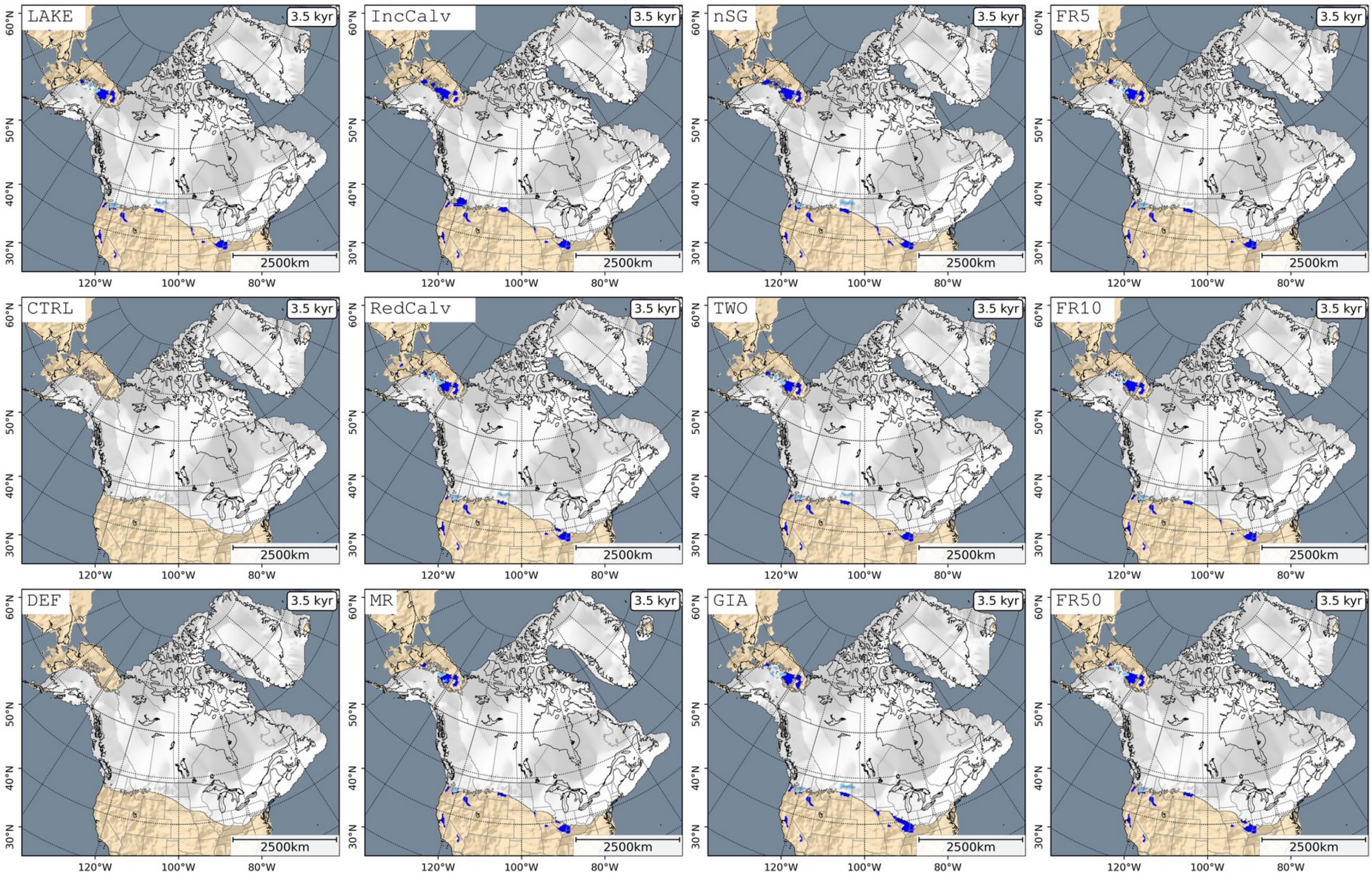

Figure S12: Overview map at 3500yr for the different experiments

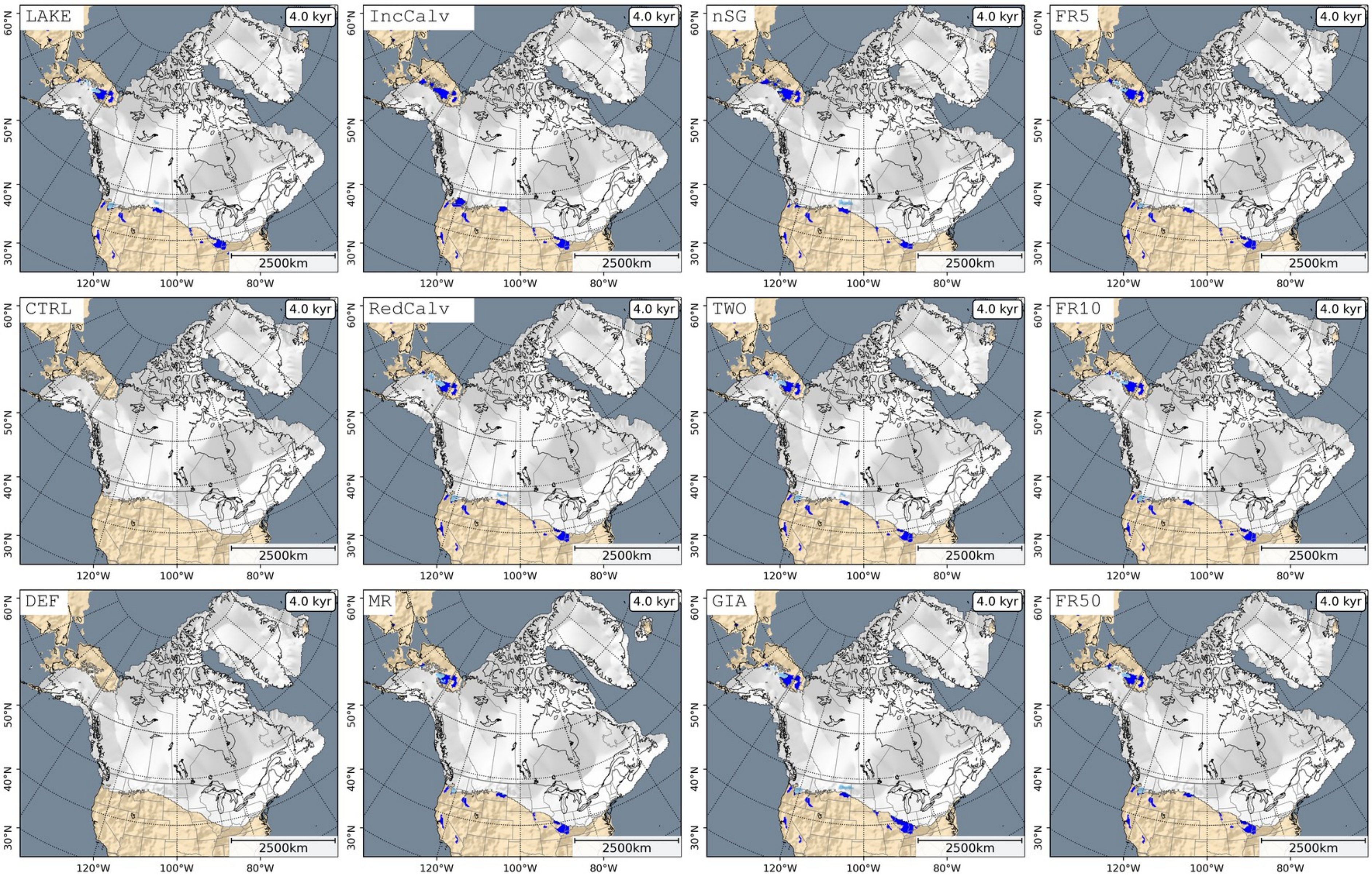

Figure S13: Overview map at 4000yr for the different experiments

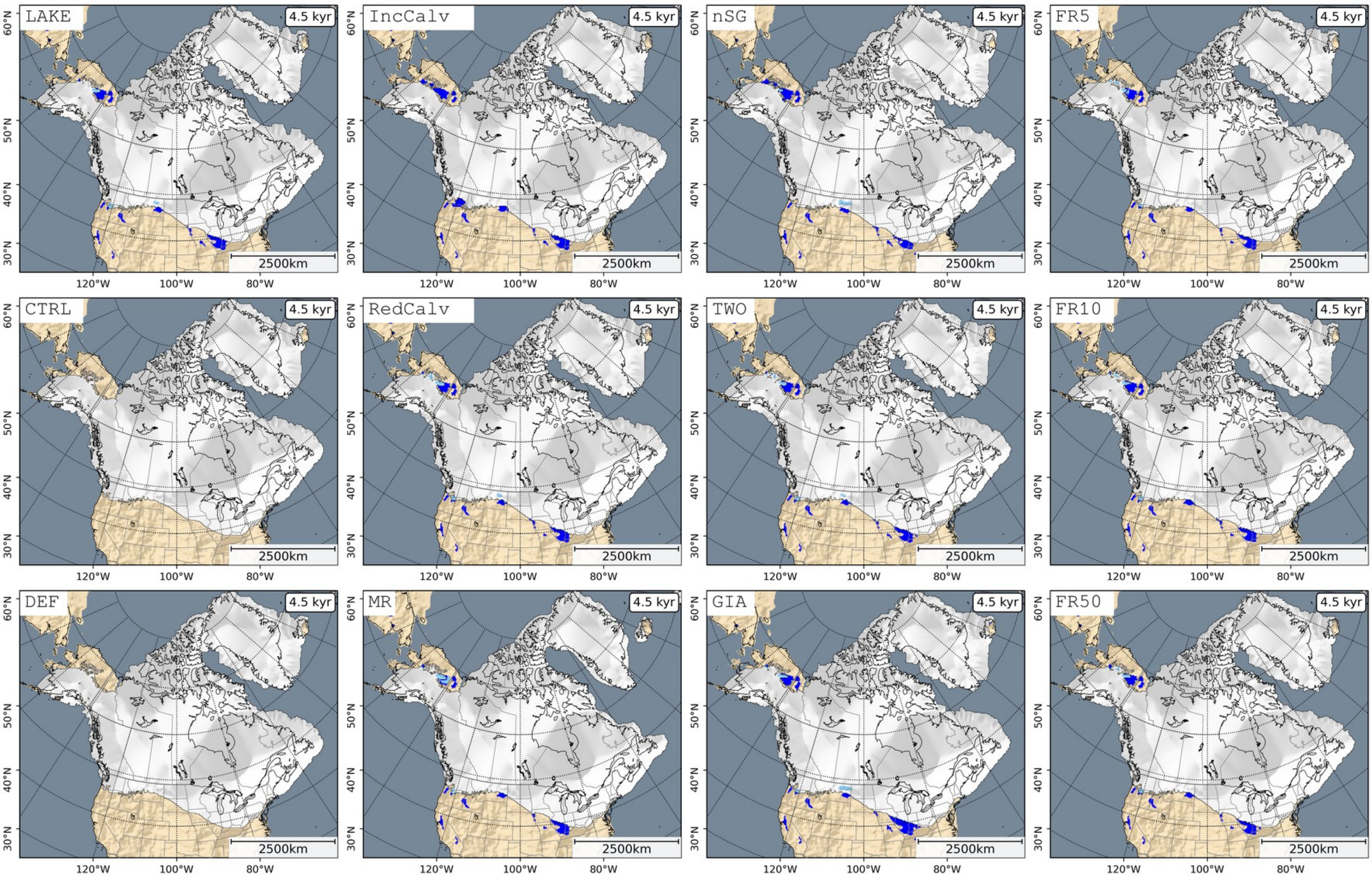

Figure S14: Overview map at 4500yr for the different experiments

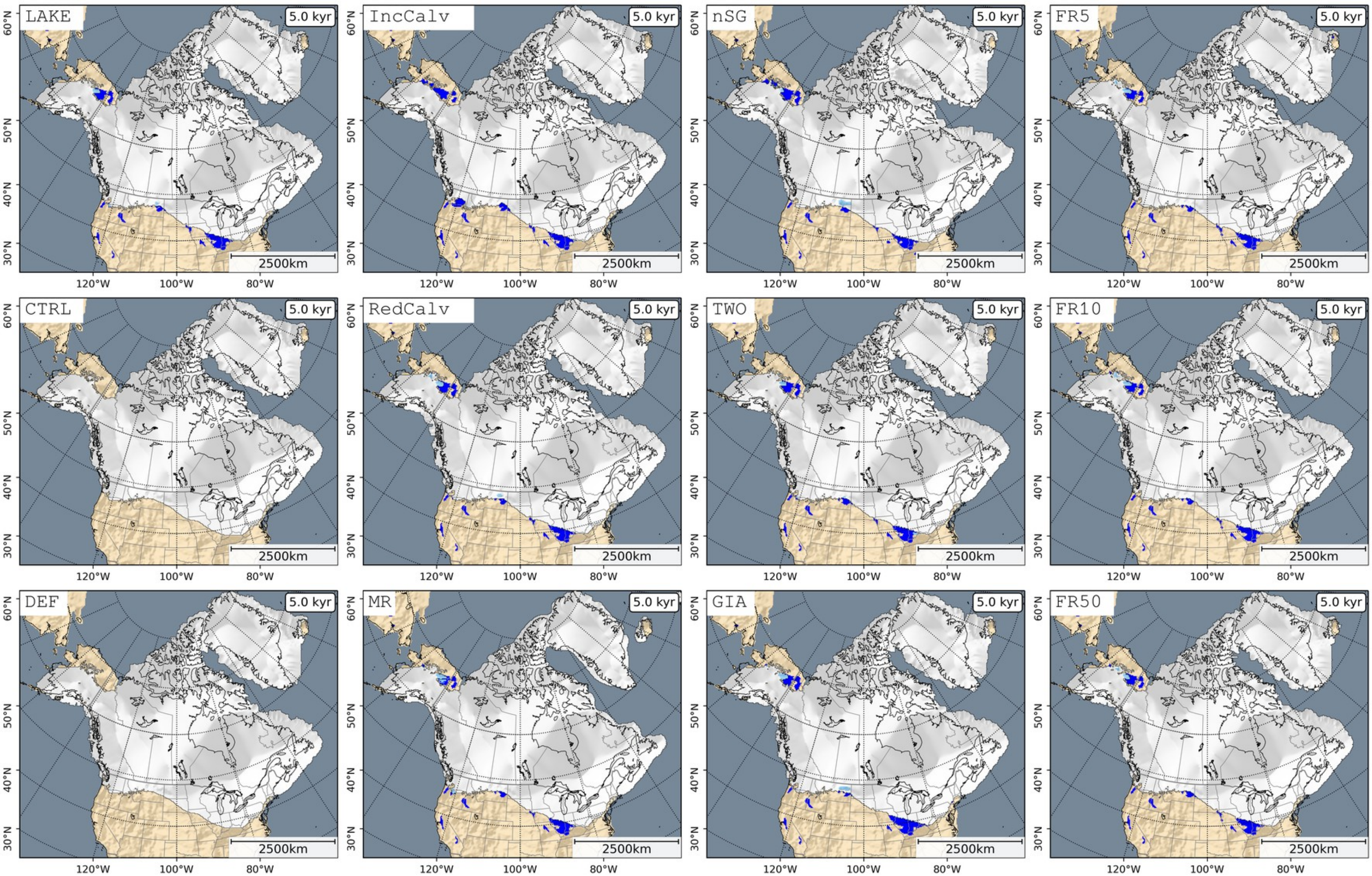

Figure S15: Overview map at 5000yr for the different experiments

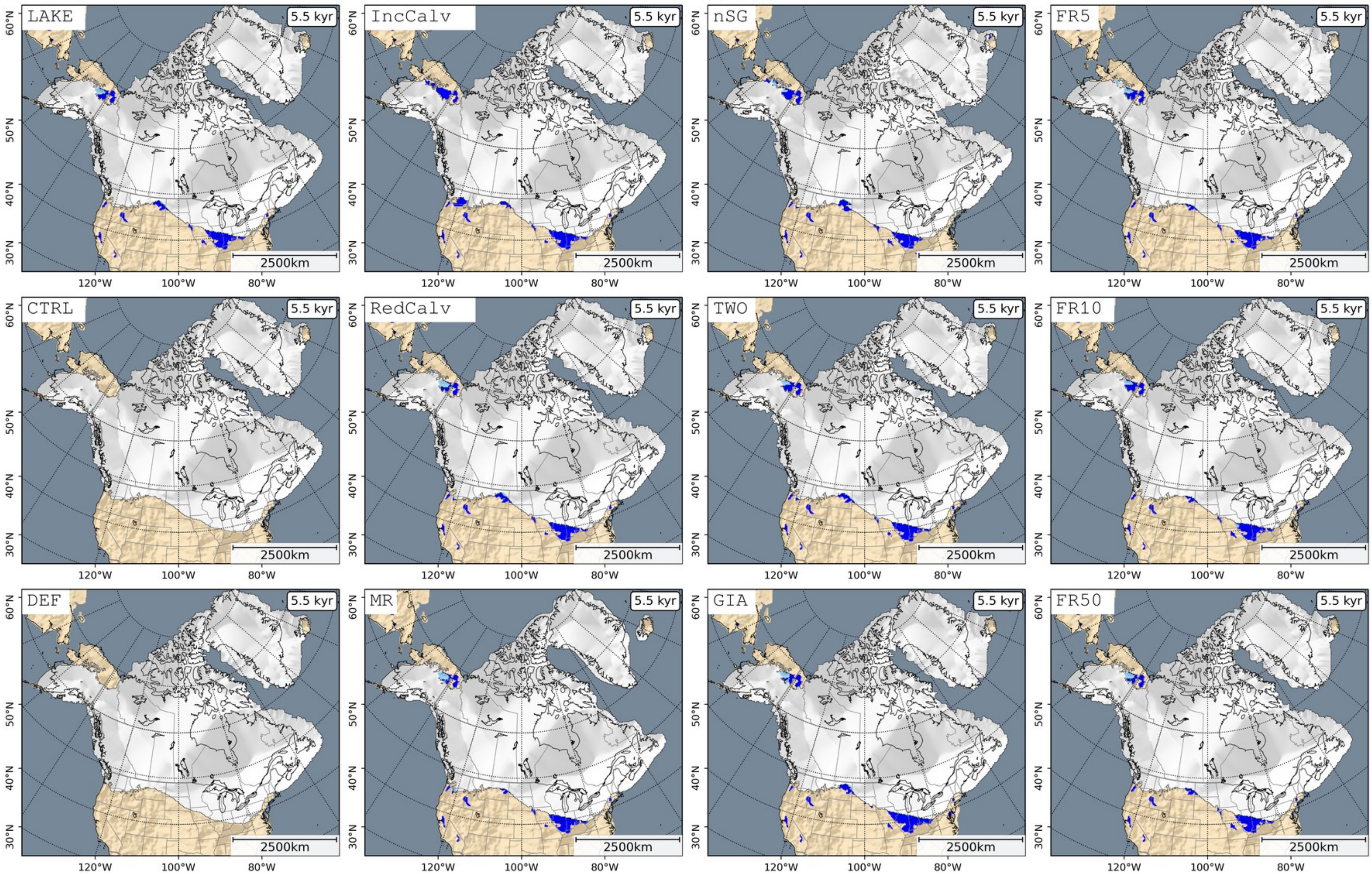

Figure S16: Overview map at 5500yr for the different experiments

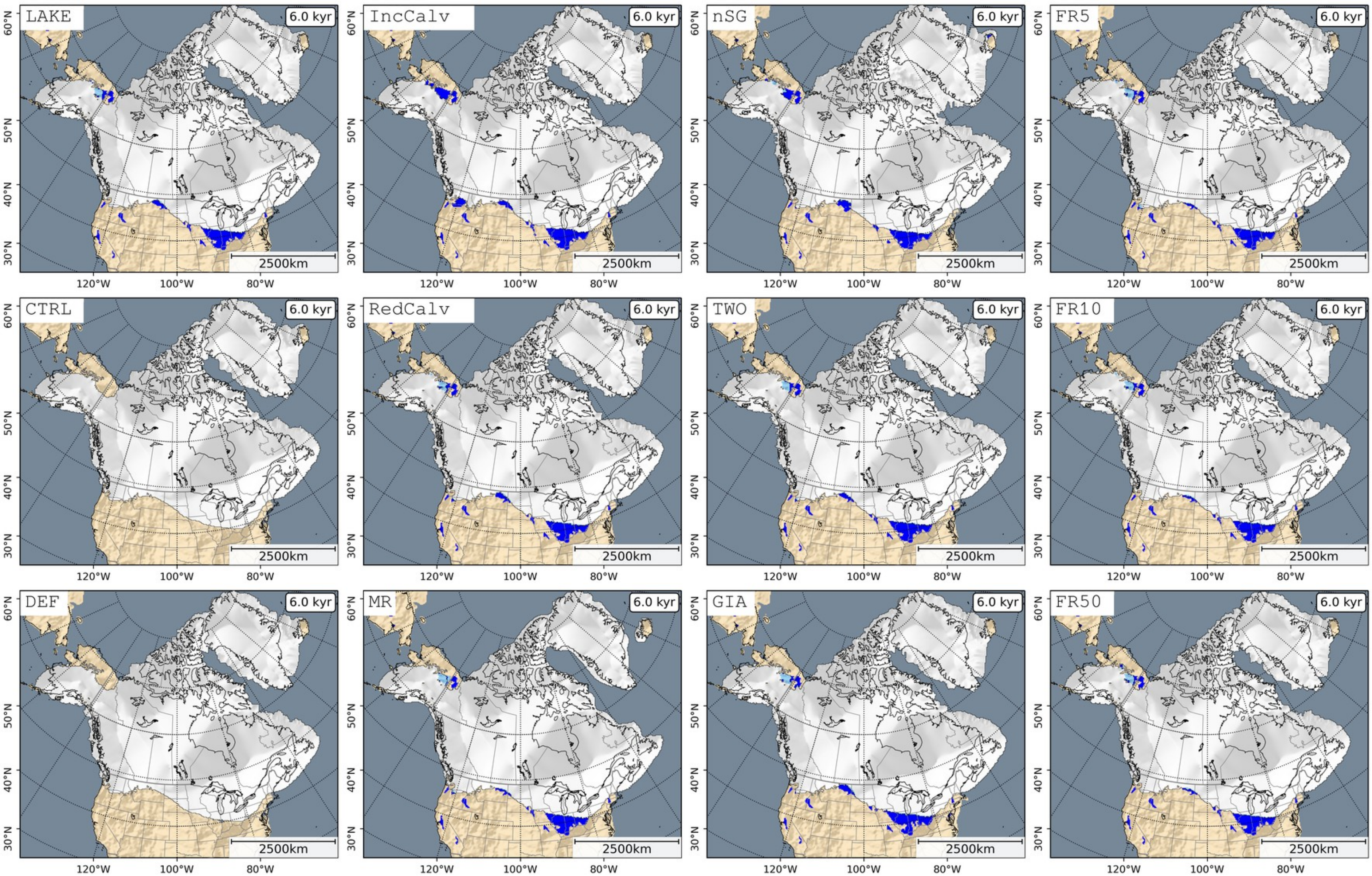

Figure S17: Overview map at 6000yr for the different experiments

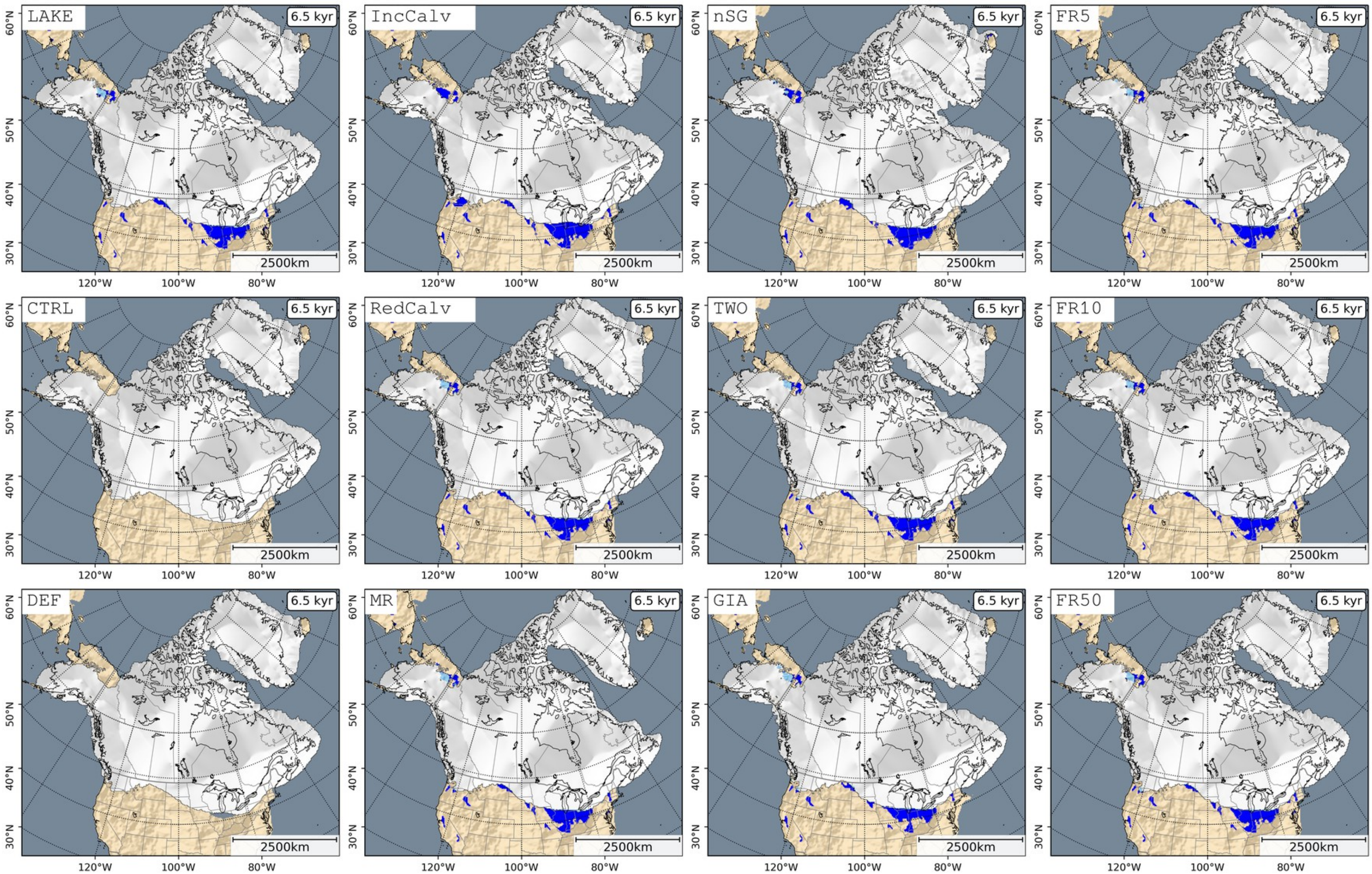

Figure S18: Overview map at 6500yr for the different experiments

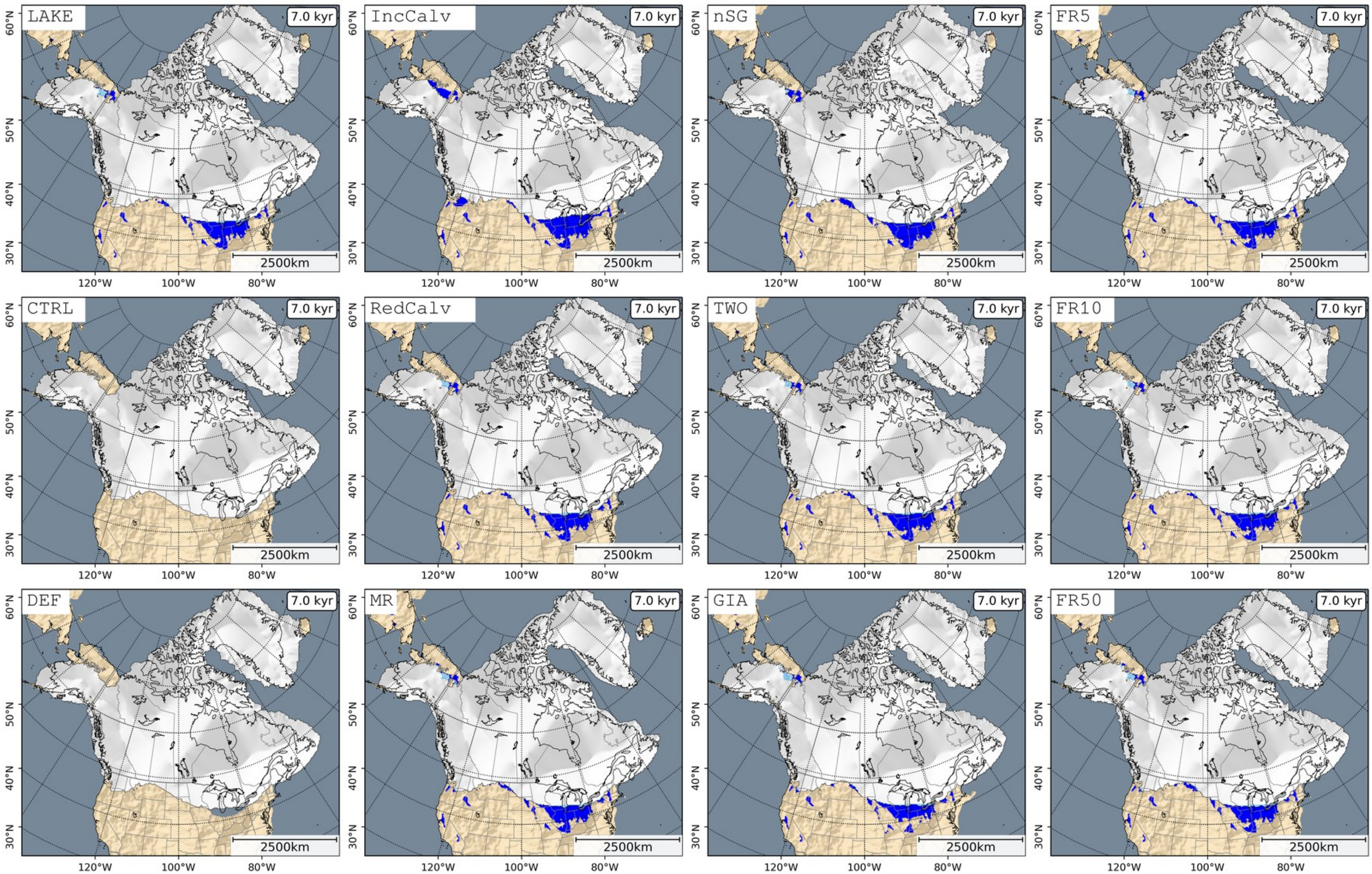

Figure S19: Overview map at 7000yr for the different experiments

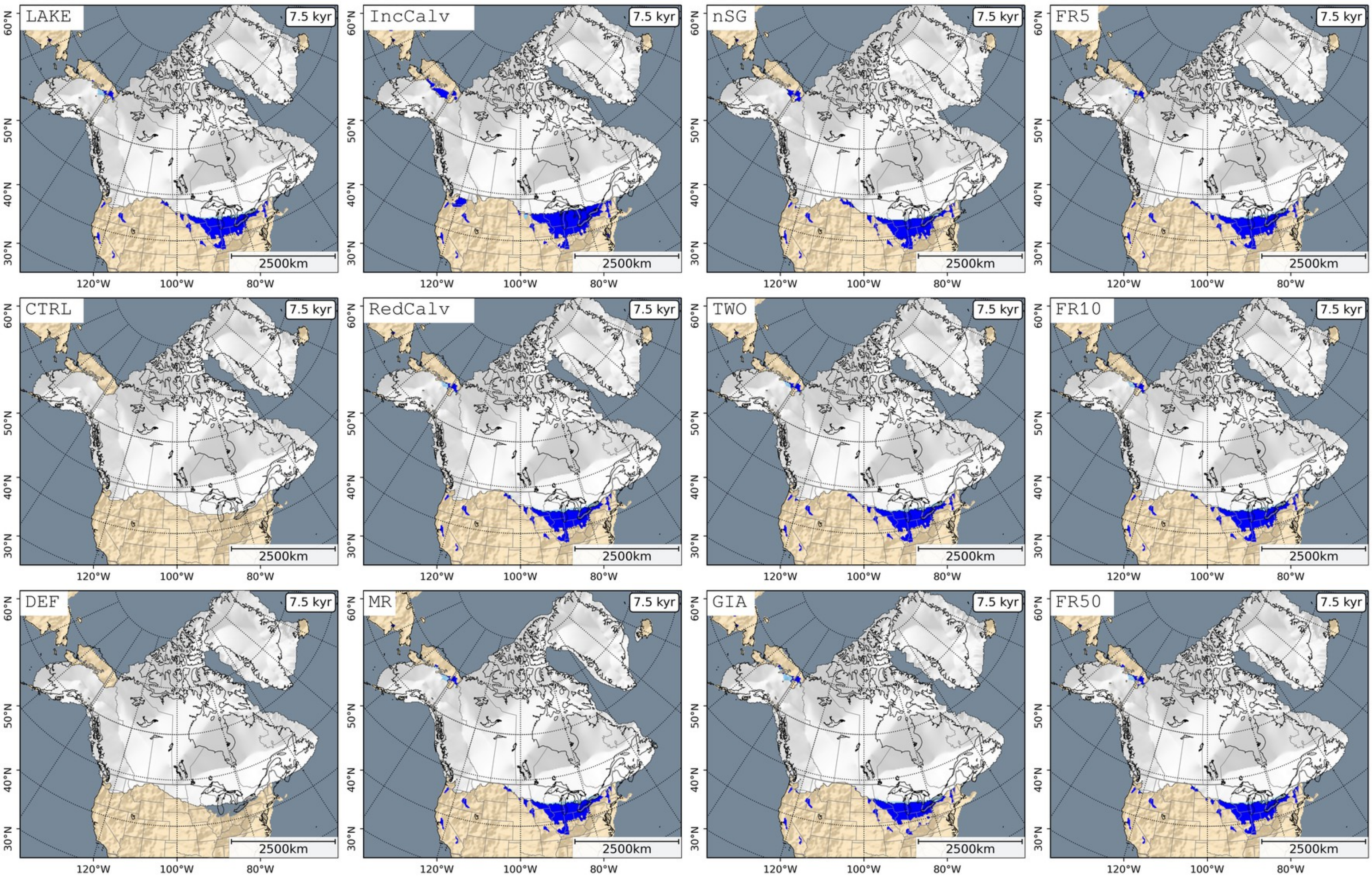

Figure S20: Overview map at 7500yr for the different experiments

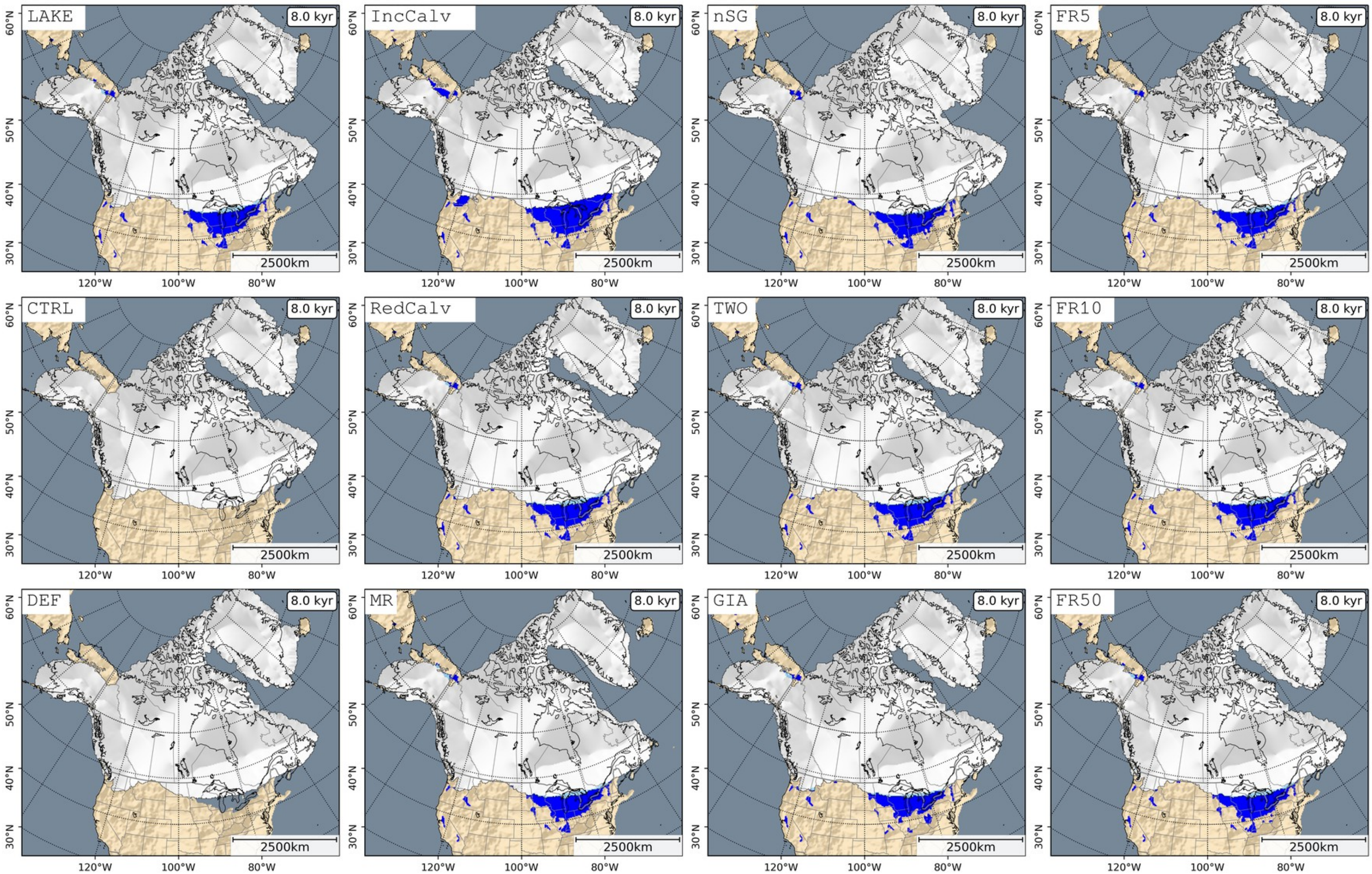

Figure S21: Overview map at 8000yr for the different experiments

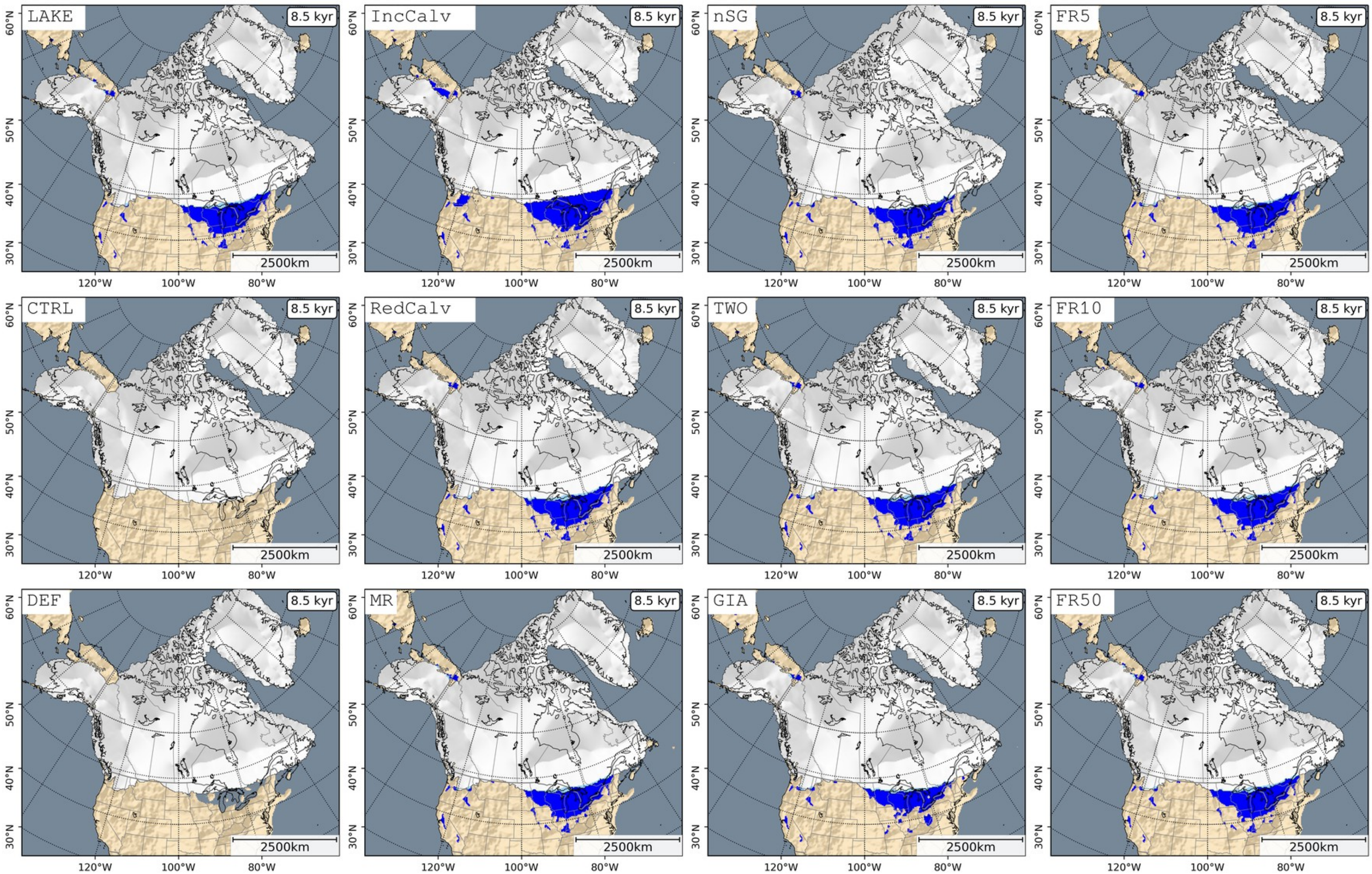

Figure S22: Overview map at 8500yr for the different experiments

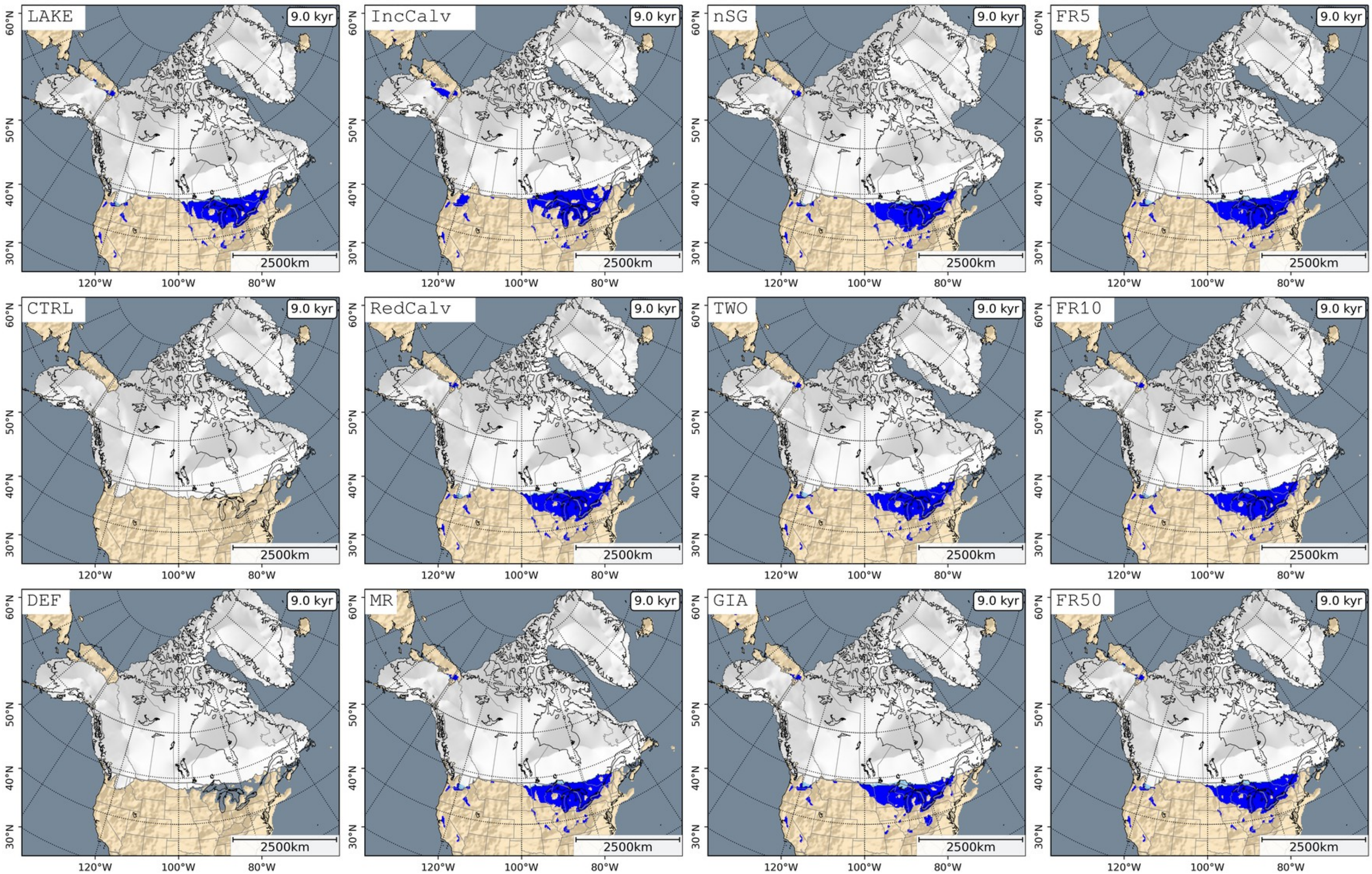

Figure S23: Overview map at 9000yr for the different experiments

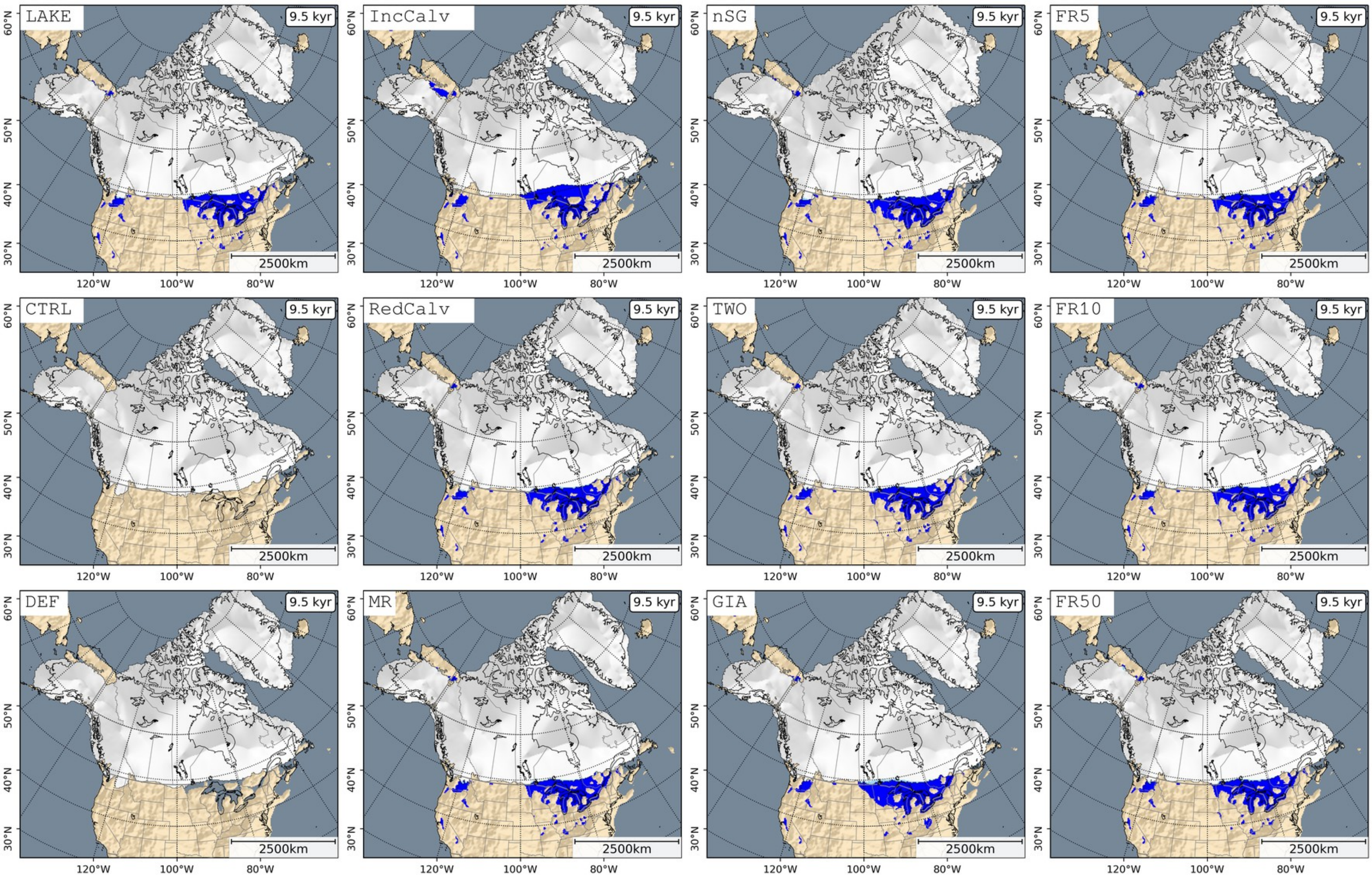

Figure S24: Overview map at 9500yr for the different experiments

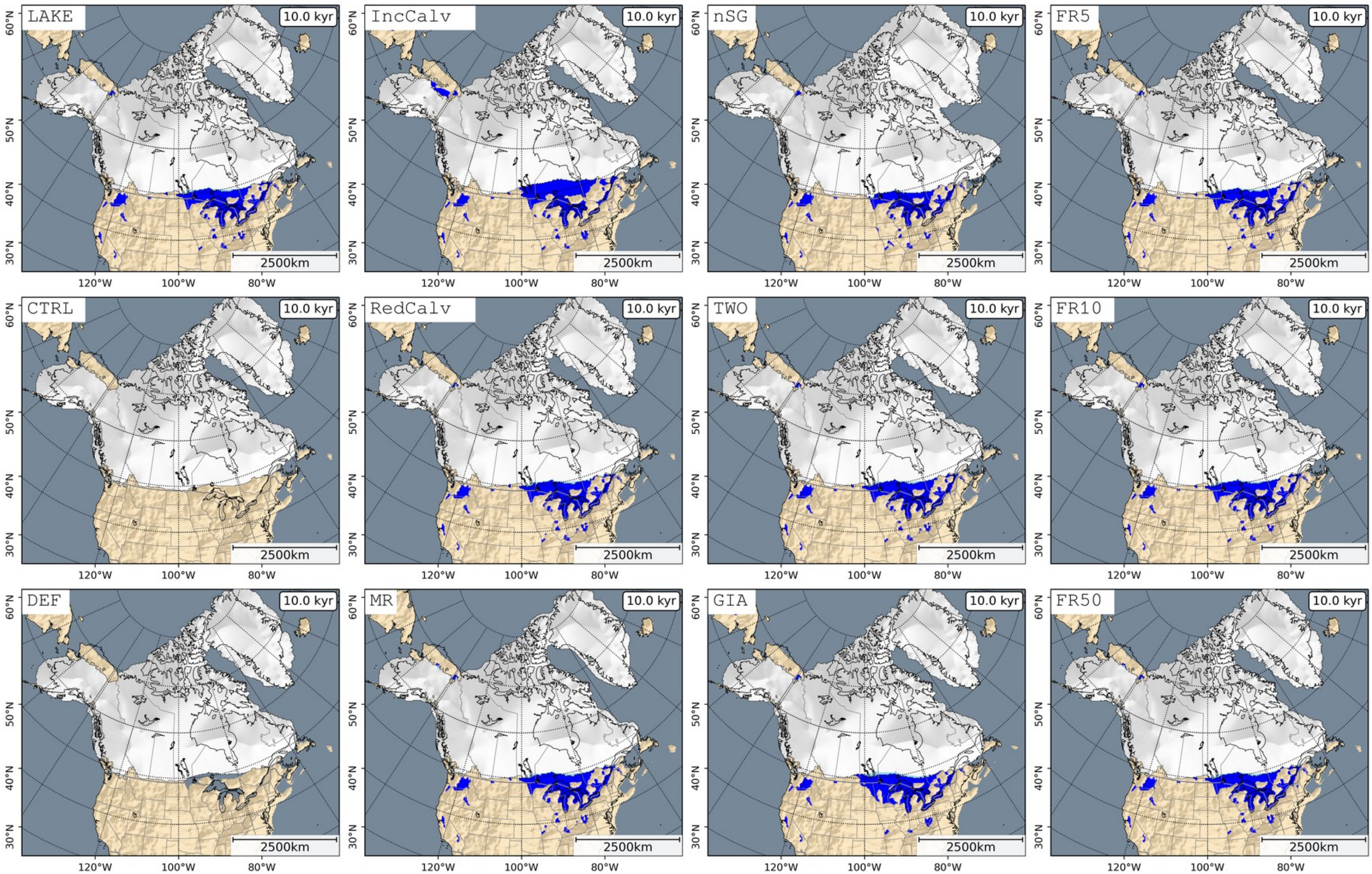

Figure S25: Overview map at 10000yr for the different experiments

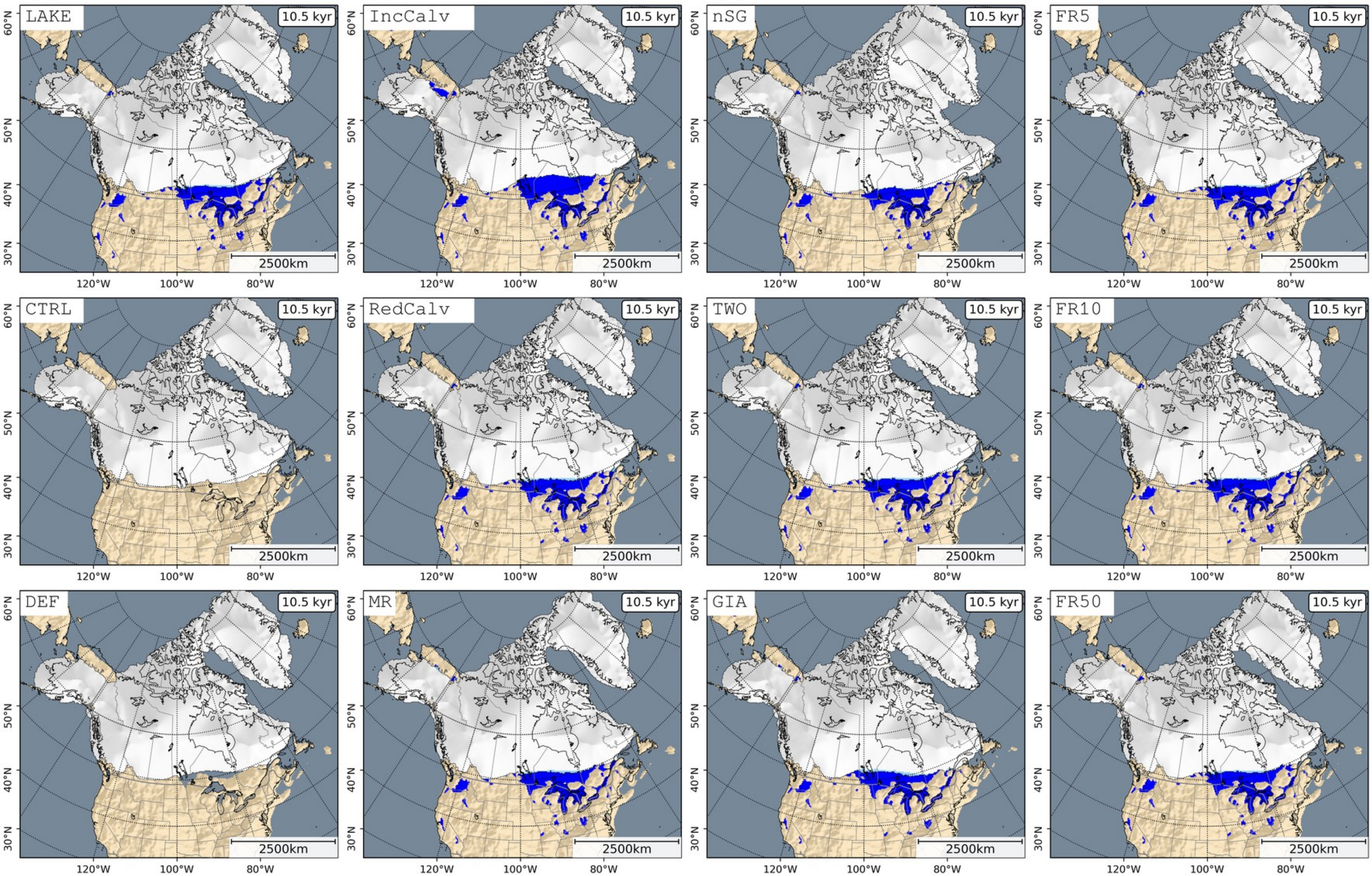

Figure S26: Overview map at 10500yr for the different experiments

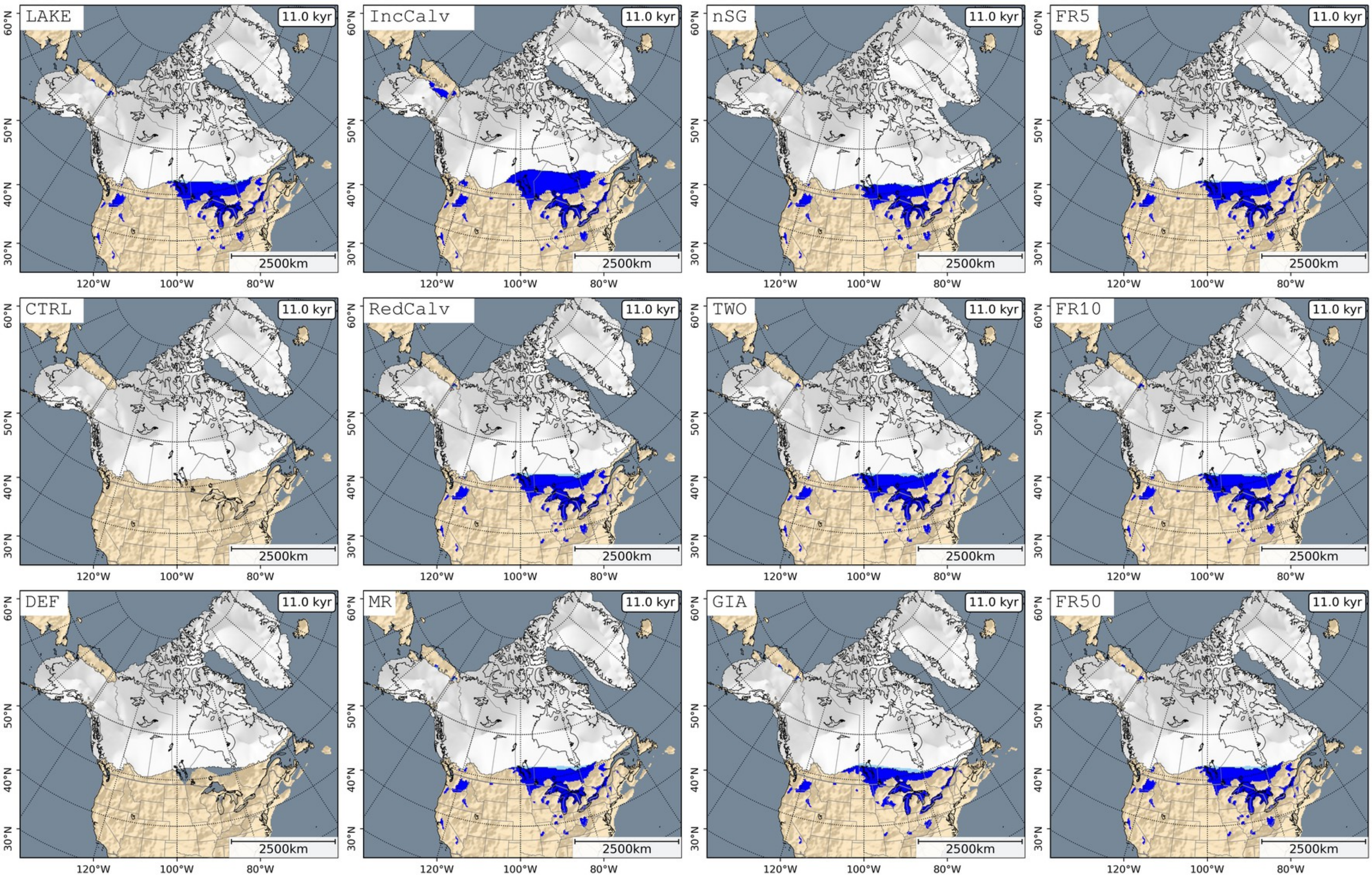

Figure S27: Overview map at 11000yr for the different experiments

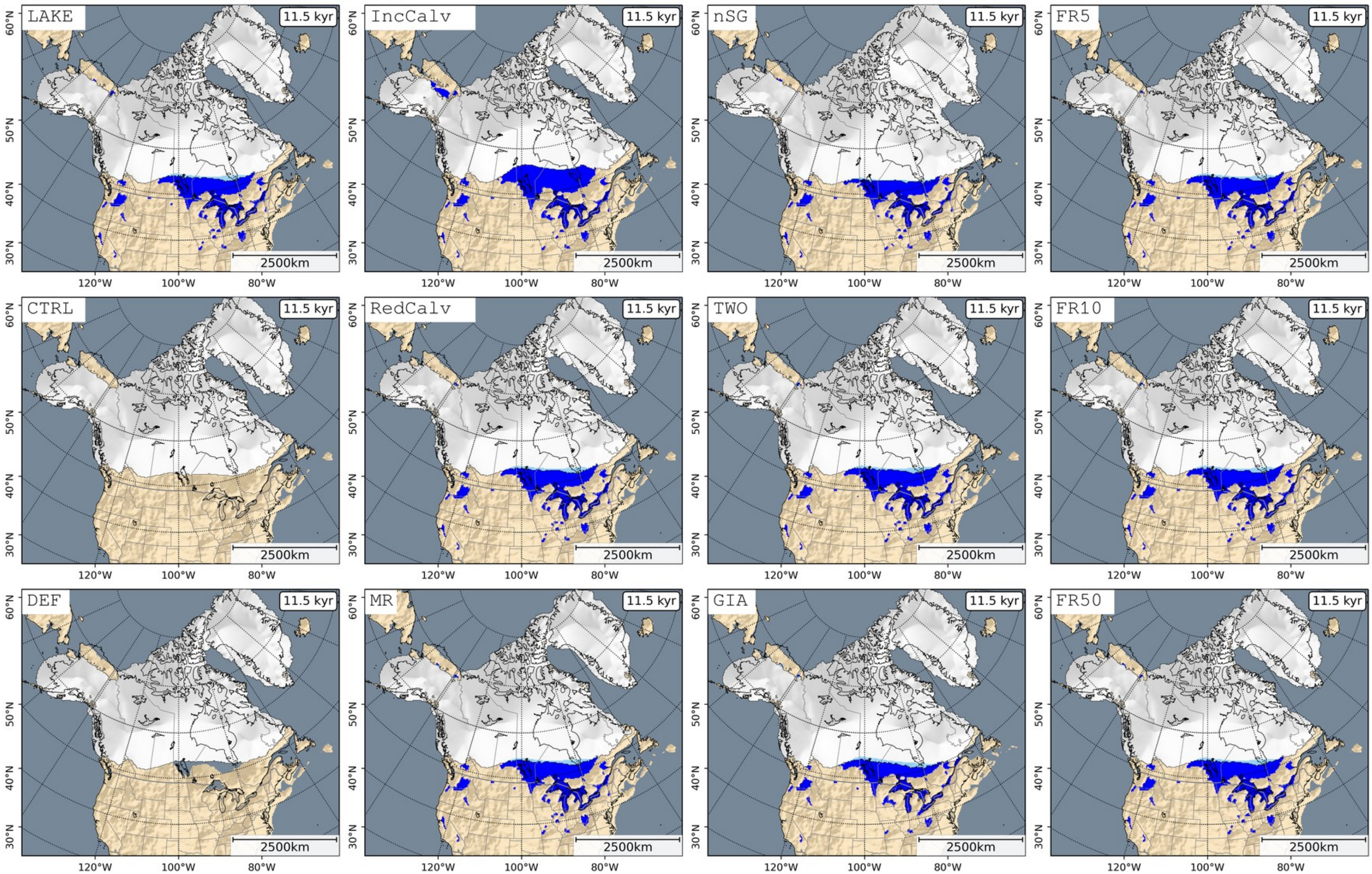

Figure S28: Overview map at 11500yr for the different experiments

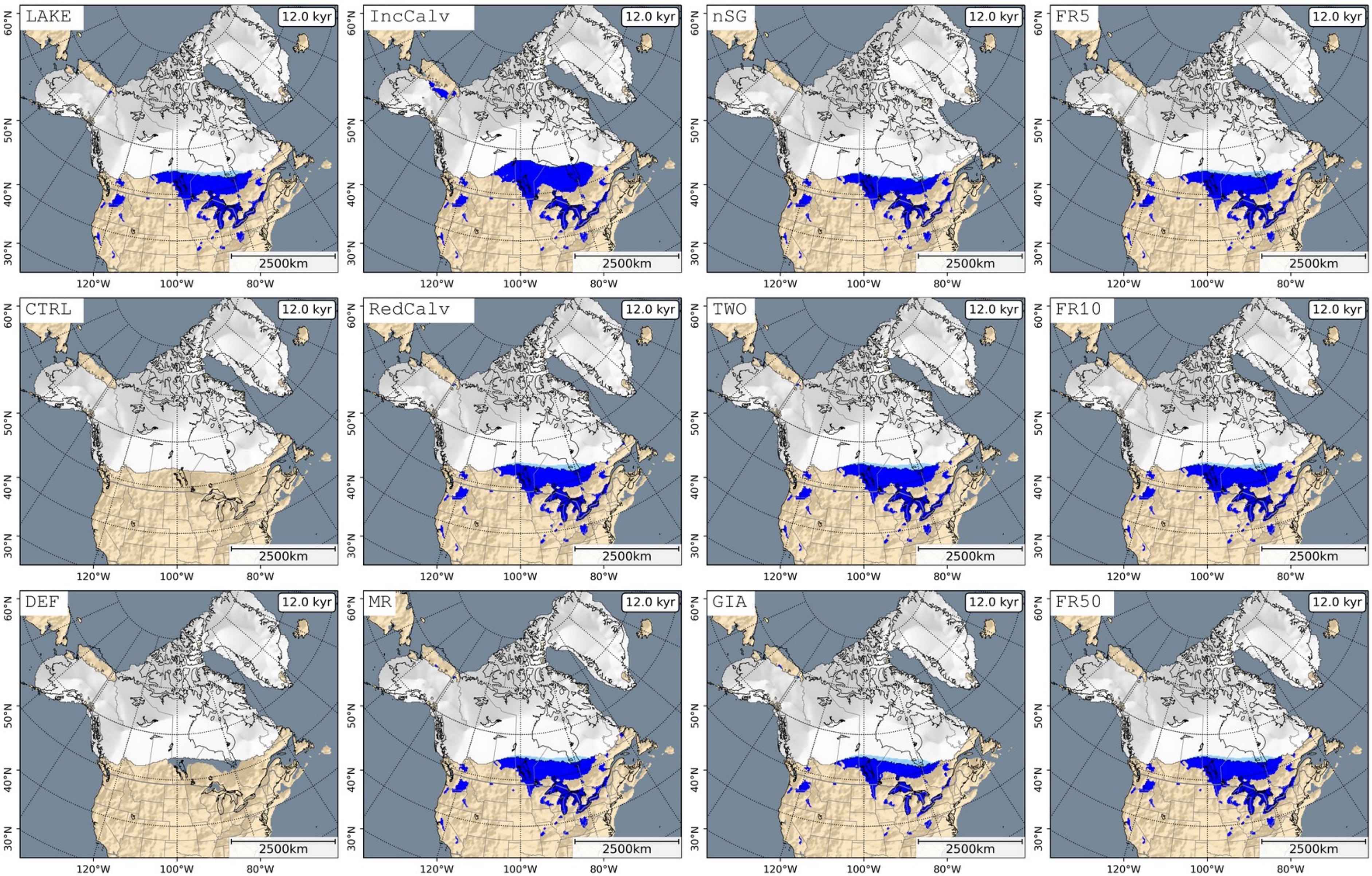

Figure S29: Overview map at 12000yr for the different experiments

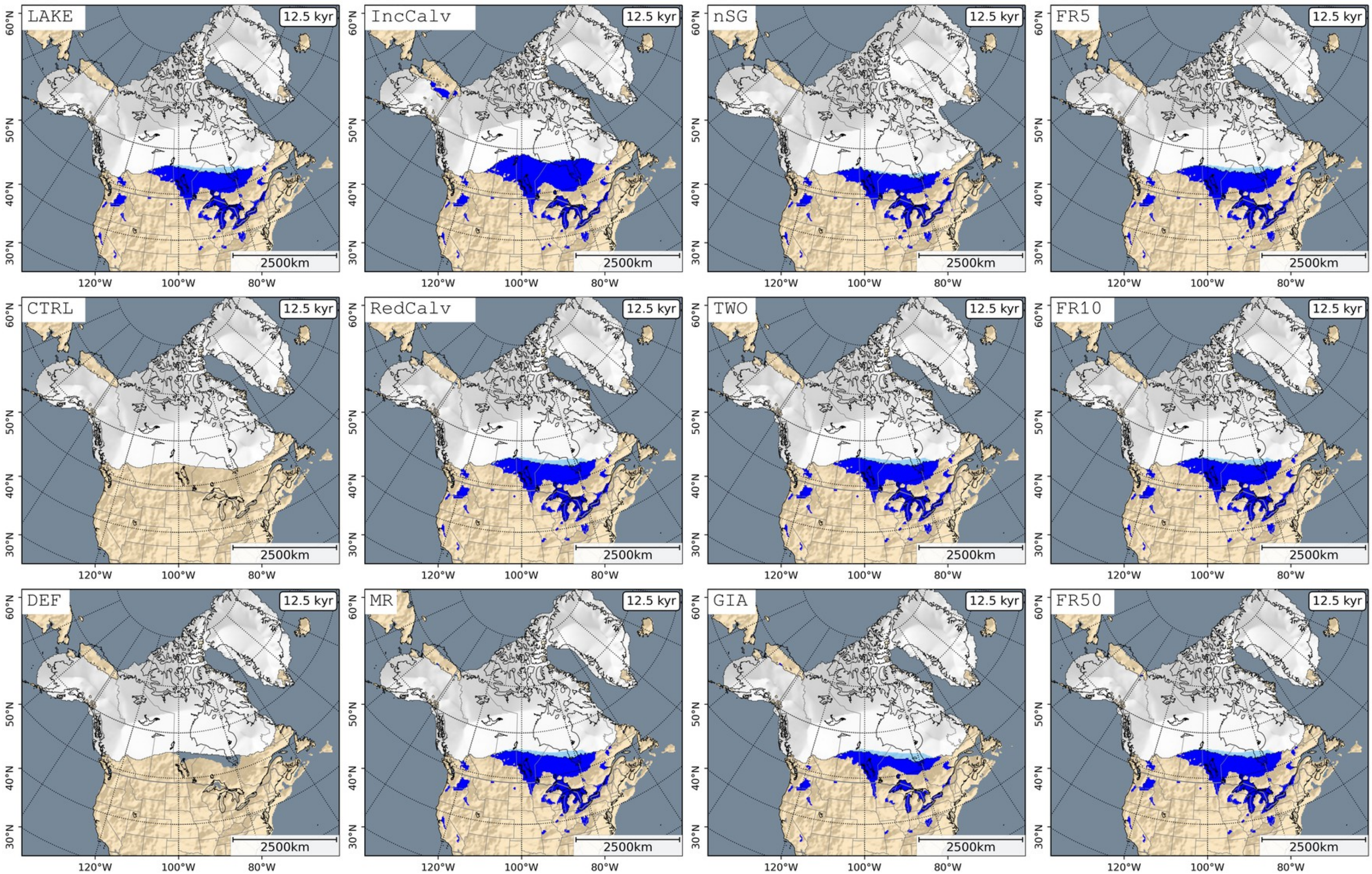

Figure S30: Overview map at 12500yr for the different experiments

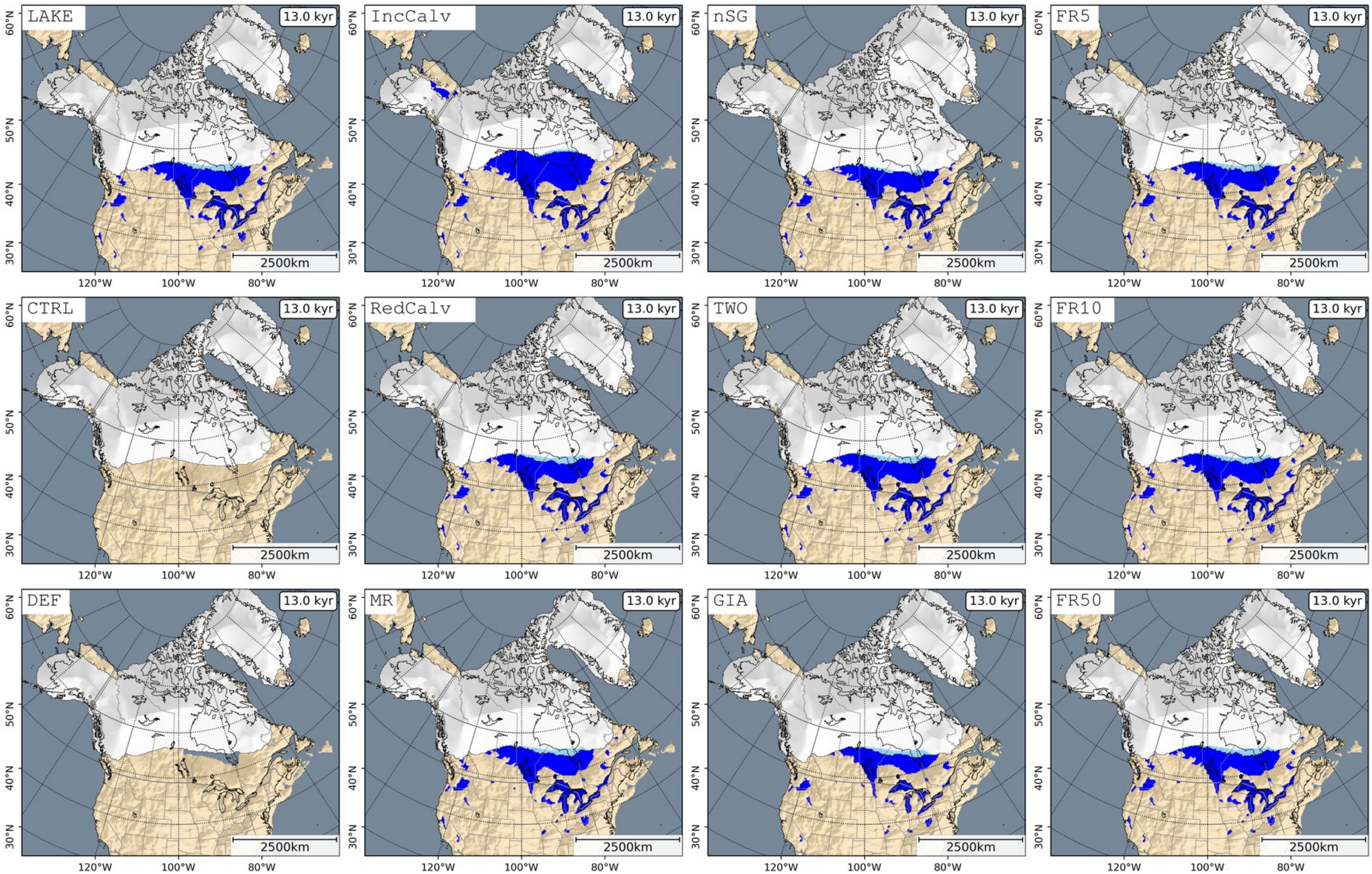

Figure S31: Overview map at 13000yr for the different experiments

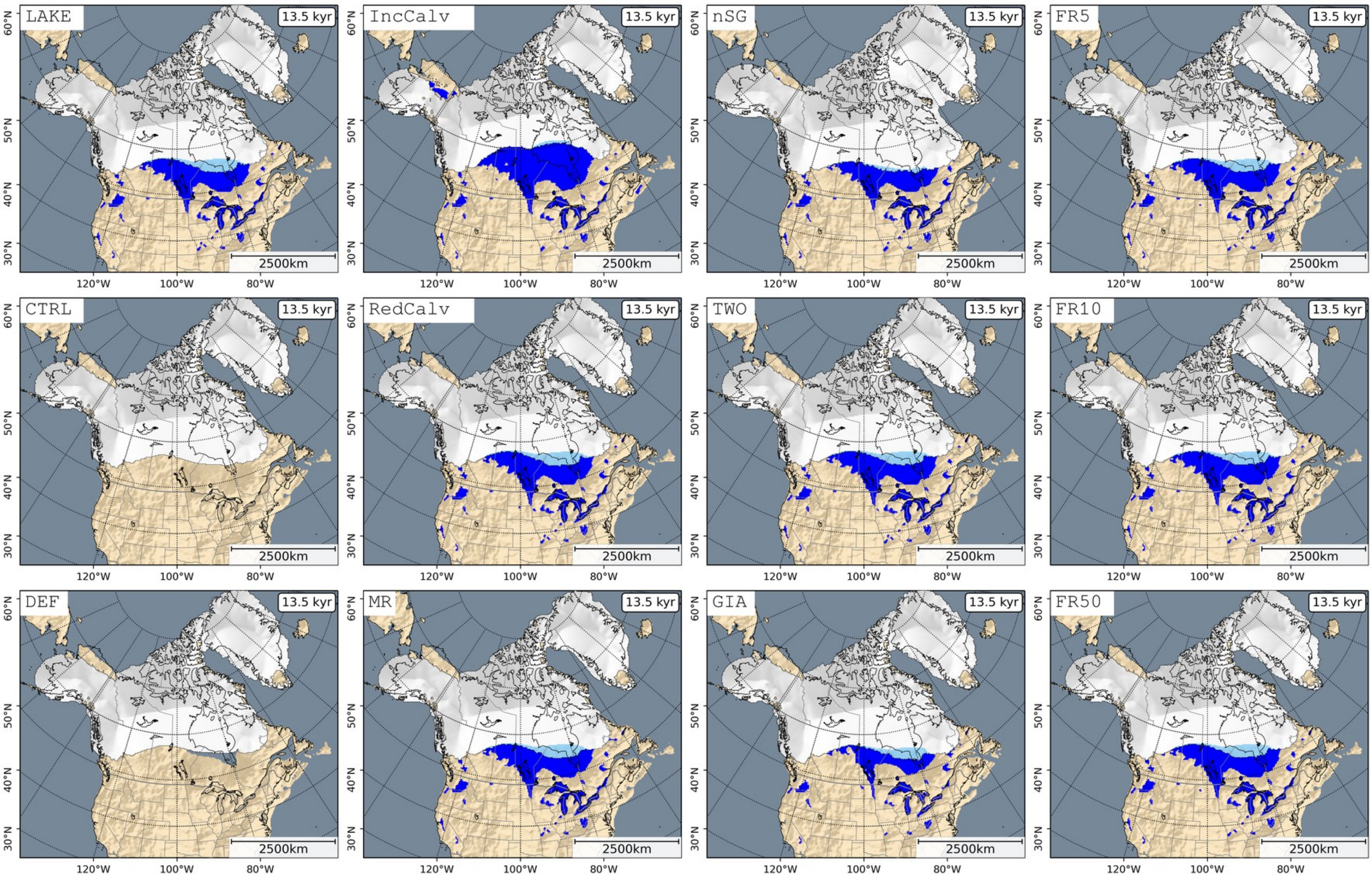

Figure S32: Overview map at 13500yr for the different experiments

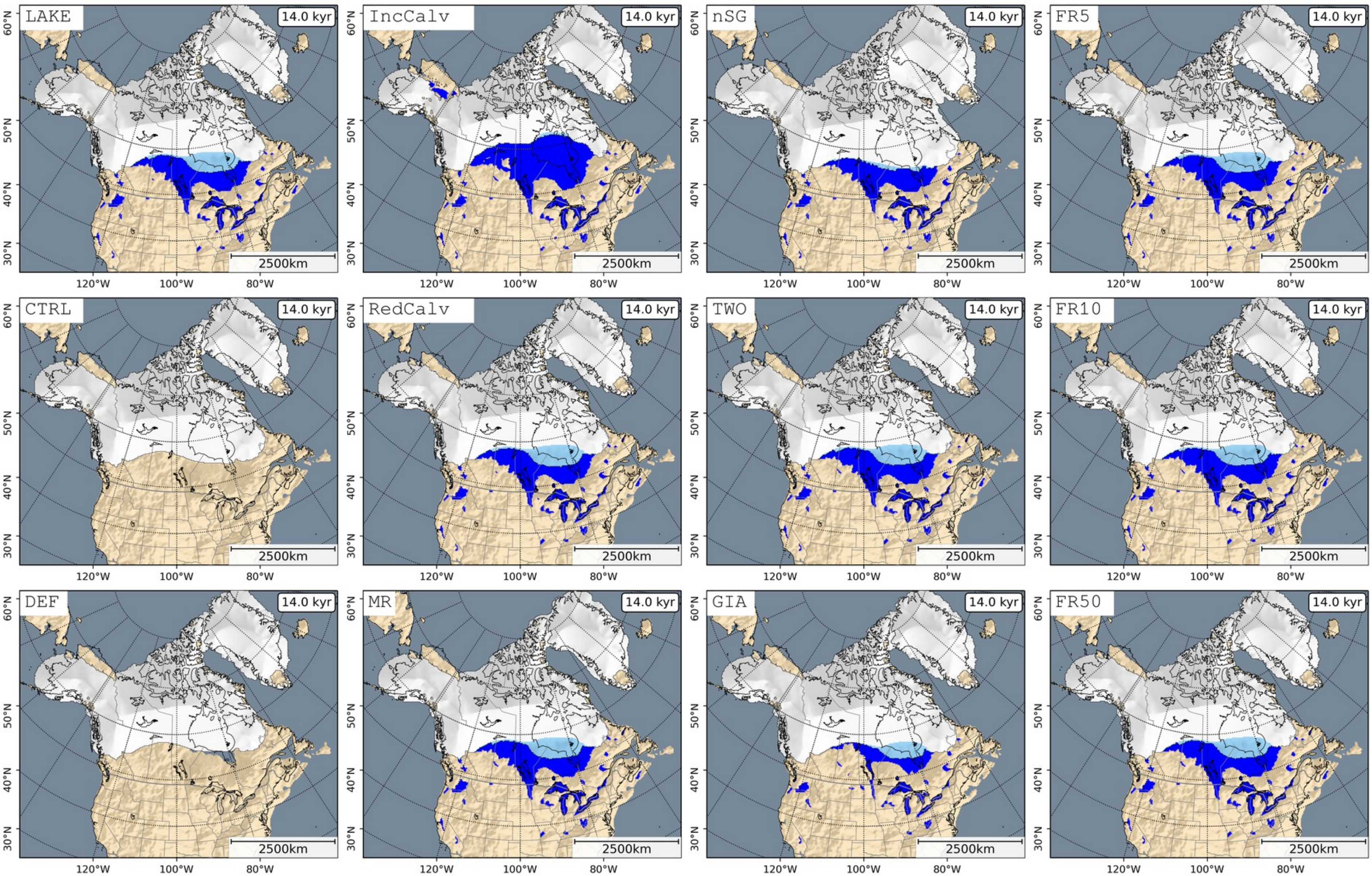

Figure S33: Overview map at 14000yr for the different experiments

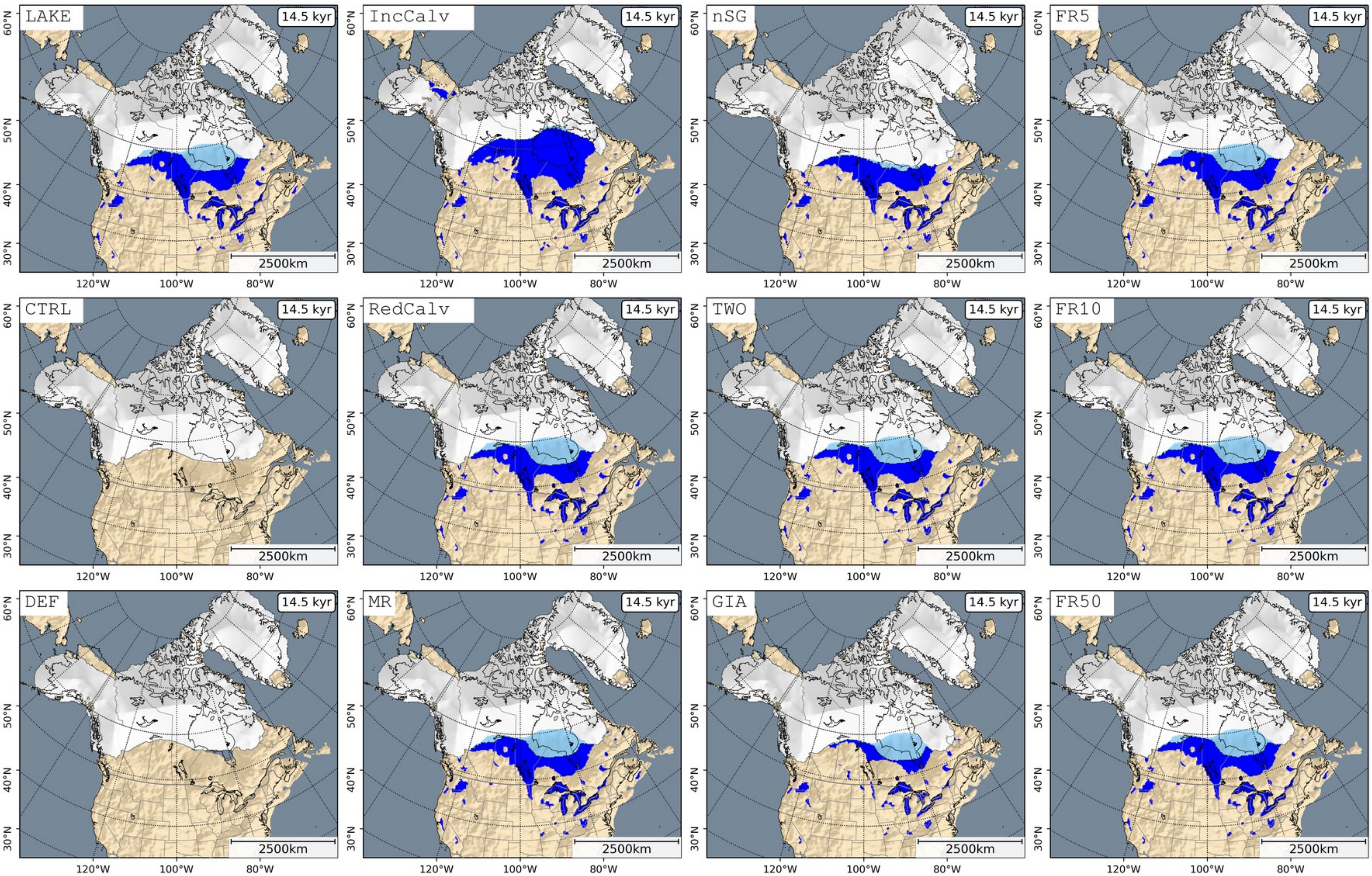

Figure S34: Overview map at 14500yr for the different experiments

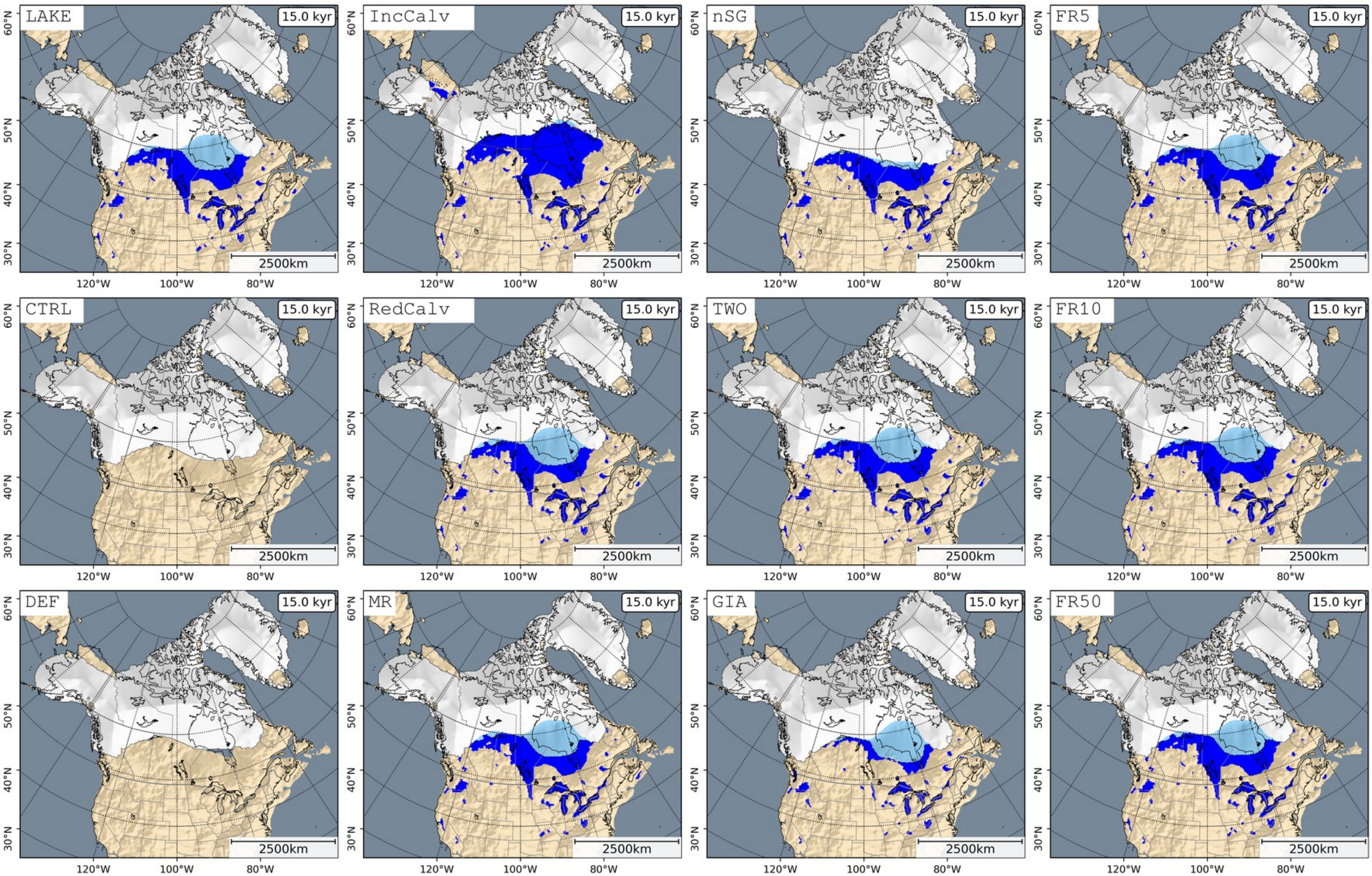

Figure S35: Overview map at 15000yr for the different experiments

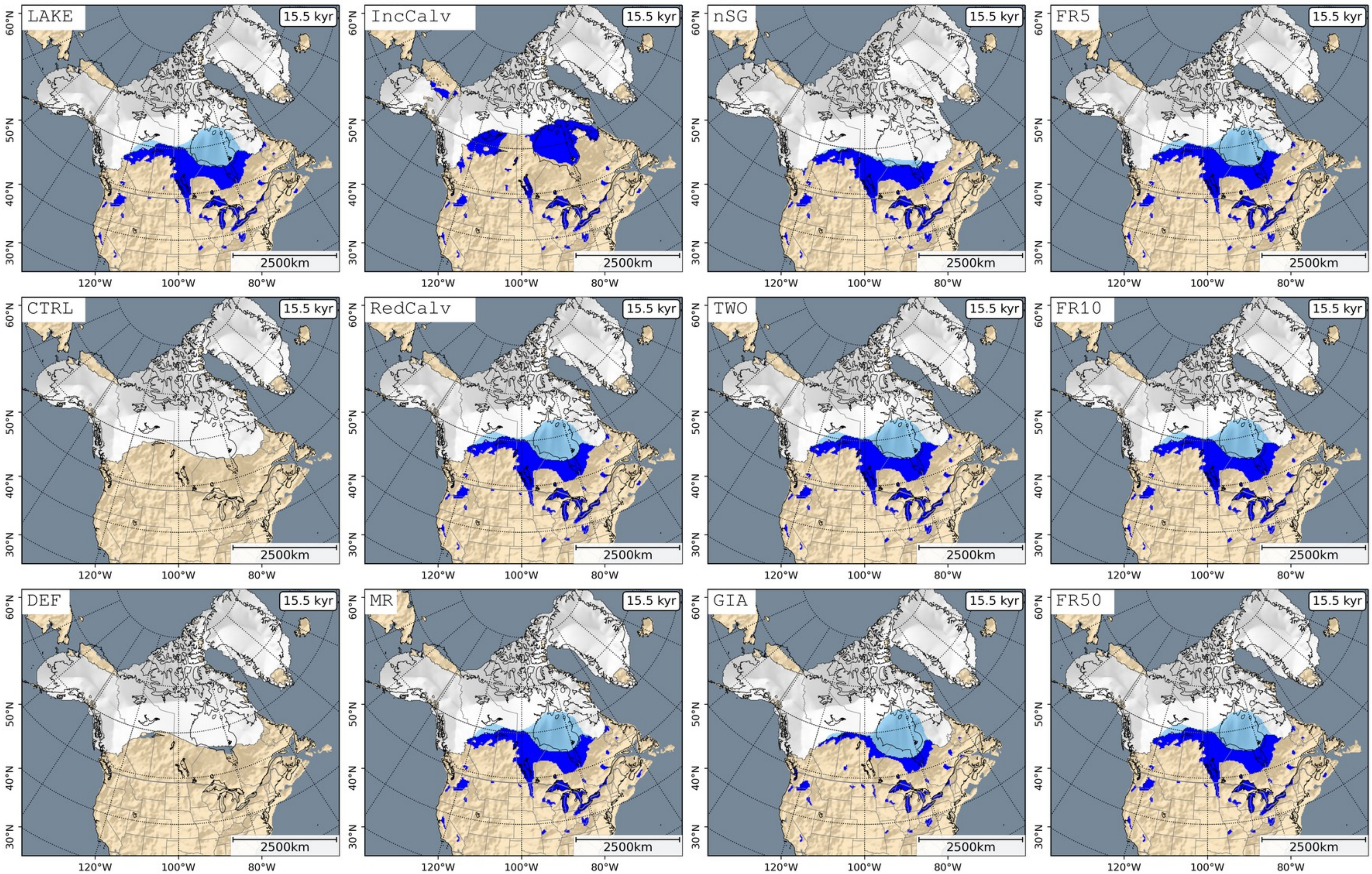

Figure S36: Overview map at 15500yr for the different experiments

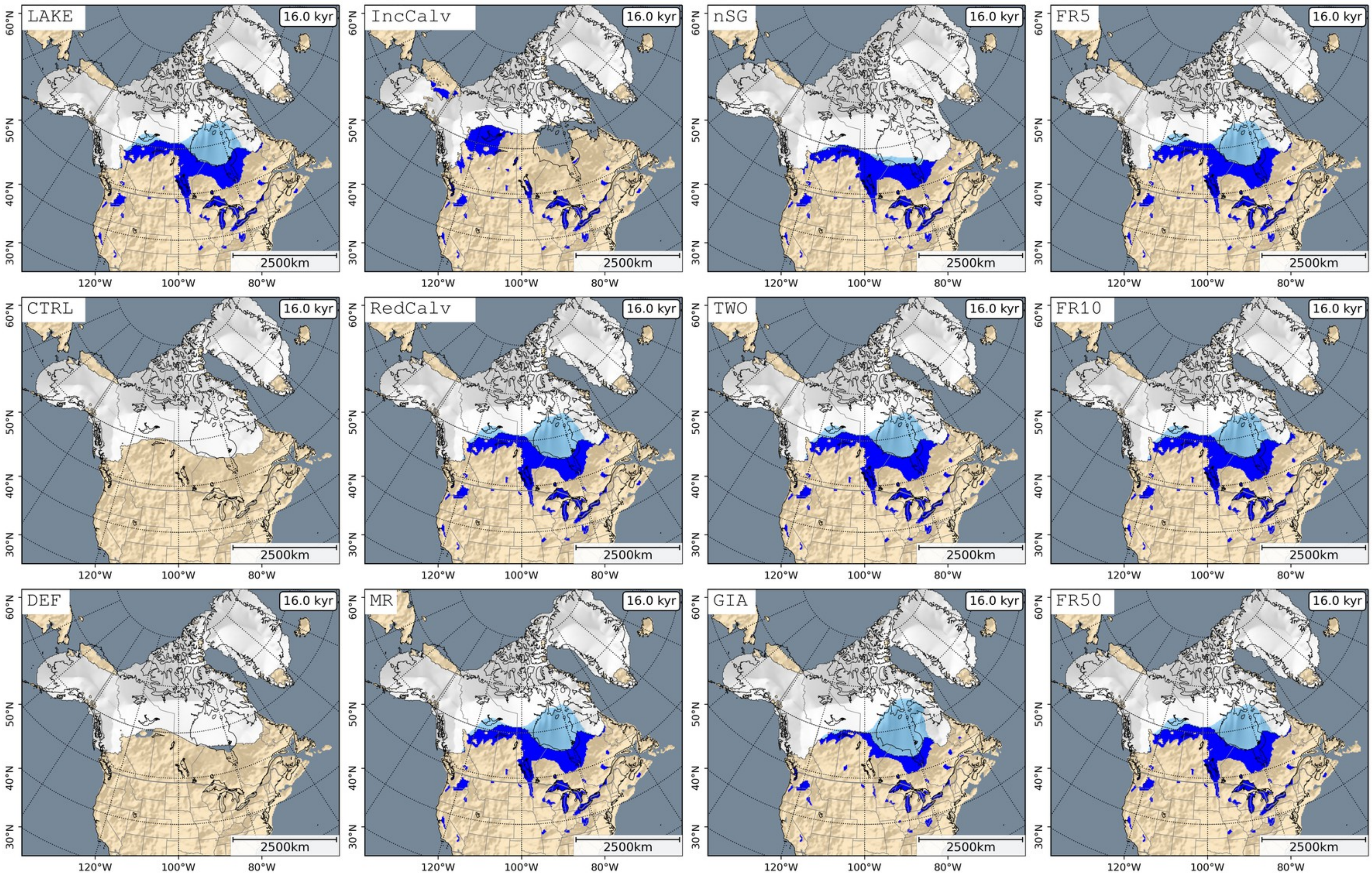

Figure S37: Overview map at 16000yr for the different experiments

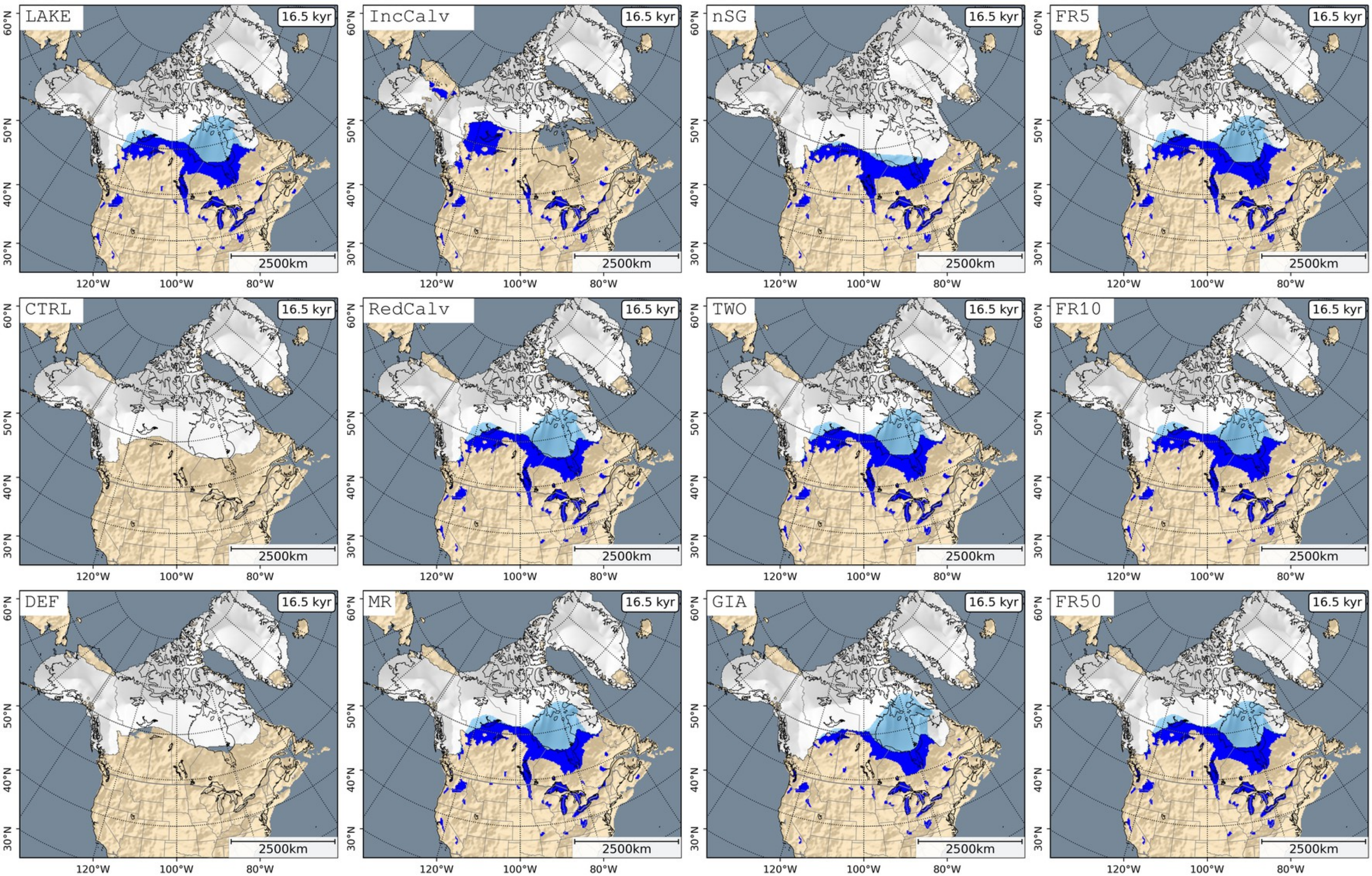

Figure S38: Overview map at 16500yr for the different experiments

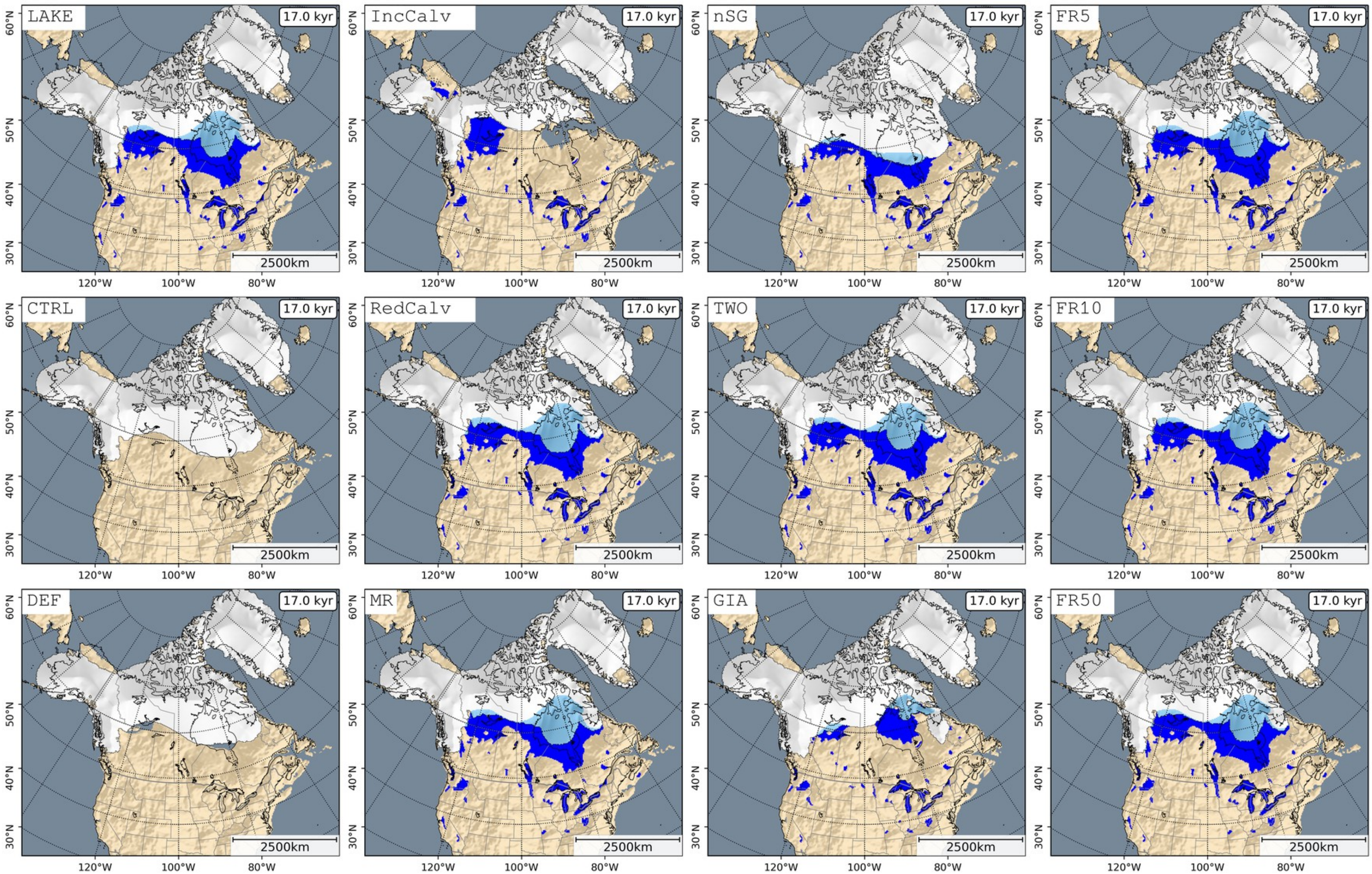

Figure S39: Overview map at 17000yr for the different experiments

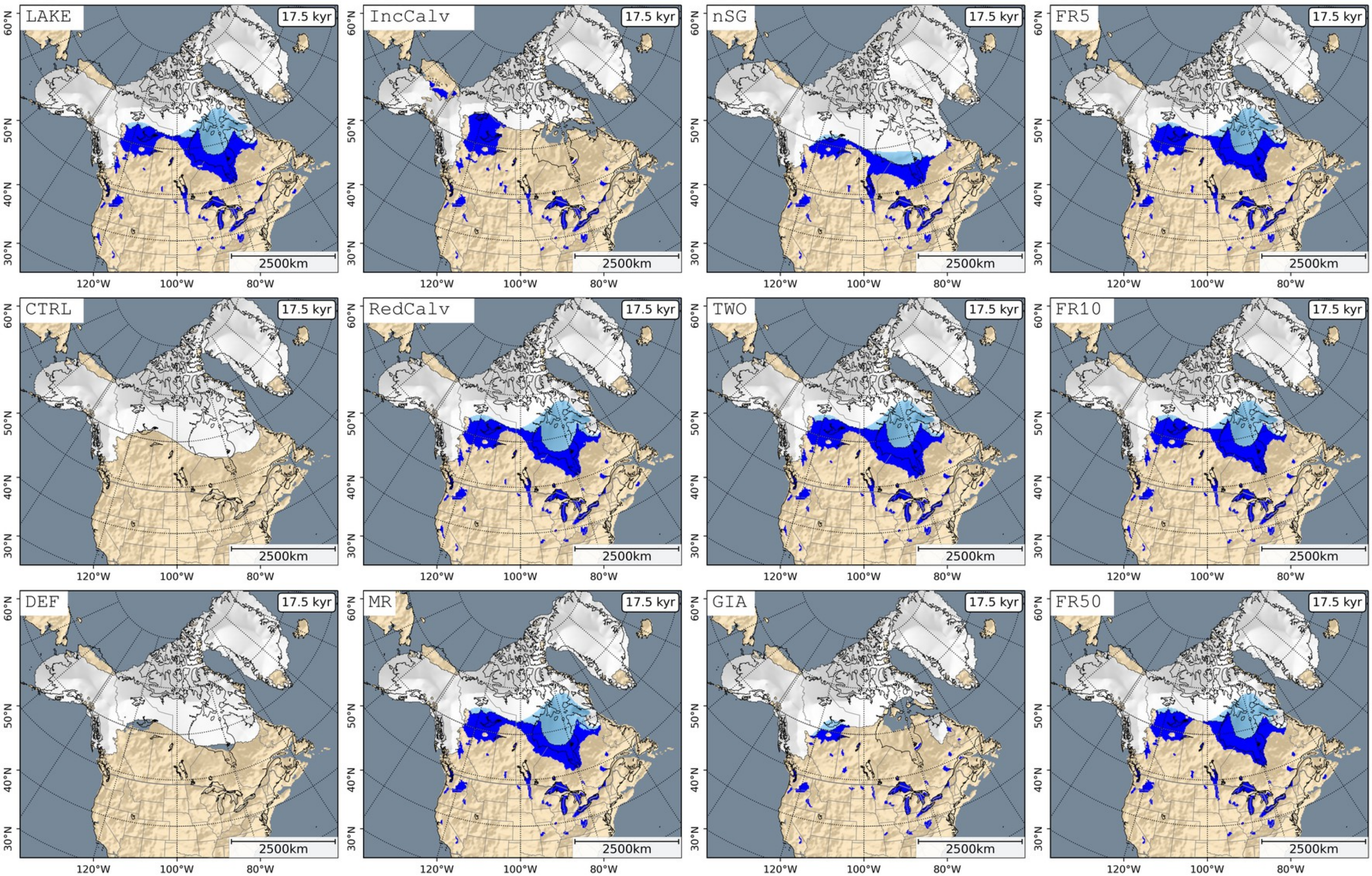

Figure S40: Overview map at 17500yr for the different experiments

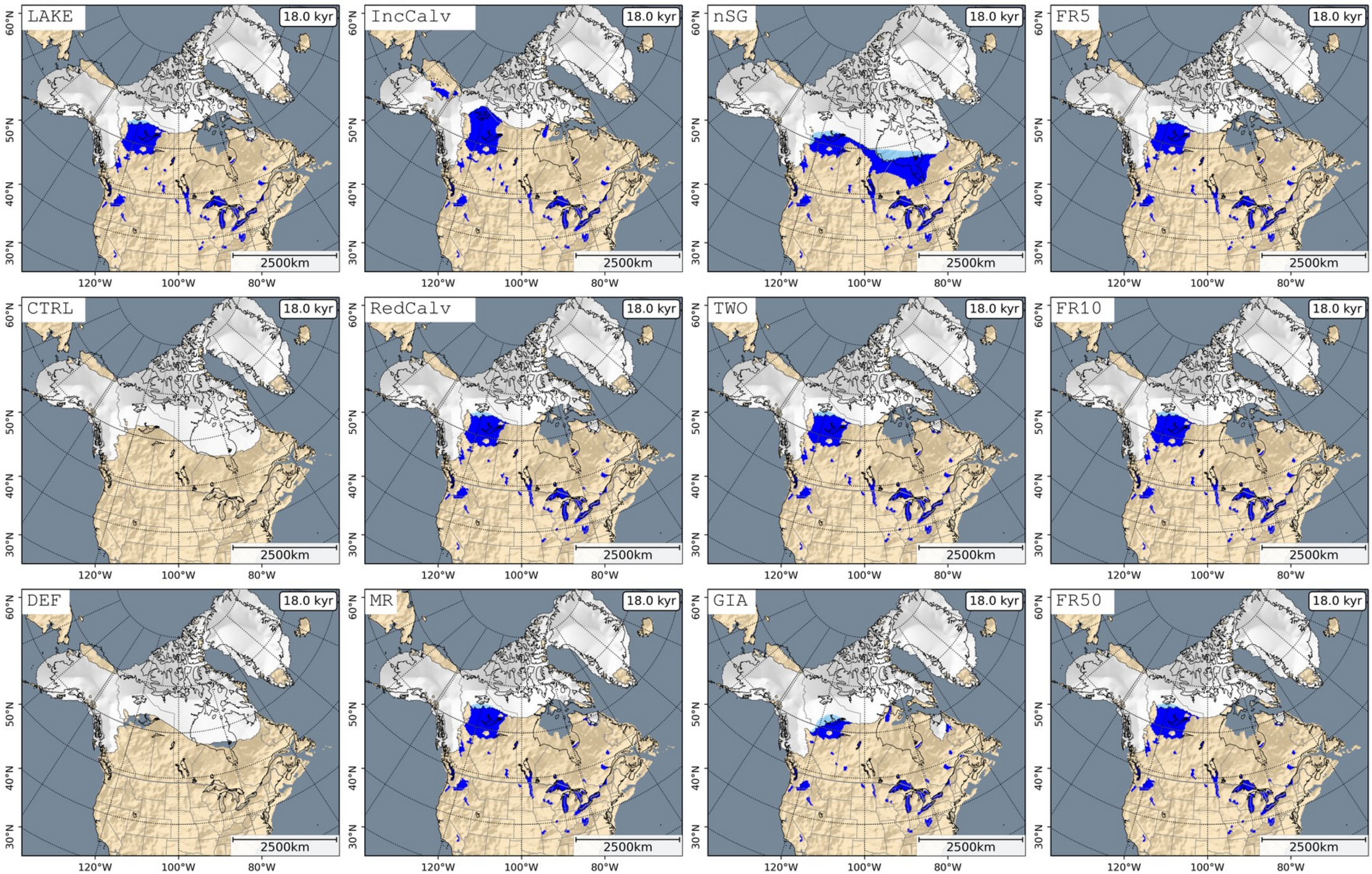

Figure S41: Overview map at 18000yr for the different experiments

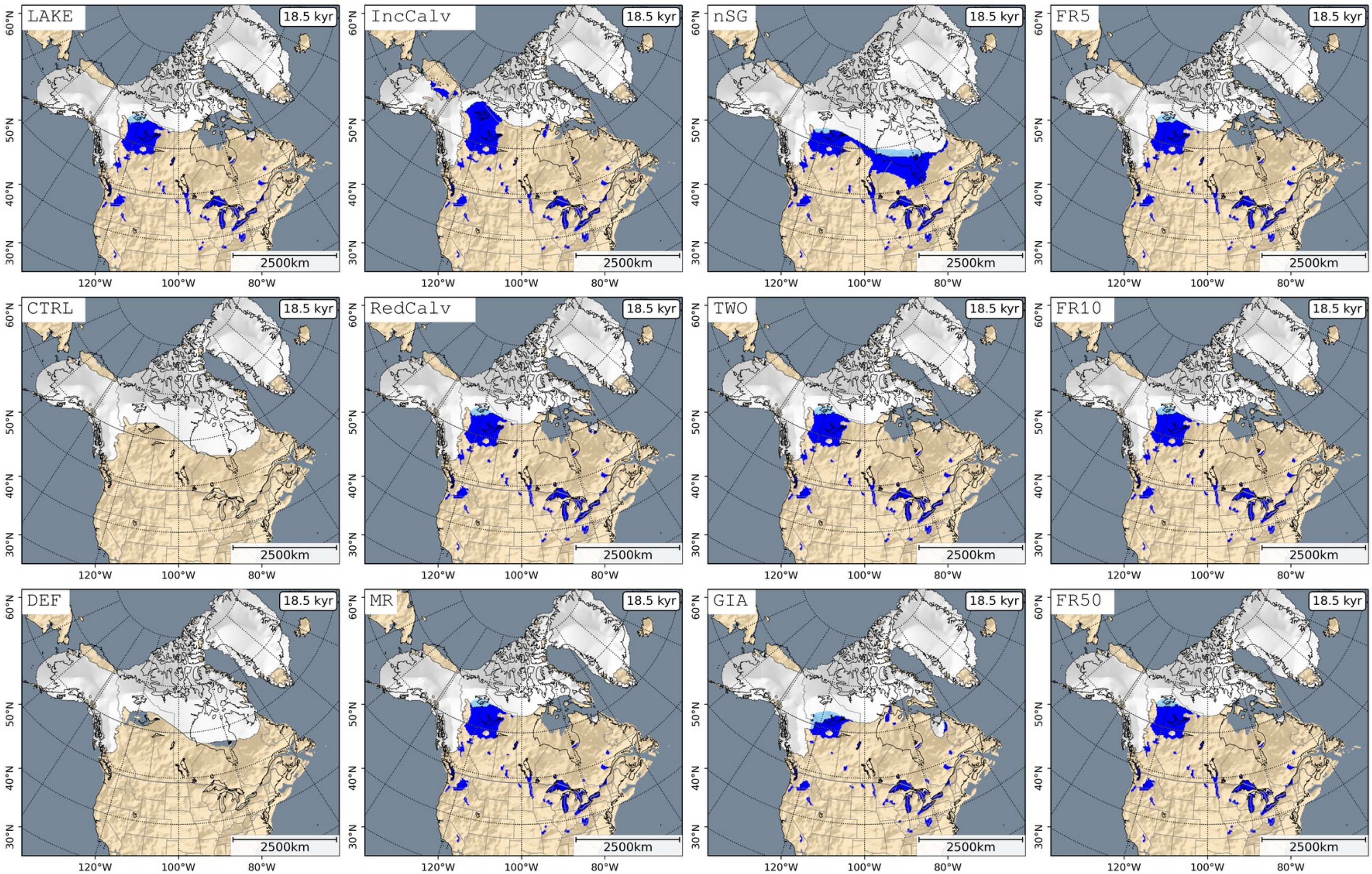

Figure S42: Overview map at 18500yr for the different experiments

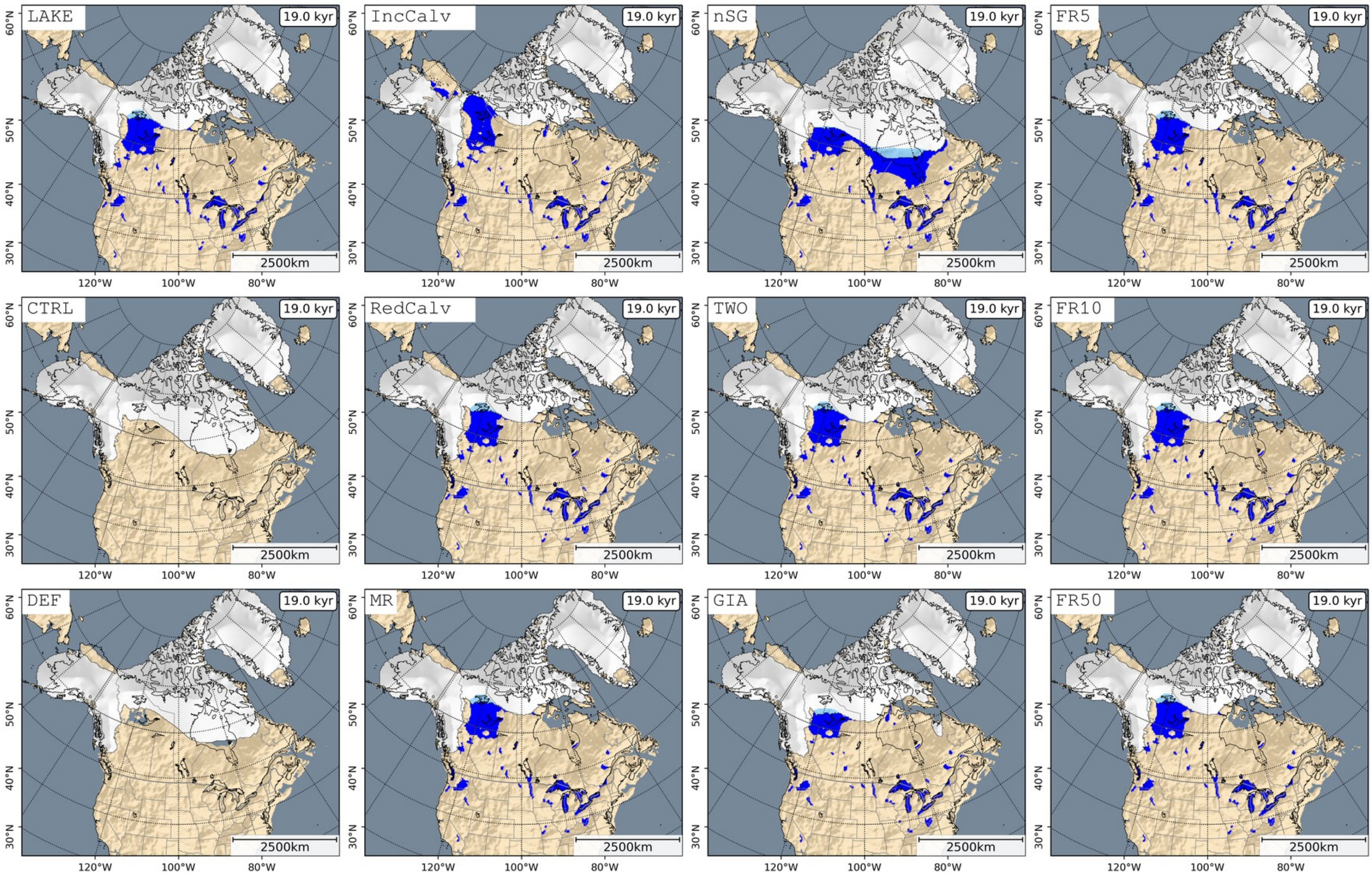

Figure S43: Overview map at 19000yr for the different experiments

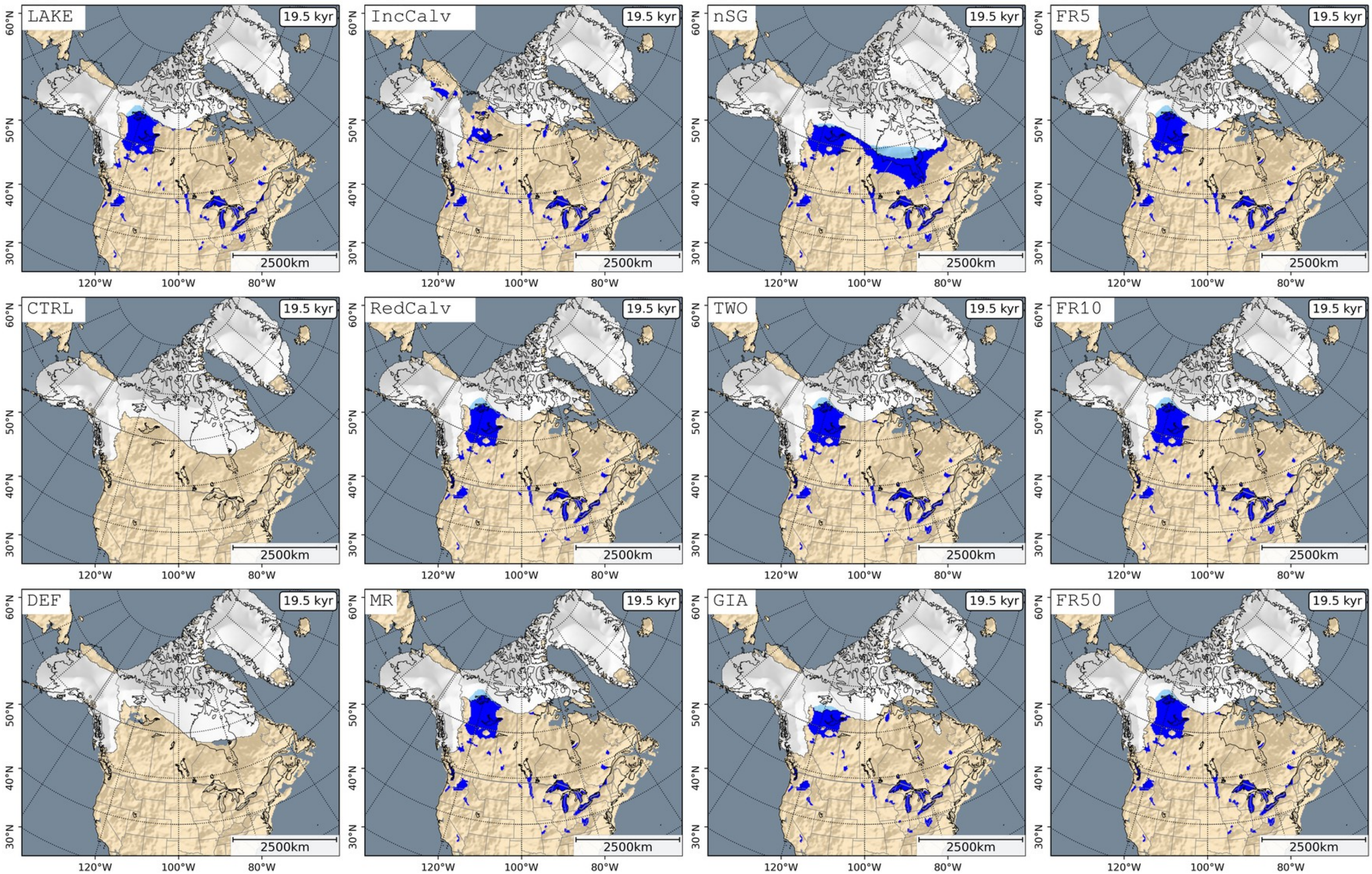

Figure S44: Overview map at 19500yr for the different experiments

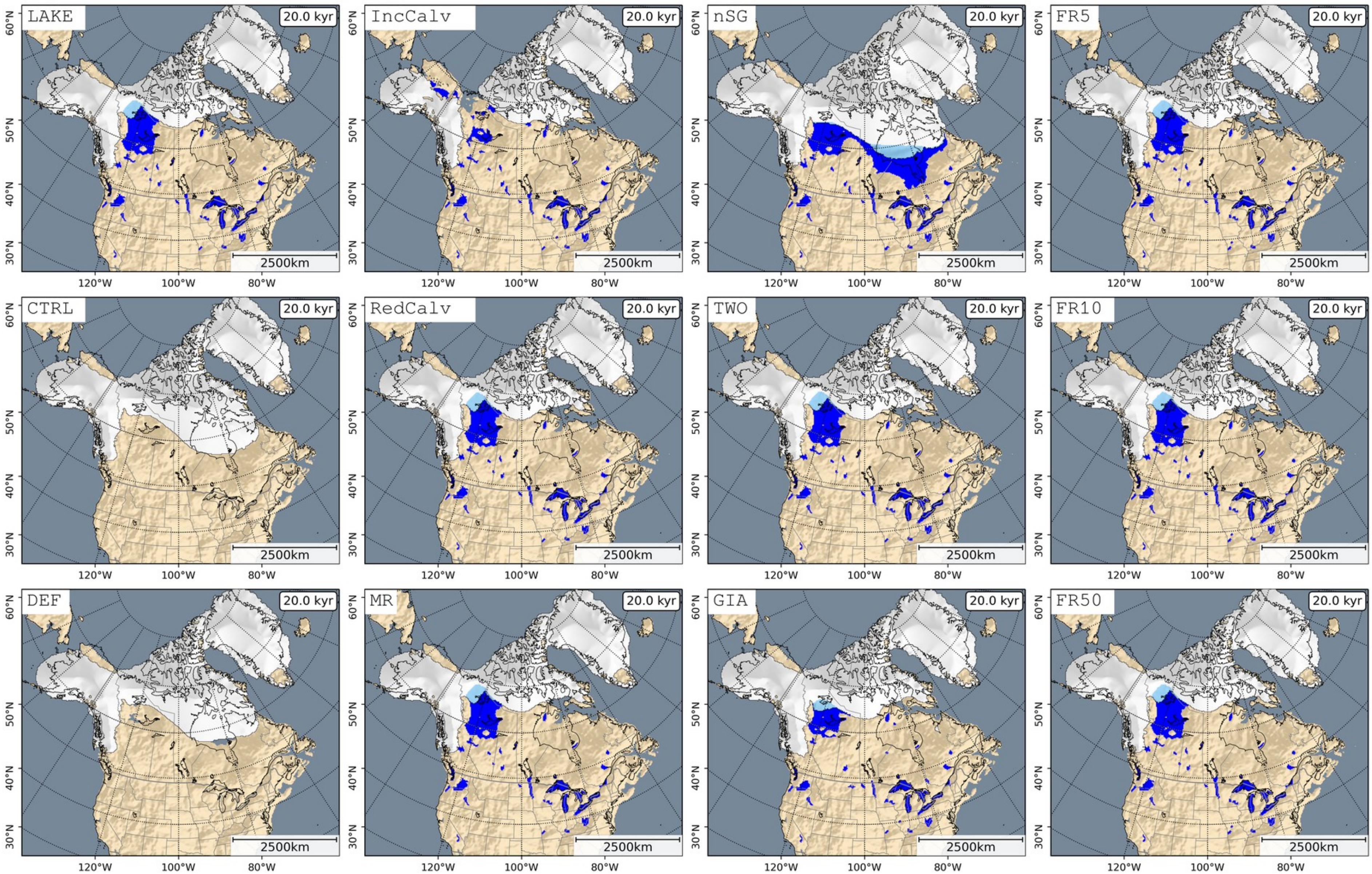

Figure S45: Overview map at 20000yr for the different experiments

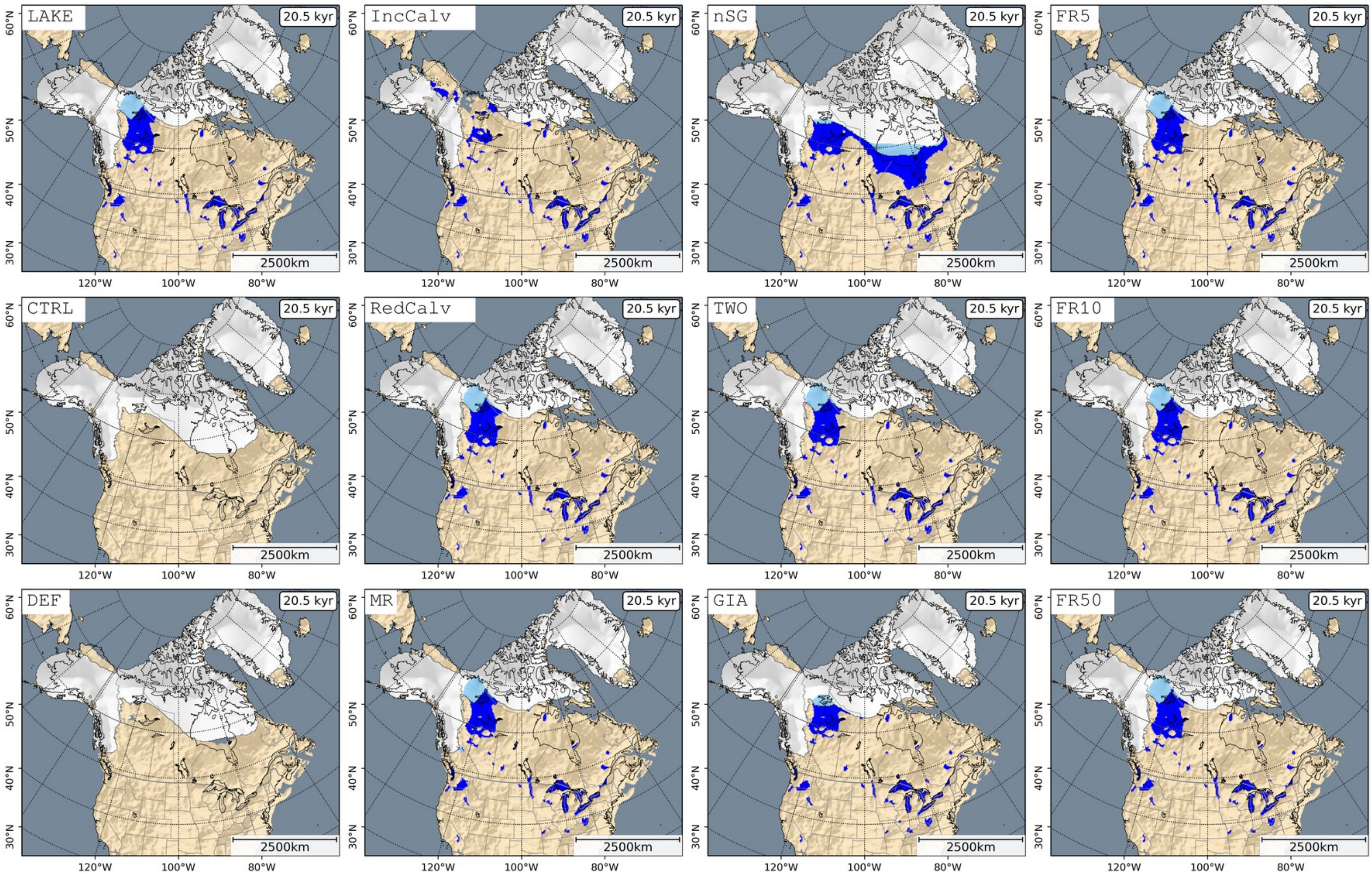

Figure S46: Overview map at 20500yr for the different experiments

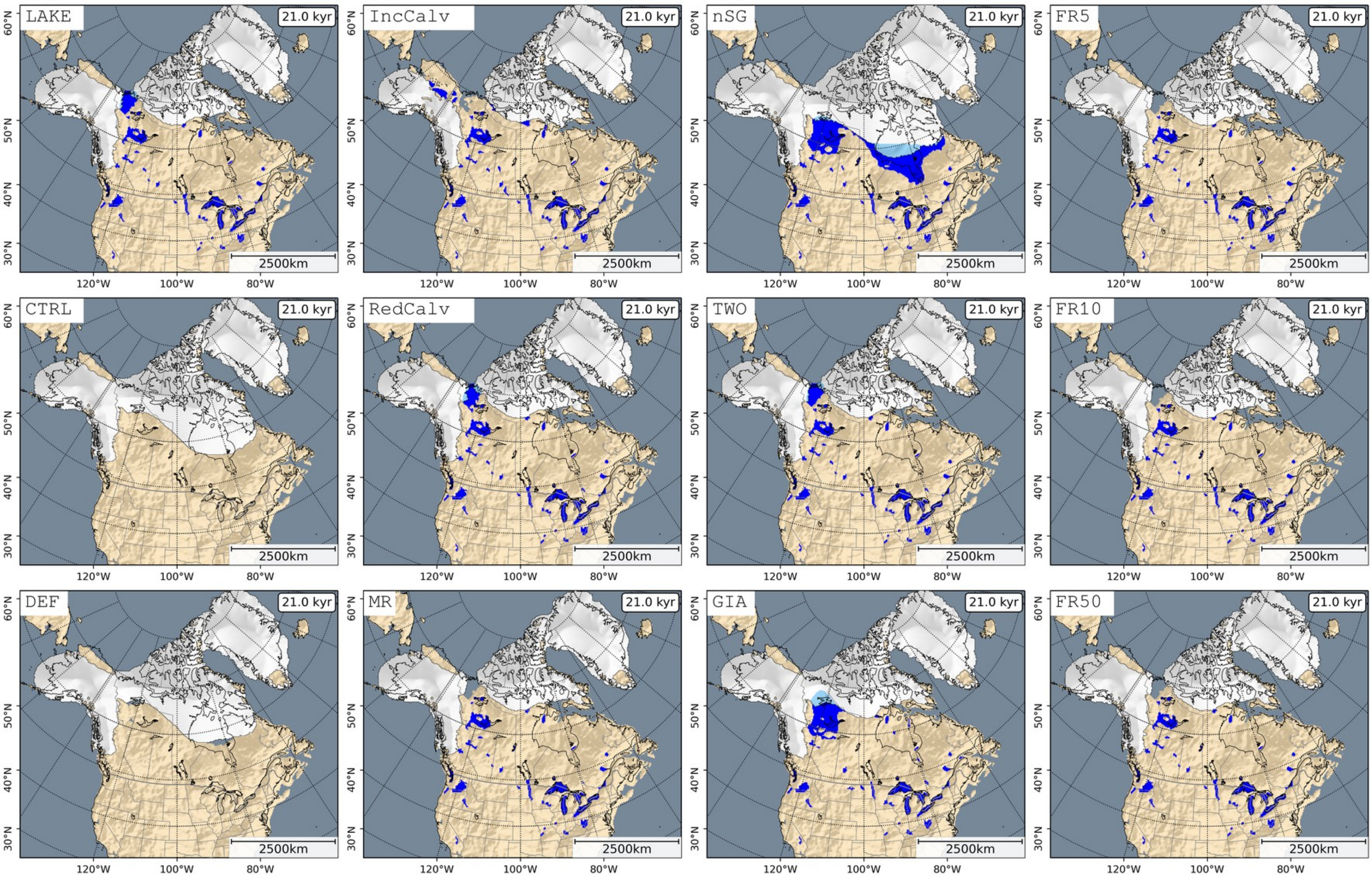

Figure S47: Overview map at 21000yr for the different experiments

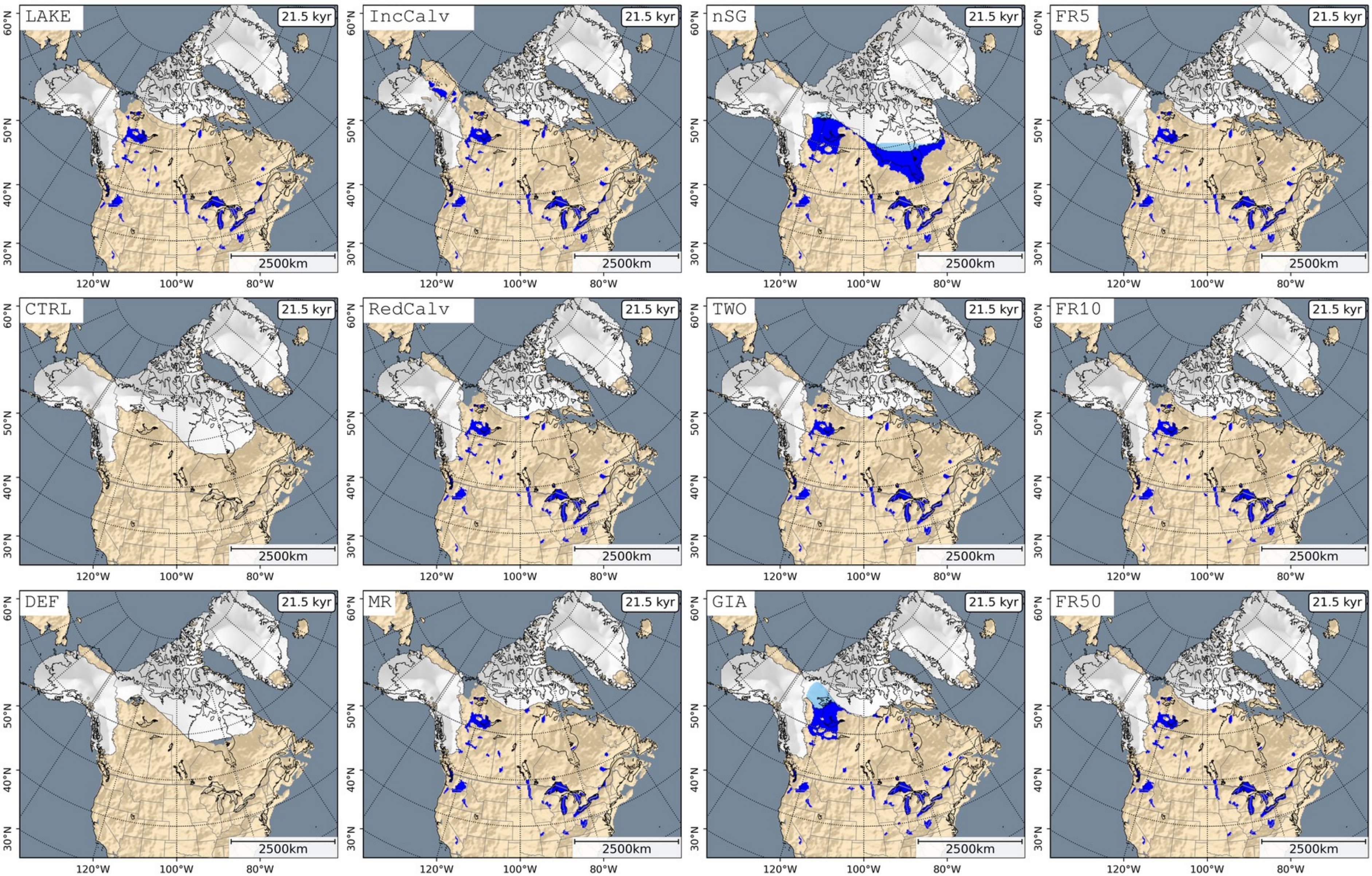

Figure S48: Overview map at 21500yr for the different experiments

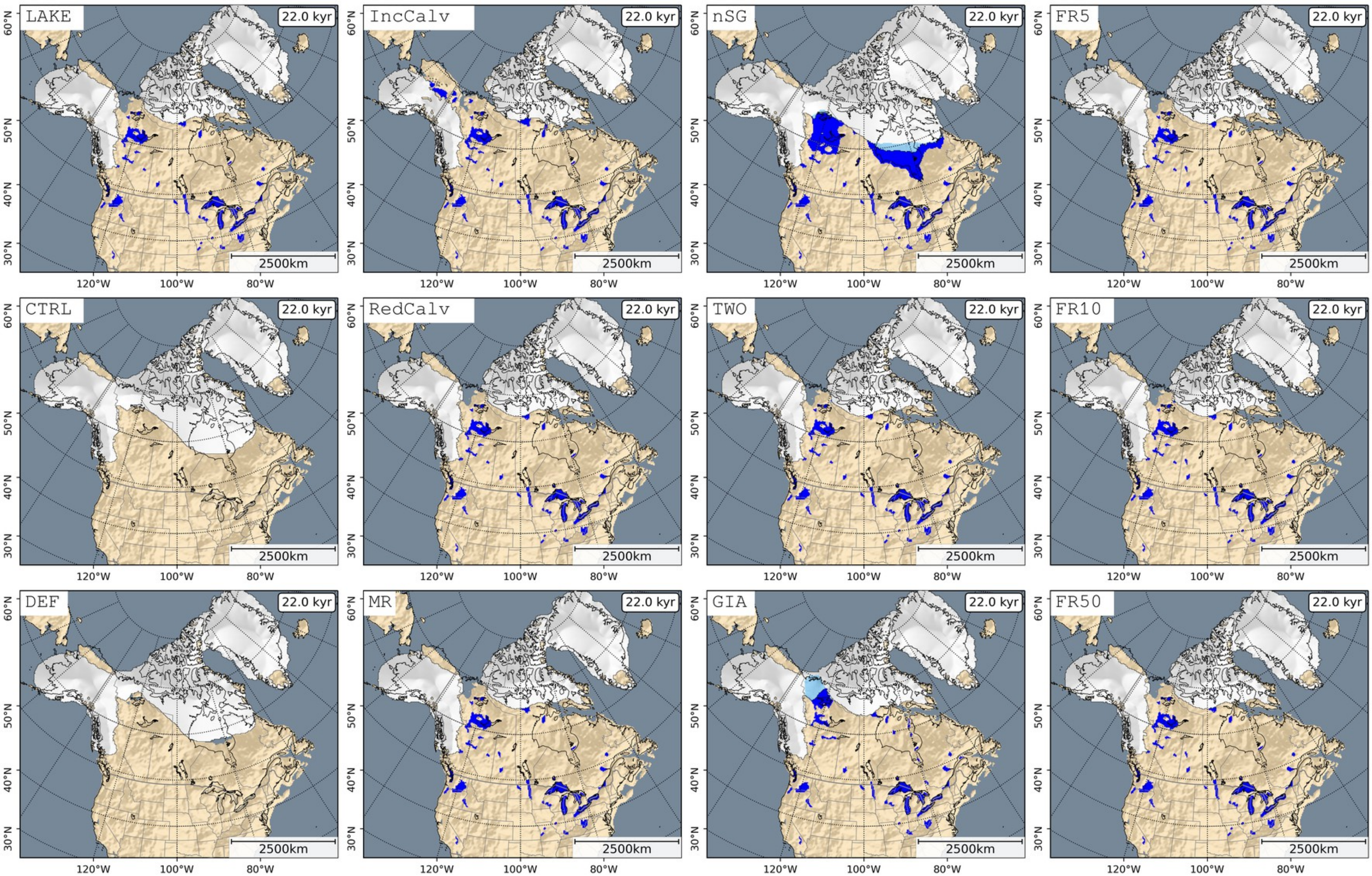

Figure S49: Overview map at 22000yr for the different experiments

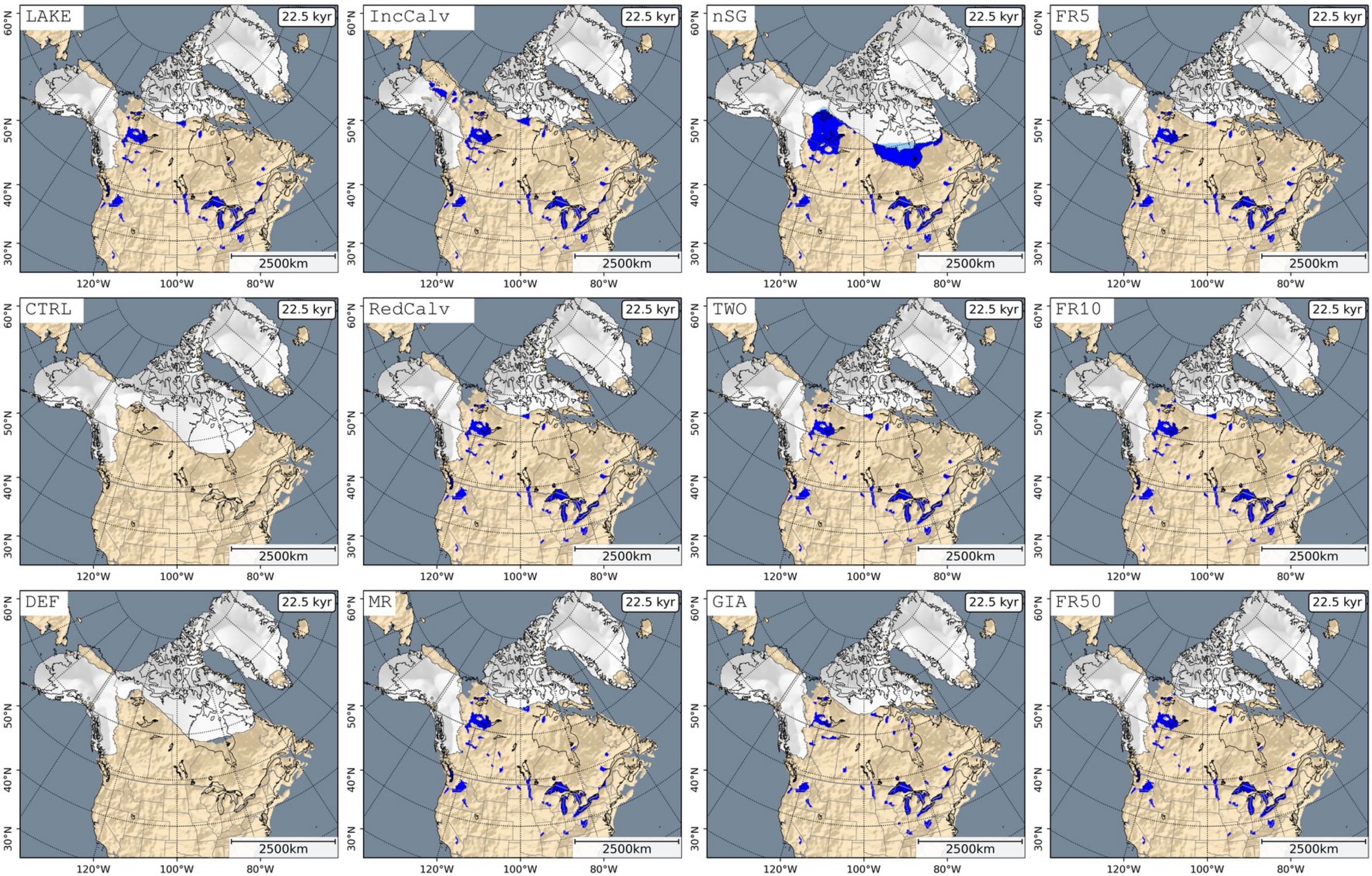

Figure S50: Overview map at 22500yr for the different experiments

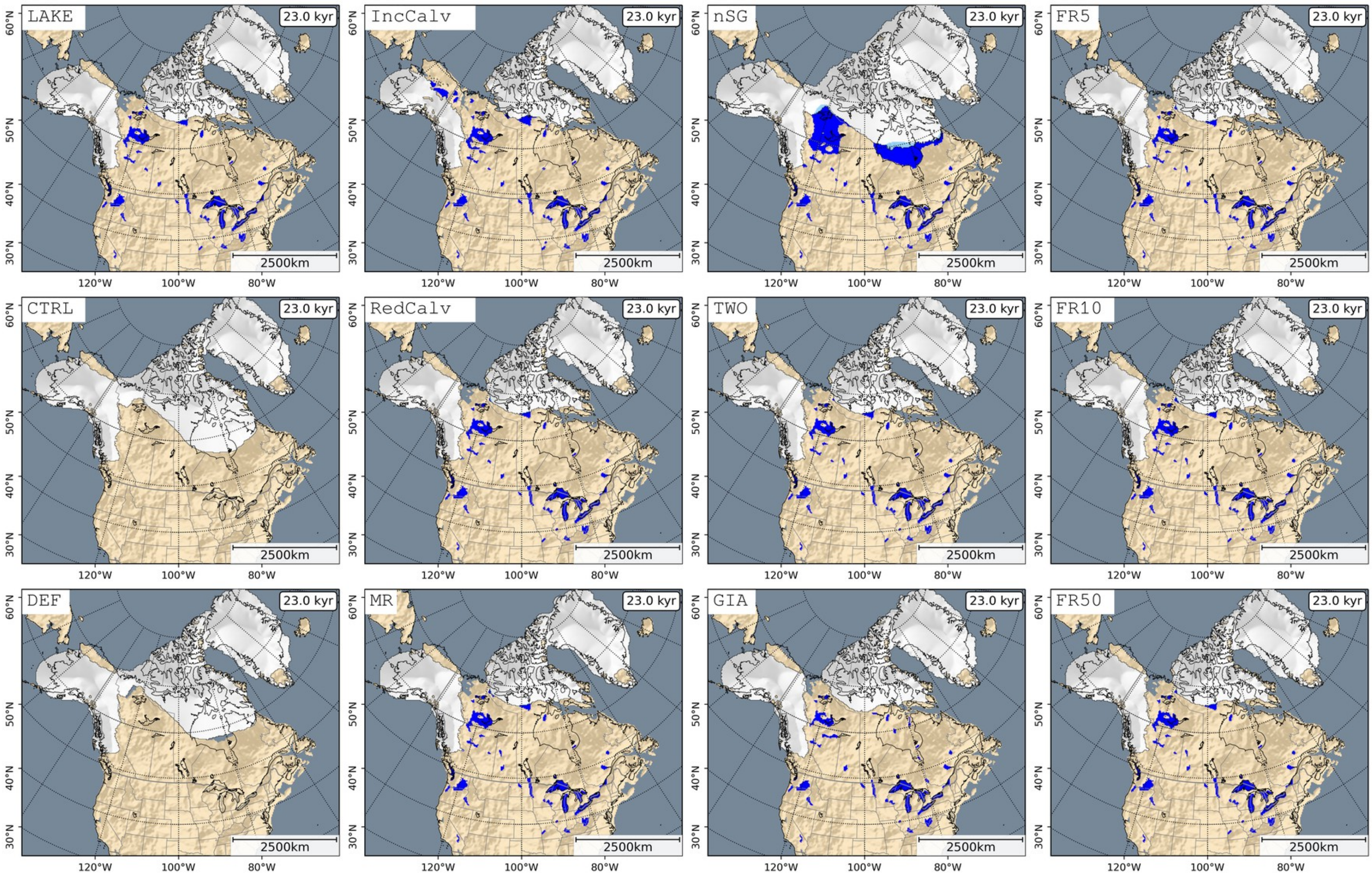

Figure S51: Overview map at 23000yr for the different experiments

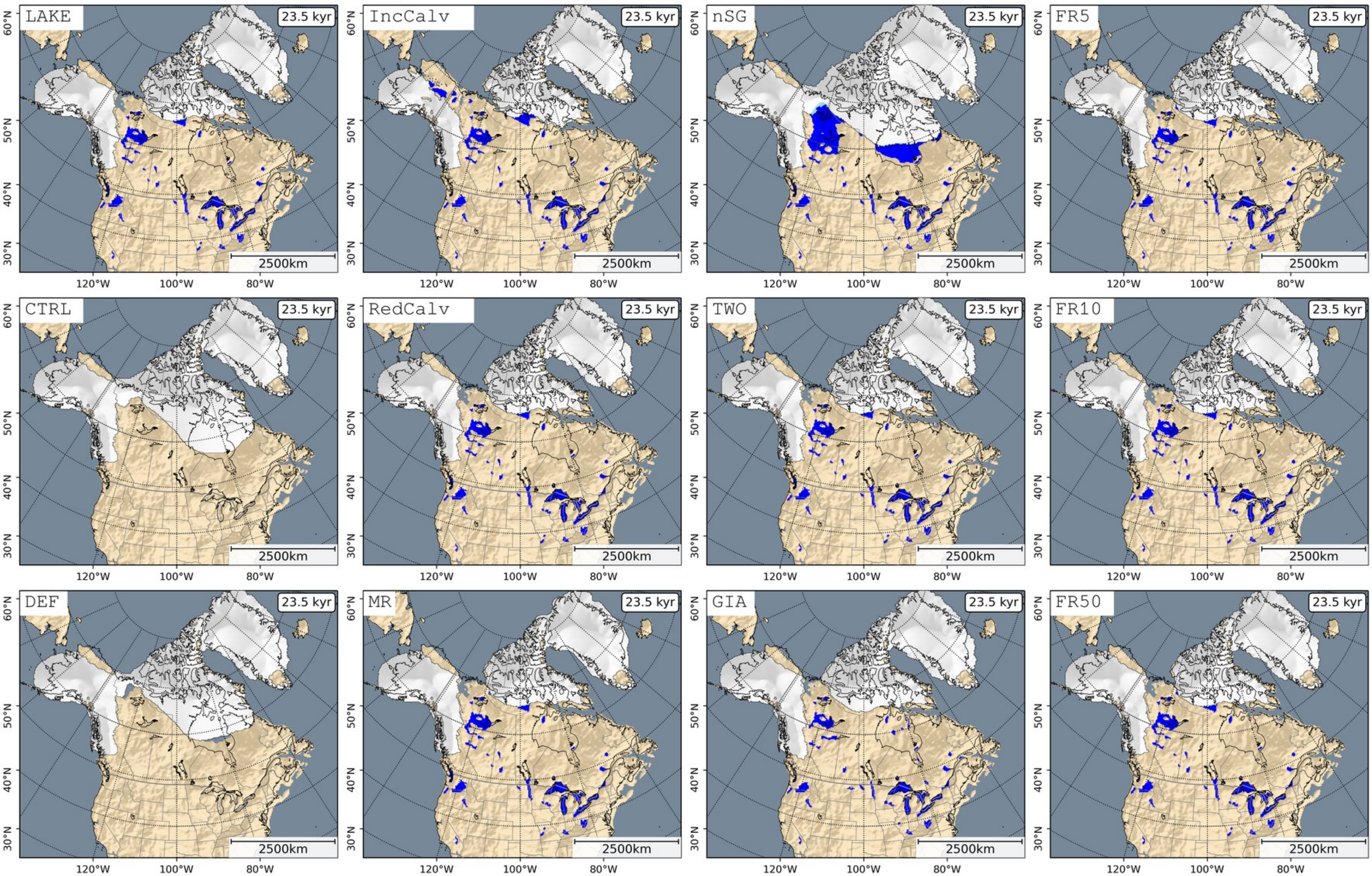

Figure S52: Overview map at 23500yr for the different experiments

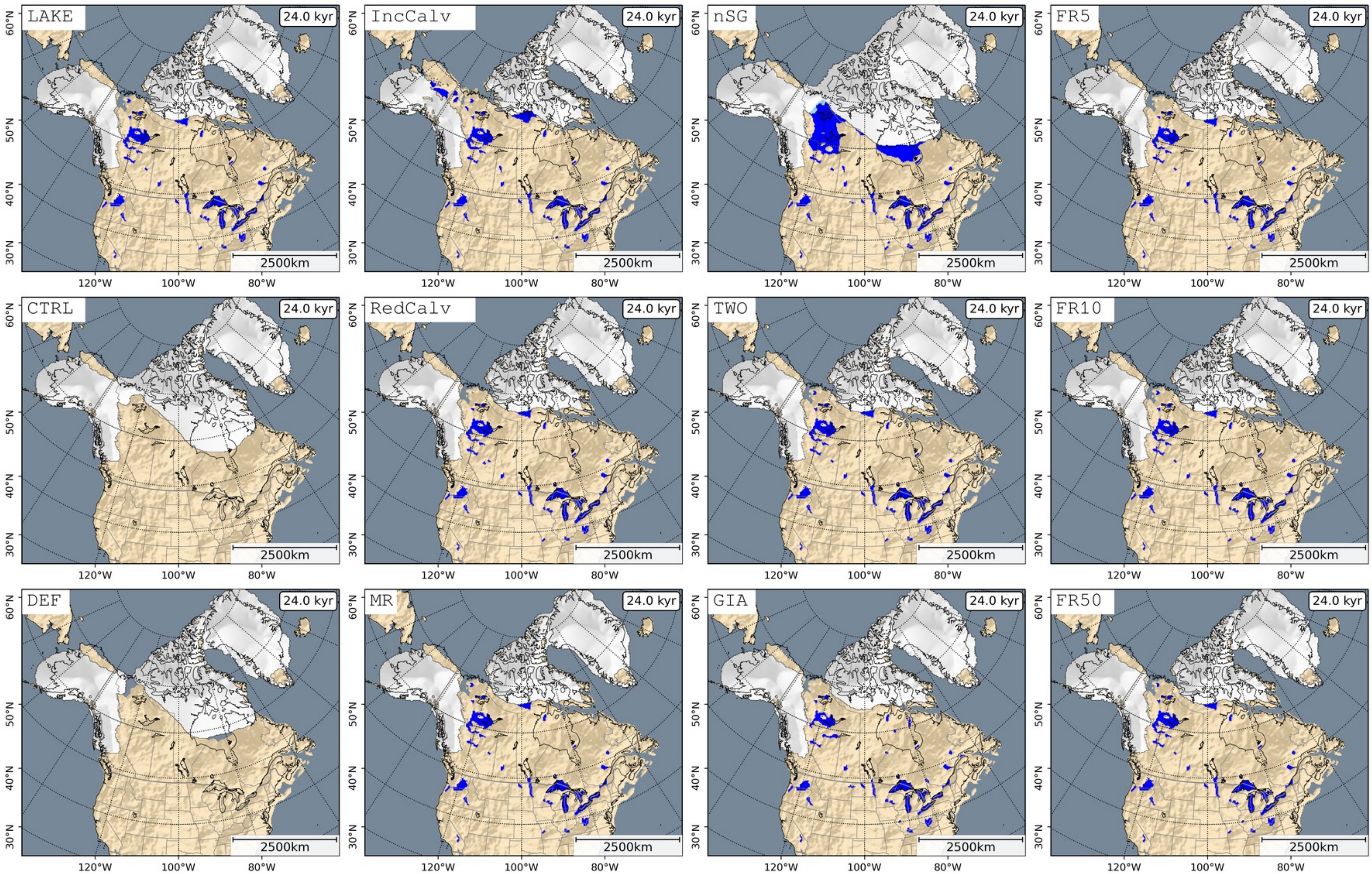

Figure S53: Overview map at 24000yr for the different experiments

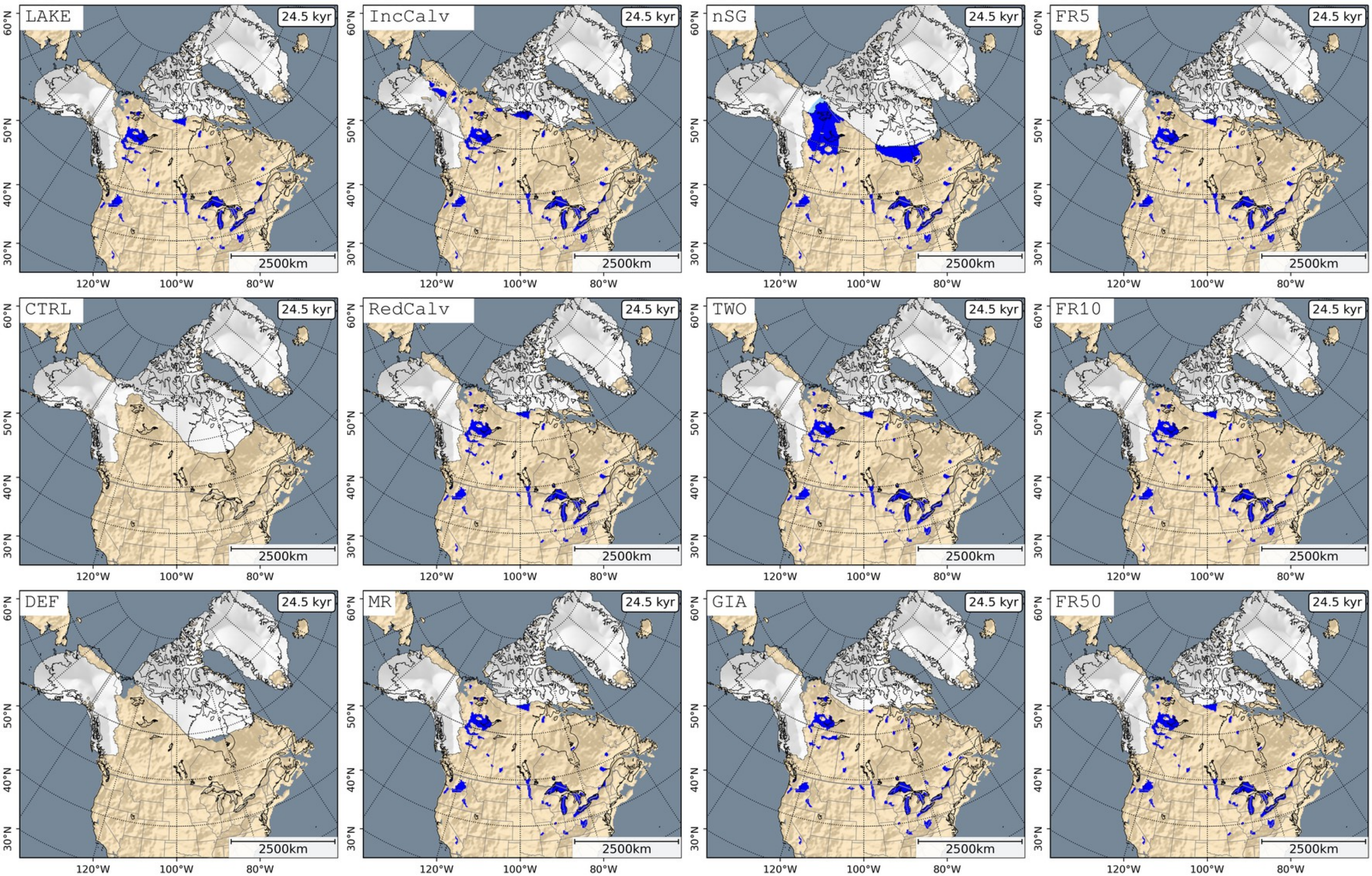

Figure S54: Overview map at 24500yr for the different experiments

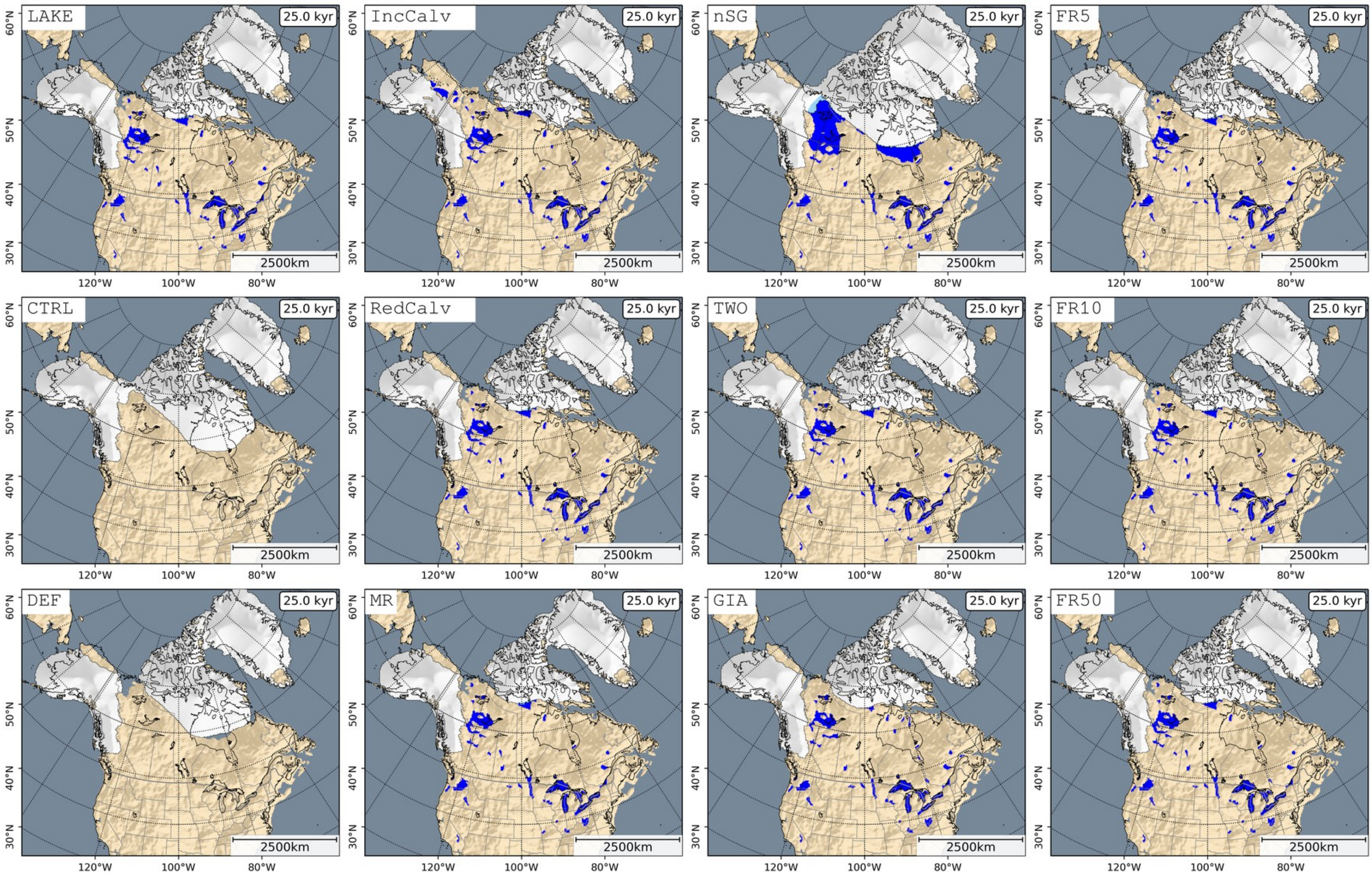

Figure S55: Overview map at 25000yr for the different experiments

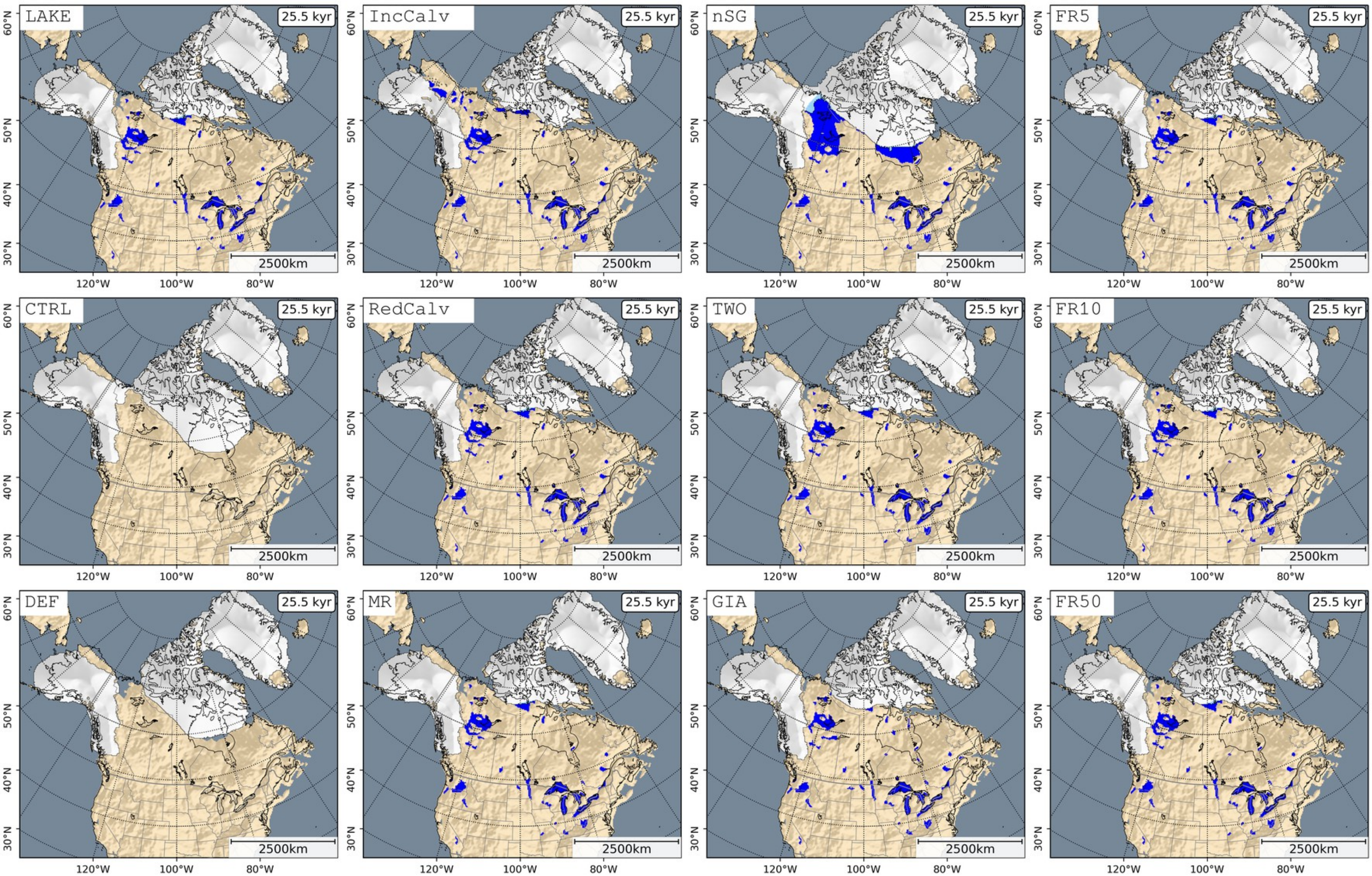

Figure S56: Overview map at 25500yr for the different experiments

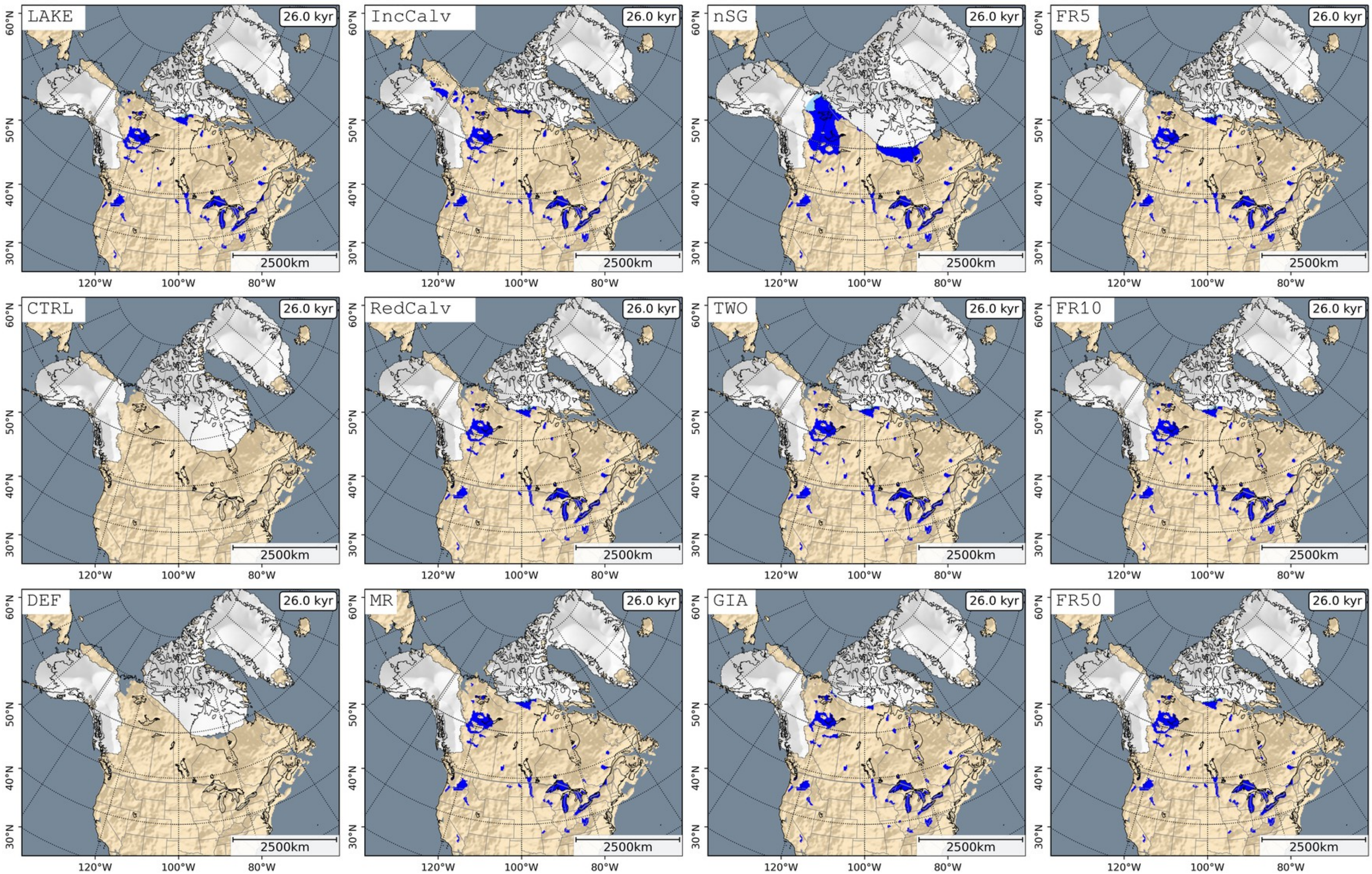

Figure S57: Overview map at 26000yr for the different experiments